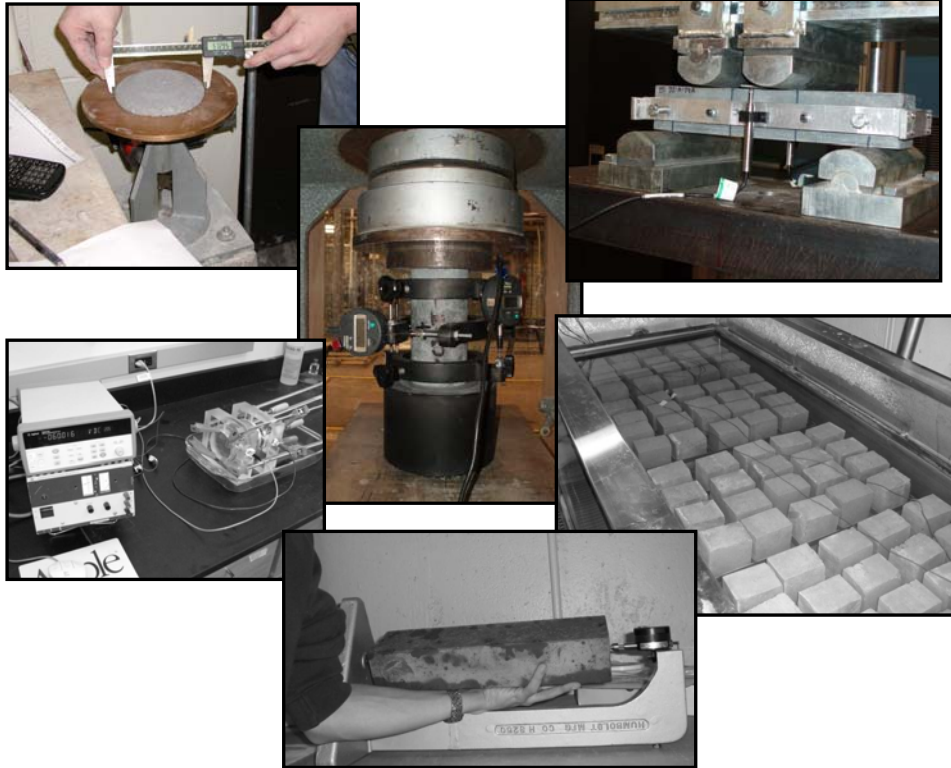**MDOT**

ULTRA-HIGH PERFORMANCE CONCRETE FOR MICHIGAN BRIDGES MATERIAL PERFORMANCE – PHASE I

FINAL REPORT – NOVEMBER 2008

Research

MichiganTech

CENTER FOR STRUCTURAL DURABILITY
MICHIGAN TECH TRANSPORTATION INSTITUTE

(This page intentionally left blank)

Technical Report Documentation Page

1. Report No. **Research Report RC-1525**	2. Government Accession No.	3. MDOT Project Manager **Roger Till, P.E.**
4. Title and Subtitle **Ultra-High-Performance-Concrete for Michigan Bridges Material Performance – Phase I**		5. Report Date **November 13, 2008**
7. Author(s) **Dr. Theresa M. Ahlborn, Mr. Erron J. Peuse, Mr. Donald Li Misson**		6. Performing Organization Code **MTU**
9. Performing Organization Name and Address **Center for Structural Durability Michigan Technological University 1400 Townsend Drive Houghton MI 49931-1295**		8. Performing Org Report No. **CSD-2008-11**
12. Sponsoring Agency Name and Address **Michigan Department of Transportation Construction and Technology Division PO Box 30049 Lansing MI 48909**		10. Work Unit No. (TRAIS)
		11. Contract Number **2003-0063**
		11(a). Authorization Number **Auth 21 Rev.1**
15. Supplementary Notes		13. Type of Report and Period Covered **Final Report**
		14. Sponsoring Agency Code

16. Abstract

    One of the latest advancements in concrete technology is Ultra-High Performance Concrete (UHPC). UHPC is defined as concretes attaining compressive strengths exceeding 25 ksi (175 MPa). It is a fiber-reinforced, densely-packed concrete material which exhibits increased mechanical performance and superior durability to normal and high strength concretes. UHPC has great potential to be used in the bridge market in the United States. However, to gain acceptance by designers, contractors, and owners this material needs to be tested according to American Society for Testing and Materials (ASTM) International and American Association of State Highway Transportation Officials (AASHTO) standards, and new practices must be developed.

    The focus of this research was to investigate how the age at which UHPC undergoes a steam (thermal) treatment affects some mechanical and durability properties. Four mechanical properties (compressive strength, modulus of elasticity, Poisson's ratio, and flexural characteristics) and properties related to durability (chloride ion penetration resistance, freeze-thaw durability, and coefficient of thermal expansion) were investigated.   The testing was conducted with differing curing conditions and at different ages to examine how these factors influence each of the measured properties. Specimens, independent of age at thermal treatment, yielded compressive strengths of over 30 ksi, modulus of elasticity values in excess of 8000 ksi, and a Poisson's ratio of 0.21. Flexural characteristics were dependent on curing regime. Testing consistently validated that UHPC had negligible chloride ion penetration, a high resistance to freeze-thaw cycling (durability factor of 100), and coefficient of thermal expansion values similar to that of normal strength concretes for both ambient cured and thermally treated specimens. Additional results revealed UHPC's autogenous healing properties while undergoing freeze-thaw cycling, low variability between batches, and the reproducibility of results between different U.S. laboratories.

    Lastly, recommendations were developed for future testing of UHPC durability properties and a preliminary life-cycle cost comparison showed that the low life-maintenance costs of UHPC can offset higher initial costs, especially as the use of UHPC in the U.S. increases and the initial cost of the material decreases.

17. Key Words: **Ultra High Performance Concrete, UHPC, Bridge Materials, Compressive Strength, Modulus, Poisson's Ratio, Flexure, Rapid Chloride Penetration, Freeze-Thaw, Coefficient of Thermal Expansion, Life Cycle Cost**		18. Distribution Statement **No restrictions. This document is available to the public through the Michigan Department of Transportation.**	
19. Security Classification (report) **Unclassified**	20. Security Classification (Page) **Unclassified**	21. No of Pages **181**	22. Price

Report RC-1525

(This page intentionally left blank)

Ultra-High-Performance-Concrete for Michigan Bridges
Material Performance – Phase I

Submitted by the Michigan Tech
CENTER FOR STRUCTURAL DURABILITY
A Michigan DOT Center of Excellence

Submitted to:

Final Report – November 2008

Submitted by:

Michigan Technological University
Civil & Environmental Eng. Dept.
1400 Townsend Dr.
Houghton, Michigan 49931
Fax: 906/487-1620

Dr. Theresa M. Ahlborn, P.E.
Associate Professor and CSD Director
906/487-2625
tess@mtu.edu

Mr. Erron J. Puese and Mr. Donald Li Misson
Former Graduate Research Assistants

(This page intentionally left blank)

ACKNOWLEDGEMENTS

DISCLAIMER

(This page intentionally left blank)

Abstract

One of the latest advancements in concrete technology is Ultra-High Performance Concrete (UHPC). UHPC is defined as concretes attaining compressive strengths exceeding 25 ksi. It is a fiber-reinforced, densely-packed concrete material which exhibits increased mechanical performance and superior durability to normal and high strength concretes. UHPC has great potential to be used in the bridge market in the United States. However, to gain acceptance by designers, contractors, and owners this material needs to be tested according to American Society for Testing and Materials (ASTM) International and American Association of State Highway Transportation Officials (AASHTO) standards, and new practices must be developed.

The focus of this research was to investigate how the age at which UHPC undergoes a steam (thermal) treatment affects some mechanical and durability properties. Four mechanical properties (compressive strength, modulus of elasticity, Poisson's ratio, and flexural characteristics) and properties related to durability (chloride ion penetration resistance, freeze-thaw durability, and coefficient of thermal expansion) were investigated. The testing was conducted with differing curing conditions and at different ages to examine how these factors influence each of the measured properties. Specimens, independent of age at thermal treatment, yielded compressive strengths of over 30 ksi, modulus of elasticity values in excess of 8000 ksi, and a Poisson's ratio of 0.21. Flexural characteristics were dependent on curing regime. Testing consistently validated that UHPC had negligible chloride ion penetration, a high resistance to freeze-thaw cycling (durability factor of 100), and coefficient of thermal expansion values similar to that of normal strength concretes for both ambient cured and thermally treated specimens. Additional results revealed UHPC's autogenous healing properties while undergoing freeze-thaw cycling, low variability between batches, and the reproducibility of results between different U.S. laboratories.

Lastly, recommendations were developed for future testing of UHPC durability properties and for a future design code, and a preliminary life-cycle cost comparison showed that the low life-maintenance costs of UHPC can offset higher initial costs, especially as the use of UHPC in the U.S. increases and the initial cost of the material decreases.

(This page intentionally left blank)

Contents

List of Figures

List of Tables

1.0 Introduction to Ultra-High Performance Concrete (UHPC)

Concrete has been one of the most widely used building materials because of its compressive strength, resistance to water, and its ability to be easily formed and placed according to need. While normal strength concrete, NSC, has long been able to achieve compressive strengths of 3,000 – 5,000 psi , issues with deterioration and an increasing desire to build larger and more robust structures with smaller members has driven researchers to explore ever stronger and more durable concrete materials. Today, high-performance concrete, or HPC (10,000 – 12,000 psi compressive strengths), with embedded steel reinforcement replaces normal strength concrete in many structural applications. However, as concrete structures begin to be constructed in ever more aggressive environments, durability in addition to strength must be considered as a principal design concern.

Research over the past decade has yielded a new classification of highly resilient concrete, called reactive powder concrete (RPC), with compressive strengths comparable to that of some steels. Now labeled and classified as ultra-high performance concretes (UHPC), these materials address many of the durability performance deficiencies associated with both NSC and HPC. Ultra-High Performance Concrete (UHPC) is one of the latest advances in concrete technology and it addresses the shortcomings of many concretes today: low strength to weight ratio, low tensile strength, low ductility, and volume instability. In addition to achieving high compressive strengths in excess of 25,000 psi (sometimes greater than 30,000 psi), UHPC is also nearly impermeable. This very low permeability allows UHPC to withstand many distresses normally associated with NSC and HPC such as freeze-thaw deterioration, corrosion of embedded steel, and chemical ingress.

The implementation of UHPC in bridge construction around the world has sparked new research investigating the potential utilization of UHPC in the U.S. bridge industry. The higher strengths afforded to UHPC could allow increased girder spans while maintaining similar or smaller cross-sectional areas. Costs may be reduced as the lower span to depth ratio of UHPC bridges require less embankment fill while providing more aesthetically pleasing profiles. Increased span lengths mean fewer support structures such as piers which can lead to improved safety when traveling under overpasses and lower environmental impact in water crossings. Additionally, beam spacing can be increased allowing for faster construction times, lower transportation costs, and increased material efficiency.

Overall, the greatest impact of UHPC materials may lie in the improved durability of concrete structures. The need for a structural material to perform in harsh environments is a reality whether the structure is a local bridge subjected to the constant winter salting, or a bridge support pier enduring the constant harsh freezing and thawing of the Straits of Mackinac. The improved durability of UHPC may lead to lower bridge repair costs and less downtime due to repair construction. UHPC bridges or structures constructed in aggressive environments may remain structurally safe for generations. Also, bridges and buildings that were all but thought impossible may now be realized. Additionally, longer lasting structures minimize the impact on the environment. Cement production is a leading contributor to industrial process-related emission sources (Hanle et al. 2004). While UHPC requires higher cement quantities than normal concretes, the amount of cement used in the lifetime of a UHPC structure may be far less than the amount used for several lifetimes of a NSC or HSC structure. Similarly, UHPC requires much less maintenance than its concrete counterparts and in turn fewer materials are required for repair or rehabilitation.

Despite these apparent benefits, material properties of UHPC need verification testing to substantiate proprietary claims on strength and durability. Similarly, results from UHPC research abroad must be validated here in the U.S. and tested according to American Society for Testing and Materials (ASTM) and American Association of State Highway Transportation Officials (AASHTO) standards where appropriate. A UHPC research initiative by the Federal Highway Administration's (FHWA) produced the first substantial UHPC research in the U.S. in late 2006 (Graybeal 2006a), but there is need for additional testing and inter-laboratory confirmation of some of the tests. Moreover, the effects of curing regimes and specimen age on the mechanical and durability properties of UHPC require a more thorough investigation.

1.2 Objectives

The primary objective of this research is to present the history of ultra-high performance concrete and to evaluate some material properties for potential use in durable highway structures. The goals necessary to accomplish this objective are outlined below:

- Characterize some UHPC material properties and build upon previous research at Michigan Tech and throughout the U.S. Properties include compressive strength, modulus of elasticity, Poisson's ratio, flexural first-crack strength, freeze/thaw behavior, chloride permeability, and coefficient of thermal expansion.

- Consider the impact that different curing regimes had on the above mentioned properties. The age at thermal treatment for curing varied from 3, 10, and 24 days, and included a baseline case of ambient-cure.

- Conduct a preliminary life cycle cost comparison between a typical prestressed concrete bridge built using standard building materials and the same bridge built using UHPC.

- Identify the impacts of UHPC material behavior on bridge design and construction.

- Develop recommendations for testing mechanical and durability properties of UHPC evaluated in this research project.

1.3   Scope

To better understand UHPC and its potential impact on the transportation industry, previous research and testing data regarding mechanical and durability properties of UHPC was compiled and synthesized. In the area of ultra-high performance concretes, Europe has led the way and produced substantial research about its material properties and durability. However, recently the U.S. also began investigating this new material and in late 2006 FHWA published the first large scale report on UHPC (Graybeal 2006a). Research is continuing at many universities and a summary of past and current research related to selected UHPC properties is presented herein.

Additionally, testing of properties was performed to analyze the effects of curing regime and cure time, age of specimen, physical distress, and ionic transport. The results were then compared to previous research to further characterize the material behavior. Moreover, due to the unique nature of the material, suggested UHPC test procedures and methods were also developed for the various tests. These suggested procedures can be used for further research on UHPC or as a foundation for developing U.S. specifications for UHPC material and durability testing.

Currently there is a large amount of research being pursued across the globe involving many different types of UHPC materials. However, the only UHPC that is commercially available in the U.S. is Ductal®, a product of Lafarge, Inc. It was for this reason that Ductal® was the only UHPC considered. More specifically, Ductal® BS1000 was used throughout this research program.

2.0   Review of UHPC

UHPC is a new family of concretes which exhibits superior mechanical and durability properties over traditional normal strength concrete (NSC) and high performance concrete (HPC). This review incorporates and condenses the current body of information related to UHPC material behavior and current applications, and serves to provide a basis for understanding UHPC durability. The majority of the information on UHPC comes from sources outside the United States that have been published since the mid-1990's. However, the U.S. Federal Highway Administration (FHWA) Turner Fairbank Laboratory recently completed an extensive material property characterization study on a proprietary UHPC material. In addition to the research completed at FHWA, several universities are conducting research on UHPC behavior including Georgia Tech, Iowa State, Ohio University, and Virginia Tech. Many of these research projects are funded through the state transportation departments (DOT) including Virginia, Georgia, and Iowa DOT's. Currently, there is no design code for UHPC in the U.S., but several other codes have been developed in Europe (AFGC 2002) and Japan (JSCE 2006). While this literature review will cover many of the known properties of UHPC, only a few studies have been conducted using accepted U.S. procedures and standards.

In the early 1990's two separate French contractors, Eiffage Group and Boygues Construction, with the help of Sika Corporation and Lafarge Corporation, respectively, developed two different UHPC's which exhibit similar properties (Harris 2004). Eiffage Group with Sika Corporation created BSI® which is noted as being coarser than other UHPCs (Jungwirth and Muttoni 2004), and the partnership between Boygues and Lafarge produced Ductal®.

Coming on the heels of continued developments in high performance concrete (HPC), the development of UHPC materials have benefited from both improved aggregate gradations and the use of a high-range water reducer, or superplasticizer. UHPC was first developed as a reactive powder concrete (RPC) with compressive strengths ranging from 29 to 116 ksi. These high strengths were the products of improving homogeneity by eliminating coarse aggregates, optimizing the granular mixture, and improving microstructure of cement paste by heat treatment application (Richard and Cheyrezy 1995). Although UHPC use of non-continuous steel fibers does not aid in increasing compressive strength, fibers do aid in improving UHPC's ductility and tensile strength. Table 2.1 compares some of UHPC's properties to HPC and NSC.

Table 2.1: Comparison of UHPC Material Properties to Other Concrete Classifications

Material Characteristics	NSC	HPC	UHPC
Maximum Aggregate Size, (in)	0.75-1.00	0.38-0.50	0.016-0.024
w/c Ratio (water/cement ratio)	0.40-0.70	0.24-0.35	0.14-0.27

Mechanical Properties	NSC	HPC	UHPC
Compression Strength, (ksi)	3.0-6.0	6.0-14.0	25.0-33.0
Split Cylinder Tensile Strength, (ksi)	0.36-0.45	-	1.0-3.5
Poisson's Ratio	0.11-0.21	-	0.19-0.24
Creep Coefficient, Cu	2.35	1.6-1.9	0.2-0.8
Porosity	20-25%	10-15%	2-6%
Fracture Energy, (k-in/in^2)	0.00057-0.00086	-	0.057-0.228
Young's Modulus, (ksi)	2000-6000	4500-8000	8000-9000
Modulus of Rupture 1st crack, (ksi)	0.4-0.6	0.8-1.2	2.4-3.2
Flexure Strength - ultimate, (ksi)	-	-	3.0-9.0
Shrinkage	-	Post Cure 40-80x10^{-5}	Post Cure <1x10^{-5}, No Autogenous Shrinkage After Cure
Coefficient of Thermal Expansion (per °F)	4.1-7.3x10^{-6}	-	7.5-8.6 x10^{-6}
Ductility	-	-	250 Times > NSC

Durability Characteristics	NSC	HPC	UHPC
Freeze/Thaw Resistance	10% Durable	90% Durable	100% Durable
Chloride Penetration (coulombs passing)	> 2000	500-2000	< 100
Air Permeability (k) at 24 hrs and 40°C, (in^2)	4.65x10^{-14}	0	0
Water Absorption at 225 hours, (lb/in^2)	4x10^{-3}	5x10^{-4}	7.1x10^{-5}
Chloride ion diffusion coefficient (by steady state diffusion), (in^2/s)	1.55x10^{-9}	7.75x10^{-10}	3.1x10^{-11}
Penetration of Carbon / Sulfates	-	-	None
Scaling Resistance, (lb/ft^2)	Mass Removal >0.205	Mass Removal 0.016	Mass Removal 0.002

Note: Table and information adapted from Kollmorgen (2004), Hartmann and Graybeal (2001), O'Neil et al. (1997), Russell (1999), Mamlouk and Zaniewski (1999), Mindess et al. (2003), Mehta and Monteiro (2006), Aitcin (1998)

2.1 UHPC Composition

While considered a relatively new material, UHPC consists mostly of the same

constituents as normal strength concrete such Portland cement, silica fume, water, and quartz

sand. However, it also includes finely ground quartz, steel fibers (0.008 in. dia. x 0.5 in. long),

and superplasticizer. While other constituents have also been investigated, including carbon

nanotubes (Kowald 2004), most UHPC mixes consist of these basic elements. The combination

of these components creates a dense packing matrix that improves rheological and mechanical

properties, and also reduces permeability (Schmidt and Fehling 2005). A breakdown of the basic

constituents of a typical UHPC is shown in Table 2.2.

Table 2.2: Composition of a Typical UHPC Mix

Constituent		lb/yd^3	% by Weight
Premix	Portland Cement	1,180 - 1,710	27 - 38
	Silica Fume	385 - 530	8 - 9
	Ground Quartz	0 - 390	0 - 8
	Fine Sand	1,293 - 1,770	39 - 41
Metallic Fibers (8.00×10^{-3} in. dia. by 0.500 in.)		245 - 320	5 - 8
Superplasticizer		20 - 30	0.5 - 1.0
Water		260 - 350	5 - 8
Water/Cementitious Material Ratio (silica fume content is considered a cementitious material and included in this ratio)		0.14 - 0.27	--

Note: Information condensed from the following references: Hartmann and Graybeal (2001),
Blais and Couture (1999), Dugat et al. (1996), and Richard and Cheyrezy (1996).

Portland cement is the primary binder used in UHPC, but at a much higher proportion

rate than in NSC or even HPC. The very low water to cementitious materials ratio prevents all

the cement from hydrating. After thermal treatment, unhydrated cement grains exist in the

matrix and act as particle packing material. Cement with high proportions of tricalcium

aluminate (CA_3) and tricalcium silicate (C_3S), and a lower Blaine fineness are desirable for

UHPC, as the CA_3 and C_3S contribute to high early strength, and the lower Blaine fineness reduces the water demand (Mindess et al. 2003). Despite the large amount of particles left unhydrated, an RPC with a water-to-cementitious material ratio of 0.20 would reach discontinuous capillary porosity when 26% hydration of cement has occurred (Bonneau et al. 2000). The addition of silica fume fulfills several roles including particle packing, increasing flowability due to spherical nature, and pozzalonic reactivity (reaction with the weaker hydration product calcium-hydroxide) leading to the production of additional calcium-silicates (Richard and Cheyrezy 1995).

Quartz sand with a maximum diameter of 0.024 in. is the largest constituent aside from the steel fibers. Both the ground quartz (4.0×10^{-4} in.) and quartz sand contribute to the optimized packing. Additionally, the most permeable portion of a concrete tends to be the interfacial transition zone (ITZ) between coarse aggregates and the cement matrix (Mehta and Monteiro 2006), and therefore, the elimination of coarse aggregates aids in improving the durability of UHPC. This zone is the area around any inclusion in the cementitious matrix, and is where the cement grains have difficulty growing because of the presence of a large surface which impedes crystal growth. Silica fume (the smallest component in UHPC with a diameter of 0.2 μm) helps fill this region, and because it is highly pozzolanic, aids in increased strength and reduced permeability. Reduction of the ITZ zone increases the tensile strength and decreases the porosity of the cementitious matrix (Mindess et al. 2003). By reducing the amount of water necessary to produce a fluid mix, and therefore permeability, the polycarboxylate superplasticizer also contributes to improving workability and durability.

Finally, the addition of steel fibers aids in preventing the propagation of microcracks and macrocracks and thereby limits crack width and permeability. For this particular application of

UHPC, straight high carbon steel fibers with a diameter of 0.008 in. and length of 0.5 in. are used. This is the largest particle in the mix and is added at 2 percent by volume to the mix. Because of its size relative to the other constituents, it reinforces the concrete on the micro level and eliminates the need for secondary reinforcement in prestressed bridge girders (Graybeal 2005). The choice and quantity of this fiber was chosen because of its availability, use in previous research, and likelihood that it will be used in the structures industry; specifically bridges. Other fiber types (polymers, organic, etc) and geometries (crimped, hooked, etc) are available, but were not investigated herein.

2.2   Types of UHPC

In Europe, there is a heavy push to develop many new and innovative types of UHPC materials. Several that have already been developed include Ductal®, BSI®, and CEMENTEC (Ahlborn et al. 2003) which are marketed by Lafarge, Eiffage Group, and Laboratoire of Central des Ponts et Chausses of France, respectively. Ductal® has been promoted in North America by the Lafarge North America group and is the brand of UHPC studied in this report. While the various UHPC materials differ slightly in composition, and many new UHPC materials are in the process of being developed, a basic understanding of UHPC material behavior and its potential implementation remains a priority for the U.S.

2.3   Applications of UHPC

As UHPC is being developed, the proper market has yet to be discovered to utilize its increased strength, durability, and flexural capacity. To date this versatile material has been used in artwork, acoustical panels, precast elements, pedestrian bridges, and a few highway bridges. Utilization of UHPC in the U.S. has been limited, but its international roots have led to many different applications in Canada, Europe, Asia, and Australia. While many of the applications

have been related to the transportation industry, more and more uses for this innovative material are being discovered to not only reap the benefits of its strength, but also UHPC's durability. Only a brief overview of UHPC functions in the world are presented here, however, more detailed investigations of these uses can be found in other sources (Behloul and Cheyrezy 2002a and 2002b; Kollmorgen 2004; Schmidt and Fehling 2005).

Development of UHPC began in the early 1990's, and in 1997 the first structure made of UHPC, the Sherbrooke pedestrian bridge, was constructed in Quebec, Canada. The 197 foot long structure is a post tension open space truss (Figure 2-1). Six match cast segments compose the main span. Among many other benefits, the enhanced mechanical properties of UHPC allowed for the use of a deck top of only 1.2 in. thick (Semioli 2001). To develop an understanding of how UHPC works in actual applications, a long term monitoring program was also implemented on the bridge to monitor deflections and forces in the prestressing tendons.
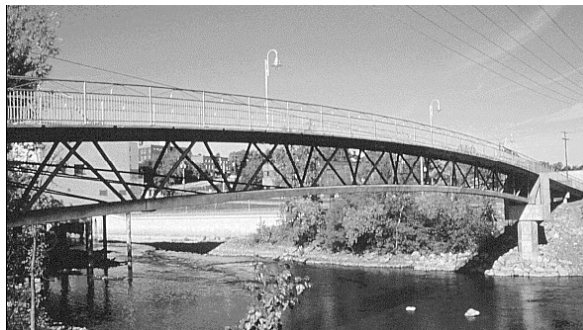
Figure 2-1: UHPC Example: Sherbrooke Footbridge (Resplendino and Petitjean 2003)

In 1997 UHPC's durability received a test when it was used to replace steel beams in the cooling towers of the Cattenom power plant, in France. The environment is extremely corrosive and UHPC was chosen because of its durability properties with the expectation of reduced or eliminated maintenance. Three years later an AFGC-SETRA working group visited the site and

under a normal layer of sediment no deterioration of the UHPC was noted (Resplendino and

Petitjean 2003).

Other transit applications include footbridges constructed in South Korea, Japan, France,

and Germany. The Footbridge of Peace in Seoul, South Korea (Figure 2-2a and Figure 2-2b), is

an arch-bridge with a span of 394 ft, arch height of only 49 ft , and a deck thickness varying

anywhere between 1.2 in. and 4 in. (Brouwer 2001). In Japan, the Sakata-Mirai footbridge

(Figure 2-2c) was completed in 2002 and demonstrated how a perforated webs in a UHPC

superstructure can both reduce weight and be aesthetically pleasing (Tanaka et al. 2002). France

utilized UHPC's fire resistant capabilities and high load carrying properties to construct an

aesthetically pleasing yet, highly fire resistant footbridge (Figure 2-2d) at a Chryso Plant in

Rhodia (Behloul and Cheyrezy 2002a). Most recently, the Gärtnerplatz Bridge was completed in

Kassel, Germany (Figure 2-2e) (Fehling et al. 2008).
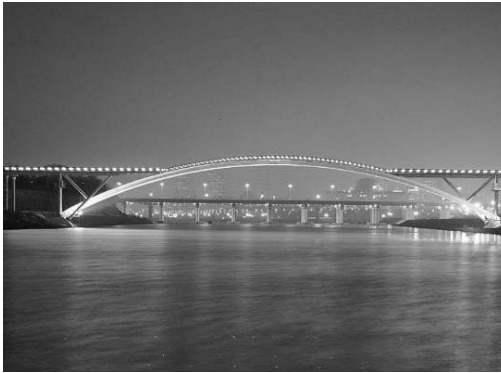
(a)

(b)

(c)

(d)

(e)

Figure 2-2: UHPC Footbridges (a) Footbridge of Peace in Seoul, South Korea at night (Behloul and Cheyrezy 2002a); (b) and during the day (Lafarge in Searls 2007); (c) perforated hollow UHPC bridge girder (Tanaka et al. 2002); (d) fire resistant UHPC footbridge in Rhodia, France; (e) Gärtnerplatz Bridge - Kassel, Germany

In 2001 the Bourg Les Valence Bridge in France was the 1st vehicle bridge constructed using UHPC. It spans approximately 145 feet with two equal spans consisting of 5 π-shaped prestressed elements. The π-shaped elements were connected by casting UHPC in situ (Resplendino and Petitjean 2003). Additionally, the Shepards Creek Bridge in New South Wales, Australia used UHPC to carry four lanes of traffic over a skewed (16°) single span of 49 ft. while reducing the dead weight by over half (Rebentrost and Cavill 2006).

UHPC made the transition to the United States in 2001 with the construction of the roof of a clinker silo (Figure 2-3a) in Joppa, Illinois (Perry 2003). The 24 wedge-shaped precast panels with a thickness of 0.5 in. covered the 58 ft. diameter silo. Utilizing UHPC saved time and labor as the roof was constructed faster and with fewer workers than the two companion metal roofed silos. Continuing in the cement industry, UHPC has since been used to create columns with a smaller cross section in a cement terminal in Detroit, Michigan (Figure 2-3b) which allows for five more feet of truck width clearance for the three loading bays (Lafarge North America 2006a).
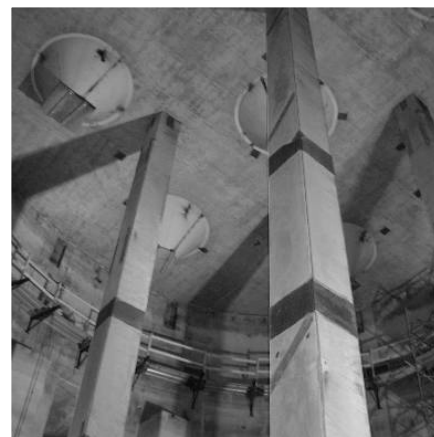
(a)   (b)

Figure 2-3: UHPC Construction Examples (a) UHPC panels on Joppa clinker silo (Behloul and Cheyrezy 2002a); (b) 54 ft UHPC columns in Detroit

14

2.4   Mechanical Properties

Characterization of the mechanical properties is imperative to the efficient design and use of UHPC. The following sections discuss the basic mechanical properties.

2.4.1 Compressive Strength

One of the most noticeable assets of UHPC is its high compressive strength. Perry and Zakariasen (2003) demonstrated that UHPC is capable of reaching compressive strengths of 25-33 ksi. This was supported by Kollmorgen (2004) with research showing a compressive strength of over 28 ksi. The increase in compressive strength, over NSC or HPC, can be attributed to the particle packing and selection of specific constituents, and thermal curing of UHPC. When undergoing a 48 hour thermal treatment of 194°F at 95 percent relative humidity, Graybeal (2005) showed an increase of 53 percent over non-thermally cured specimens of the same age. This increase in compressive strength may allow UHPC to get a foot hold in the long span and low span-to-depth ratio market segments which have been dominated by steel; creating choices for designers and owners.

Testing UHPC with traditional standards is difficult because of its high compressive strength. In the United States the standard size for a concrete cylinder is 6 x 12 in.; however, a 28 ksi cylinder of this size would require almost 800 kips to break. If the load rate of 35 psi per second specified by ASTM C 39 *Standard Test Method for Compressive Strength of Cylindrical Concrete Specimens* was followed, the same cylinder would take over 13 minutes to bring to failure instead of the normal 2 to 6 minutes with NSC. The size of compression machine and the length of the test may prove to be a barrier for production use in the U.S. Kollmorgen (2004) showed that there was no size effect for UHPC for cylinders as small as 3 x 6 in., and suggested that a 3 x 6 in. cylinder be used for standard testing of UHPC. In addition, Graybeal and

Hartmann (2003) showed that increasing the load rate to 150 psi per second does not affect the results and greatly reduces the time required to complete a compression test. For a 3 x 6 in. cylinder, the total load required to break the cylinder is decreased to approximately 200 kips and the test duration reduced to just over three minutes.

Kollmorgen (2004) investigated the mechanical behavior of thermally treated UHPC at different ages and with different sized specimens. Three cylindrical, two cube, and two prismatic geometries were used to complete the testing. Specimens were cured under ambient conditions for three days before being demolded, then tested or thermally treated. Thermal treatment included a six hour ramp up to 194°F at 100 percent relative humidity, a 48 hour hold period, and a ramp down over night. Over 240 compressive specimens were tested at various ages and with different geometries. Specimens were tested before thermal treatment (3 days after mixing), and after thermal treatment (7, 14, 28, and 56 days after mixing). Three different cylindrical (4 x 8 in., 3 x 6 in., and 2 x 4 in.) and two different cube (3.94 x 3.94 x 3.94 in. and 2 x 2 x 2 in.) geometries were tested in compression. The average compressive stress exceeded 8.5 ksi for specimens tested 3 days after casting before thermal treatment and over 28 ksi for all specimens undergoing thermal treatment regardless of age.   It was shown that the age and size effects were minimal on compression specimens, and a 3 x 6 in. cylinder was recommended for use for compression testing.

Graybeal (2005) conducted a material characterization study prior to performing full scale tests on AASHTO Type II girders made of UHPC. This characterization study included defining mechanical and durability properties, as well as the long term stability under various loading and environmental conditions. To reduce the time before the specimens could be demolded, an accelerator was added to the mix and the specimens were demolded at

16

approximately 24 hours after casting. Specimens were then subject to one of the four curing treatments of air, steam, delayed steam, and tempered steam treatments. Specimens undergoing air curing treatment remained at standard laboratory atmospheric conditions until the time of testing. Steam treatment began within 4 hours of demolding and consisted of a 2 hour ramp up to 194°F at 95 percent relative humidity, followed by a 44 hour hold, and a 2 hour ramp down to atmospheric conditions. Delayed steam treatment was similar to steam treatment except it commenced on the 15th day after mixing. Tempered steam treatment was similar to steam treatment except the temperature was limited to 140°F.

Graybeal (2005) tested nearly 1000 cylindrical and cubic compression specimens which underwent one of the four curing treatments and yielded an average 28 day compressive stress of 18.3, 28.0, 24.8, and 24.8 ksi for air, steam, delayed steam, and tempered steam, respectively. Several recommendations were made based on the research; 3 x 6 in. cylinders can be utilized for compression testing and the load rate for compression testing can be increased to 150 psi per second.

2.4.2 Modulus of Elasticity and Poisson's Ratio

The modulus of elasticity is a material dependent property which is often described as a mathematical relationship between stress and strain. Typically when the value is given for concrete, it is referencing the elastic portion of the compressive stress-strain curve up to 40 percent of the ultimate compressive strength ($0.40\,f\grave{}_c$) as specified in ASTM C 469 *Standard Test Method for Static Modulus of Elasticity and Poisson's Ratio of Concrete in Compression*. The slope of the elastic portion of the stress-strain curve is the modulus of elasticity. The modulus of elasticity is used in design calculations to predict deflection behavior of the element so the design can often satisfy the specified limit states. Because testing the modulus of

elasticity is time consuming, and requires additional testing jigs and software to determine; efforts have been undertaken to develop a relationship between modulus of elasticity and compressive strength.

ACI Committee 318 (ACI 2005) presents an equation which relates the 28 day compressive strength ($f`_c$) of normal strength concrete to the modulus of elasticity (E_c), for concrete with a unit weight (w_c) of 90 to 155 pcf. The ACI 318-05 equation, is shown as Equation 2.1

$$E_c = w_c^{1.5} * 33 * \sqrt{f`_c} \quad \text{(psi)}$$ Equation 2.1

However, HPC has a much greater compressive strength than normal strength concrete. ACI Committee 363 (ACI 1997) produced a relationship for higher strength concrete with compressive strengths from 3,000 to 12,000 psi. The equation is shown below.

$$E_c = 40,000 * \sqrt{f`_c} + 1.0 * 10^6 \quad \text{(psi)}$$ Equation 2.2

The previous two equations do not apply as the high compressive strength of UHPC lies above the range of applicable compressive strengths. Additionally, the Interim Recommendations for UHPC, which was requested by the Association Française de Génie Civil (AFGC) and published by Service d'études Techniques des Routes et Autoroutes (SETRA), does not have an equation relating compressive strength to modulus of elasticity (AFGC 2002). The document states that the material property should be determined in the later design stages by conducting a test. However, a relationship is given from the work conducted at the Cattenom nuclear power plant on 196 cylindrical specimens with diameters of 7 cm (2.76 in.). The equation is shown below after it was converted to English units.

$$E_c = 262,000 * \left(\sqrt[3]{f`_{ATT}} \right) \quad \text{(psi)}$$ Equation 2.3

18

Where: $f\hat{}_{ATT}$ = Compressive stress of UHPC after thermal treatment.

Research conducted by Sritharan et al. (2003) at Iowa State University on five 3 x 6 in. cylinders produced an equation which took the following form.

$$E_c = 50,000 * \sqrt{f\grave{}_{ATT}} \text{ (psi)}$$ Equation 2.4

Where: $f\hat{}_{ATT}$ = Compressive stress of UHPC after thermal treatment.

Work completed by Kollmorgen (2004) at Michigan Tech resulted in an equation relating compressive strength of thermally treated specimens to modulus of elasticity. The modulus of elasticity was determined using local deformation transducers (LDT) made out of strips of phosphorus bronze with strain gauges attached to each side of the metallic strip. Hinges were glued to the specimens at a set gage distance and the LDT installed. Twenty-four cylindrical specimens of 2 x 4 in., 3 x 6 in., and 4 x 8 in. were used to determine the following relationship with an applicable range of 5 to 30 ksi.

$$E_c = 351,000 * \left(\sqrt[3.14]{f\grave{}_{ATT}} \right) \text{ (psi)}$$ Equation 2.5

Where: $f\hat{}_{ATT}$ = Compressive stress of UHPC after thermal treatment.

Graybeal (2005) developed yet another relationship using a total of 148 specimens undergoing one of four different curing regimes. As previously noted, the curing treatments were air, steam, delayed steam, and tempered steam. Two parallel solid rings with a gage distance of 2 in. were solidly attached to the specimens. The upper ring held three LVDTs which end bears on the lower ring. The relationship was shown to apply to UHPC with compressive strengths between 4 and 28 ksi, and any of the aforementioned curing treatments.

$$E_c = 46,200 * \sqrt{f\grave{}_c} \text{ (psi)}$$ Equation 2.6

Poisson's ratio (v) is defined as the relationship of the transverse strain (ε_{trans}) divided by the longitudinal strain ($\varepsilon_{longitudinal}$) as shown in the equation below.

$$v = \frac{\varepsilon_{trans}}{\varepsilon_{longitudinal}}$$

Equation 2.7

This ratio is also used to relate the shear modulus, G, and modulus of elasticity, E.

$$E = 2*G*(1+v)$$

Equation 2.8

SETRA (AFGC 2002) gives a Poisson's ratio of 0.2 if it is not determined by direct testing. This value is also the widely accepted value for Portland cement concrete of normal strength.

2.4.3 First-Crack Flexural Strength and Flexural Toughness

ASTM C 1018 *Standard Test Method of Flexural Toughness and First-Crack Strength of Fiber-Reinforced Concrete (Using Beam with Third-Point Loading)* is used to evaluate the first crack strength and flexural toughness of portland cement concrete. However, no standards are available for UHPC but ASTM C 1018 can be adapted. Small prismatic specimens are loaded at the third point to create a region of constant moment in the specimen. The applied load and resulting deflection are recorded to be used in determining the first-crack strength and post crack flexural toughness. The first-crack strength is a useful indicator of the tensile strength of UHPC, however it can overestimate the tensile strength when small scale prisms are utilized (Graybeal 2005). Flexural toughness is calculated as the area under the load deflection curve and is an indication of the energy absorption capabilities.

Research by Cheyrezy et al. (1998) showed that UHPC was capable of reaching a flexural strength as high as 7.0 ksi and had a toughness of 250 times that of normal strength

concrete. Perry and Zakariasen (2003) showed that UHPC had flexural strengths ranging from 5.0 – 7.0 ksi which confirmed Cheyrezy's findings. Dugat et al. (1996) reported average modulus of rupture values of 3.2 ksi and an ultimate flexural strength of 4.6 ksi. Graybeal and Hartmann (2003) attributed the increase in the flexural behavior of UHPC to the particle packing and the addition of fibers which hold the cement matrix together after cracking has occurred. UHPC exhibits ductility because as the specimen begins to microcrack the small scale fibers reinforce the matrix causing smaller, less damaging cracks to form.

Kollmorgen (2004) conducted flexural testing on 58 specimens. The specimens had two different geometries to determine if a size effect existed on small scale prisms. Testing was conducted on 2 x 2 x 11.25 in. and 3 x 3 x 11.25 in. prismatic specimens with 9 in. spans and loading applied at the third points. A constant displacement rate of 1.50×10^{-4} in/sec, at the testing machine head, was used to test both specimen geometries. Average values of first-crack strengths, maximum loads, and toughness values, based on AGFC (2002) were reported.

Graybeal (2005) tested 71 flexural specimens utilizing the procedure outlined in ASTM C 1018, which controls the rate of deflection of the prism. As previously noted the specimens underwent one of four curing treatments, and utilized five different geometries/loading configurations. Specimens had span lengths of 6 in., 9 in., 12 in., and 15 in. with a cross section of 2 x 2 in. and a 12 in. span with a 3 x 4 in. cross section. Corrections were applied to calculate a more representative tensile strength from the first-crack strength. Ultimate load and toughness values based on the procedure outlined in ASTM C 1018 were reported.

2.4.4 Thermal Treatment

Due to the very low water-to-cementitious material ratio in UHPC, the full hydration potentials of the cement and silica fume are never reached. However, improved performance has

21

been observed after thermally treating UHPC using combinations of heat, steam, and pressure treatments (Loukili et al. 1998; Kollmorgen 2004; Graybeal 2006). The thermal treatment appears to allow continued hydration of the portland cement and pozzolanic reaction of the silica fume (Gatty et al. 1998; Cheyrezy et al. 1995). Loukili et al. (1998) noted that after treating UHPC in 194°F water, up to 65% of the cement is hydrated (compared to 48% before treatment). In addition to improved mechanical properties, Graybeal (2006) observed improved durability characteristics including increased resistance to chloride penetration and abrasion. These findings indicate that the full promises of UHPC's benefits are not only realized because of particle packing, but also due to the method of curing.

2.5   Durability Improvements

Concrete durability has become an ever more important aspect in the design of structural concrete. While compressive strength has long been the standard for determining the quality of a concrete, more and more research is focused on investigating the durability aspects of concretes. Aitcin (1998) defines durability of concrete as "the resistance of concrete to the attack of physical or chemical aggressive agents". The American Concrete Institute, or ACI, further details the durability of concrete as that which is able to resist weathering, chemical attack, abrasion, or other processes of deterioration (ACI 2002). In general, the durability of a concrete can be summarized as the capability of a concrete to continue performing its designed functions while maintaining its dimensional stability in a given environment. Concrete can experience deterioration from either physical attack (abrasion, freezing and thawing, fire, or salt crystallization) or chemical agents (alkali-silica reaction, chloride ingress and corrosion of embedded steel, sulfate attack, or delayed ettringite formation). All of these issues can lead to additional durability problems or build upon already existing problems. Generally, outside of

poor material selection leading to internal attack (high chloride content in cement paste or alkali-aggregate reaction) or poor construction practices, high permeability in a concrete is the main cause of durability failures (Mindess et al. 2003; Mehta and Monteiro 2005). On the other hand, UHPC has an extremely low water/cement ratio and a densely packed matrix that may contribute to a very low permeability.

2.5.1 Chloride Ion Penetration

Chloride ion migration through a concrete by means of capillary absorption, hydrostatic pressure, or diffusion (Stanish et al. 2000) is one of the most problematic durability issues associated with low permeability concretes. Mehta and Monteiro (2005) define permeability as the ease with which a fluid under pressure flows through a solid. A concrete with high permeability is, therefore, much more susceptible to chloride ingress which eventually leads to corrosion of reinforcing steel. Once chloride ions reach embedded steel, corrosion can take place through an electro-chemical reaction that expands the steel up to 600%. Steel corrosion is such a large problem that a 1991 FHWA report on the status of reinforced concrete bridges linked corrosion as a cause of distress for a majority of cases (Mehta and Monteiro 2005).

However, previous research demonstrated that UHPC exhibited almost no permeability and was not susceptible to chloride ingress. The very low water/cement ratio and densely packed matrix of UHPC contribute to permeability results even lower than HPC. Permeability testing demonstrated that UHPC has an oxygen permeability of less than 1.6×10^{-15} in.^{2} which is on the extremely low end of testing (AFGC 2002), while O'Neil et al. (1997) reported water absorption of 7.1×10^{-5} lb/in.^{2}. HPC on the other hand had an air permeability of 1900×10^{-15} in.^{2} and water absorption of 49.7×10^{-5} lb/in.^{2} (O'Neil et al. 1997). Cheyrezy et al. (1995) used mercury

intrusion to demonstrate that the porosity of an RPC is less than 9% in volume for the pore diameter range of 1.48×10^{-7} in. to 3.74×10^{-3} in.

Another method to determine whether a concrete is susceptible to chloride ingress uses an applied electric potential across a specimen load cell to determine concrete's conductance (ASTM C 1202). Bonneau et al. (1997) reported less than 10 Coulombs passing (over a six hour period) through UHPC specimens (negligible chloride ion penetrability) that were water cured at varying times and temperatures. In the U.S., additional research by Graybeal (2006a) demonstrated that UHPC had negligible chloride ion penetration when thermally treated and only very low penetration when not thermally treated. While Graybeal (2006a) demonstrated that the steel fibers did not contribute to a short circuit effect during UHPC testing, Toutanji et al. (1998) revealed that adding 0.75 in. polypropylene fibers increased the permeability of concrete and adding shorter fibers 0.50 in. reduced the permeability of the concrete. Furthermore, the addition of silica fume greatly reduced the conductivity of the specimen. However, the reduction was not proportional to the amount of silica fume added (Toutanji et al. 1998). Therefore, results from rapid chloride penetration testing of UHPC should reflect these claims and demonstrate UHPC's high resistance to chloride penetration.

Similarly, the French recommendations report that UHPC has an electrical resistivity of 2878 kW/in, a rate of reinforcement corrosion less than 0.39 μin/yr, and only surface corrosion of steel fibers when exposed to corrosive chemical conditions (AFGC 2002). Work by Schmidt et al. (2003) supported claims of high resistance to aggressive agents such as de-icing salts, carbonization, and chloride ion attack. The highly dense structure of the composite and the reduction in pore volume restricts aggressive chemicals and water from entering UHPC's cementitious matrix, thus preventing deterioration. The Japan Society of Civil Engineers

24

acknowledges this characteristic by mandating only a 0.79 in. cover for prestressed strands used in UHPC (JSCE 2006). Australian publications also reported chloride diffusion on the order of 31×10^{-12} in.^{2}/s to have replaced collapsed weir covers exposed to salt-water spray at the Eraring Power Station with UHPC panels having a life expectancy greater than 100 years (Rebentrost and Cavill 2006).

2.5.2 Freeze-Thaw Testing

Another mechanism of concrete distress that hinges on a concrete's permeability is freeze-thaw durability. Typically, concrete specimens exhibit distress, and eventually deterioration, in the form of cracking, spalling, and disintegration as freeze-thaw cycling persists. Freezing and thawing of saturated concrete occurs regularly in northern climates and over a period of time can disintegrate both cement matrix and aggregates. Several mechanisms are believed to be at work in this process including hydraulic pressures developed due to expanding ice (water expands 9% when frozen) (Powers 1945), osmotic pressure (Powers and Helmuth 1953), water expulsion (Litvan 1972), or the movement of water towards frozen water to form ice lenses (Collins 1944). While some or all of these theories may be at work in a specimen, the methods to avoid freeze-thaw damage are more regularly accepted. The two methods of producing freeze-thaw resistant concrete are: entraining air voids that allow pressure to dissipate or using a sufficiently low w/c ratio to reduce capillary porosity which reduces the amount of freezable water (Pigeon and Pleau 1995). The freeze-thaw durability of UHPC comes from its highly impermeable matrix that effectively eliminates capillary porosity (Bonneau et al. 2000).

Most research to date has revealed that UHPC has a durability factor of 100 or greater (no deterioration of specimens after 300 freeze-thaw cycles) (Bonneau et al. 1997). In fact, research by Lee et al. (2005) and Graybeal (2006a) demonstrated that UHPC actually increased its

25

relative dynamic modulus, or RDM (ratio of squared resonant frequency at the end of freeze-thaw testing to squared resonant frequency before testing – revealing amount of deterioration in specimen), and gained mass as the freeze-thaw cycles continued. A mass increase of 0.2% after 125 cycles was documented by Graybeal and Tanesi (2007) and led to a further study of mass change in UHPC specimens submerged in water. Normally, concretes lose mass due to material spalling and experience a decrease in relative dynamic modulus as micro-cracking occurs.

In spite of this, compiled research on autogenous healing (sometimes referred to as self healing) revealed that concrete can heal when exposed to water after or during deterioration (Jacobsen and Sellevold 1996). Jacobsen and Sellevold also demonstrated that high strength concretes can recover from damage due to freeze-thaw if submerged in water after testing. Concretes that lost up to 50% of their RDM values, gained nearly all of it back after being submerged in water for three months. However, the submerged specimens regained only 4-5% of their compressive strengths after losing nearly 22-29% of it due to freezing and thawing. Granger et al. (2007) investigated self-healing cracks in a UHPC material and determined that precracked specimens stored in water regained stiffness upon reloading while precracked specimens stored in air did not regain stiffness. The methods for self healing may come from the gathering of debris in the cracks, hydration of unhydrated cement particles in low w/c concretes, or precipitation of calcium carbonate ($CaCO_3$) (Edvardsen 1999; Granger et al. 2007). This phenomenon was further investigated by Graybeal (2006a) on air treated and steam treated UHPC specimens not subjected to distress. Untreated UHPC specimens that were submerged in water, but not subjected to freeze-thaw cycling, gained 0.25 – 0.35% mass compared to 0.09 – 0.18% mass gain for specimens remaining in an ambient air environment. Additionally, the untreated UHPC specimens submerged in water increased in compressive strength by 12%

26

relative to the compressive strengths of specimens remaining in air. On the other hand, the compressive strengths of the steam treated specimens submerged in water increased by only 3% relative to their counterparts that remained in an ambient air environment (Graybeal and Tanesi 2007).

2.5.3 Coefficient of Thermal Expansion

Temperature fluctuations that are not in the freezing range can also play an important role in structural design. The coefficient of thermal expansion (CTE) of a material is the strain in the material per a given change in temperature. The coefficient of thermal expansion needs to be considered when more than one type of material is used in construction or when member expansion could lead to overstressing under large strains. Thermal strains of concrete structural elements can lead to cracking and, therefore, susceptibility to chloride ingress or freeze-thaw damage. Given UHPC's unique material composition, establishing an appropriate CTE value for UHPC is extremely important before utilizing it with other structural materials.

Because concrete is a composite material, its coefficient of thermal expansion value correlates to the proportions (volume) of its constituents (Walker et al. 1952). As concretes generally contain a majority coarse aggregate by volume, the CTE value largely depends on the CTE of the aggregate (Mindess et al. 2003). Other important factors when considering a material's CTE are the w/c ratio, specimen age, and moisture content (Mindess et al. 2003). Some of these factors can greatly affect the recorded CTE value of a material. Partially saturated specimens can have CTE values as much as 1.8 times higher than fully saturated specimens (Emanuel and Hulsey 1977), and the CTE of cement pastes can increase as much as 25% as the cement fineness increases from 590 ft^2/lb to 1300 ft^2/lb (Mitchell 1953). However, dry specimens exhibit only slightly higher CTE values on the order of 1.17 times larger than fully

saturated specimens (Emanuel and Hulsey 1977). Emanuel and Hulsey used these factors and

developed the following equation to estimate the CTE of a concrete:

$$\alpha_C = f_T \left[f_M f_A \beta_P \alpha_S + \beta_{FA} \alpha_{FA} + \beta_{CA} \alpha_{CA} \right]$$

Equation 2.9

where: α_C = CTE of concrete
α_S = CTE of cement paste
α_{CA} = CTE of coarse aggregate
α_{FA} = CTE of fine aggregate
f_T = correction factor for temperature alternations
(1.0 - controlled, 0.86 - outside)
f_M = correction factor for moisture
f_A = correction factor for age
β_P = proportion by volume of paste
β_{FA} = proportion by volume of fine aggregate
β_{CA} = proportion by volume of coarse aggregate

The CTE value can be very important where differential heating occurs or where a

variety of materials are used. However, little research is published about the coefficient of

thermal expansion of UHPC, with most coming from manufacturers. The Japanese specification

for UHPC design states that the coefficient of thermal expansion can change substantially and

depends on the moisture content. CTE values of $7.5 \times 10^{-6}/°F$ are given by the specification for

specimens after thermal treatment (JSCE 2006). Values of approximately $8.3 \times 10^{-6}/°F$ have

been document by Graybeal (2006a). These CTE values are slightly higher than those of most

normal strength concretes which are on the range of $4.1 \times 10^{-6}/°F$ to $7.3 \times 10^{-6}/°F$ (Mindess et al.

2003). However, the French Recommendations for UHPC (AFGC 2002) use CTE values from

European UHPC suppliers of $6.6 \times 10^{-6}/°F$ for Ductal® and $5.8 \times 10^{-6}/°F$ for BSI® which are

more in line with typical concretes.

To date, the coefficient of thermal expansion of UHPC has not been tested in the United

States.

2.5.4   Additional Durability Research

Despite these findings, the body of research on UHPC durability, especially in the United States, is limited and incomplete. Variables such as specimen age at time of thermal treatment and procedure variations (ASTM C 666 - Procedure A vs. Procedure B) have not been considered. Current research has provided information about the durability properties of UHPC, but has seen little done in the way of showing that these results can be replicated in other laboratories or that variability between batches is low. Relatively few statistical analyses of the test results have been reported due to the small sample sizes tested.

The research reported here will address several of these issues including the age of thermal treatment, procedure variations, and inter-laboratory repeatability. These findings will help provide the body of UHPC research in the U.S. with a more comprehensive and thorough understanding of UHPC and its distinctive material properties. Additionally, areas of potential future research will be addressed so that continual progress can be made towards providing stronger, more sustainable, and aesthetically pleasing bridges and concrete structures.

2.6   Other UHPC research

Several state Department's of Transportation and a few universities have been investigating this relatively new material, however, the main material property tests have been conducted by FHWA at their Turner-Fairbank Highway Research Center (TFHRC). The FHWA material property characterization research was completed in 2006 (Graybeal 2006a) and provided a broad, yet basic, understanding of how UHPC performs under ASTM and AASHTO testing methods. Both mechanical and durability properties of a UHPC were investigated. Also, full scale testing of two 80 ft prestressed AASHTO Type II UHPC girders (Figure 2-4a) was completed in 2001 (Hartmann and Graybeal 2002). While these girders did not efficiently take

advantage of the UHPC properties by minimizing the cross-sectional area of the beams, they

provided valuable information about how UHPC can be cast in U.S. precast facilities. Current

research at the TFHRC is investigating an optimized girder/deck configuration for use on short

span road bridges (Graybeal et al. 2004). Initially, four 33 in. deep, 70 ft span girders with a

double-tee (or π-shaped) cross-section with an integrated 8 ft wide, 3 in. deep UHPC deck were

tested for both long-term and loading effects (Figure 2-4b). However, testing revealed problems

with the girder shape, including transverse loading and fiber distribution, and a new design has

been proposed (Keierleber et al. 2007). Results from the follow-up investigation are pending.

(a)   (b)

Figure 2-4: UHPC Girder Testing (a) Testing of a UHPC I-girder (Hartmann and Graybeal 2002) (b) UHPC π-girder at the TFHRC (Keierleber et al. 2007)

Using the research from FHWA and collaborating with Iowa State University, the Iowa

Department of Transportation and Lafarge North America constructed the first UHPC bridge in

the United States in Wapello County, Iowa in 2006 (Figure 2-5). The 110 ft simple span Mars

Hill bridge, replacing the 73-year-old dilapidated truss bridge, was comprised of three 110 ft

Modified Iowa Bulb-Tee prestressed UHPC beams (Graybeal 2006b). In addition, no mild steel

reinforcement was used (steel use was limited to the steel fibers in the UHPC matrix and to the prestressing tendons). To monitor the behavior of the beams and bridge, a 2-year performance monitoring program was implemented.

Figure 2-5: Mars Hill Bridge in Wapello County, Iowa (Lafarge 2006b)

Additional UHPC research at the Virginia DOT and Virginia Polytechnic Institute & State University characterized some of the structural aspects of UHPC including punching shear of thin UHPC plates (Harris and Roberts-Wollmann 2005) and horizontal shear between bridge decks and beams (Banta 2005). Both studies demonstrated that current AASHTO and ACI design standards could be used for design of UHPC members for punching shear and horizontal shear.

(This page intentionally left blank)

3.0   Methodology

3.1   Introduction

The objectives of this chapter are to outline the materials and equipment used to mix, cast and cure UHPC. The areas investigated were compressive strength (ASTM C39), modulus of elasticity and Poisson's ratio (ASTM C 469), and flexural properties (ASTM C 1018), rapid chloride penetration testing (ASTM C 1202), freeze-thaw cycling (ASTM C 666), and coefficient of thermal expansion (AASHTO TP 60-00). Some ASTM standards were modified slightly to facilitate use for UHPC. Modifications are discussed herein. Additionally, studies were performed for the freeze-thaw and coefficient of thermal expansion tests specimens, to determine the impact of water absorption on UHPC specimens under testing.

While previous research by Graybeal (2006a) showed a strong intra-batch correlation in the durability data (i.e. – test results correlated well when specimens were from the same batch), an inter-batch correlation is desirable to demonstrate repeatability of the batching and curing process. Therefore, one sample for each test and corresponding test age was often cast in each batch. For example, only one thermal treatment cured specimen for the 28-day coefficient of thermal expansion test was cast in Batch A, and Batch B similarly had only one thermally cured specimen for the 28-day coefficient of thermal expansion test. While this may have introduced some variability due the fact that there was only one sample of a test age for each test, the homogeneous nature of UHPC materials and batching processes allowed for accurate comparisons between specimens from different batches (as shown by low coefficient of variation results in upcoming sections). In addition, to ensure that any variability present did not greatly affect the results, three or four compression specimens for various age testing were cast in each batch to check the variability between each batch. If the compression cylinders did not achieve

proper strength, the batch would be considered to have had an error during the mixing or curing process.

3.2   UHPC Mixing Procedure

The Ductal® product used in this project was purchased from Lafarge North. Enough material to make about three fourths of a cubic yard was supplied in one shipment. The shipment included thirty-three 80 lbs. bags of premix, five 40 lbs. boxes of steel fibers, and five gallons of Chryso® Fluid Prema 150 superplasticizer. UHPC can be mixed with several different fiber types, but high carbon/high strength steel fibers were chosen as these were consistent with other research being conducted using Ductal® for precast bridge elements (Kollmorgen 2004; Graybeal 2005). The straight steel fibers measured 0.008 in. in diameter x 0.5 in. long. Three bags were damaged in transport and used for preliminary testing to ensure previous procedures outlined at Michigan Tech were still valid.

Mixing UHPC requires special equipment and procedures to develop consistency in batching, casting, and curing in a timely fashion. A high shear capacity mixer along with vibratory table and steam cure chamber capable of maintaining 100% humidity at 194°F is required (Kollmorgen 2004). The UHPC was batched according to procedures given by a Lafarge North America Technician and more detailed description of procedures can be found in Kollmorgen (2004). Mixing UHPC in Benedict Laboratory at Michigan Technological University used a Doyon BTF-060 planetary mixer (Figure 3-1).

Figure 3-1: Doyon Mixer

Batches of up to 0.65 cubic feet (ft^3) in volume were mixed using the amounts shown in

Table 3.1. This mix design was followed for all batches, except for one batch which was cast

without fibers to determine unreinforced mechanical properties. In that case, the batching

weights were kept consistent but the steel fibers were eliminated.

Table 3.1: Ductal® Mix Proportions for 0.65 ft^3 batch

Constituents	1.0 yd^3	0.65 ft^3
Premix	3700 lb.	96.3 lb.
Water	219 lb.	5.7 lb.
Superplasticizer	51 lb.	1.32 lb.
Steel Fibers	263 lb.	6.84 lb.
w/c ratio	0.20	0.20

UHPC was packaged as a blended premix that included the proprietary proportions of

Portland cement, silica fume, ground quartz, and quartz sand already combined. This premix

was added to the mixer first and then disturbed with dry mixing to break up any clumps in the

material. The other constituents (water, superplasticizer, and steel fibers) were added at the

appropriate times during the mixing sequence (Peuse 2008, Misson 2008). The superplasticizer

was added in two stages; half blended with water and added near the beginning of the mix, and

the other half added after the turning point (Table 3.2). The turning point of UHPC was defined

as the time at which all of premix and water, and half of the superplasticizer are completely

mixed so that the UHPC begins clumping together and falling from the sides of the mixing bowl,

Figure 3-2 (Kollmorgen 2004). The turning point was determined by the mixer attaining peak

amperage. After the turning point was reached, the remainder of the superplasticizer was added

followed by the slow addition of steel fibers.

Table 3.2: Typical and Adjusted Mixing Procedures

	Typical Mix Time	Mixer Speed	Mix Time for Premix age 2 mo.	Mix Time for Premix age 11 mo.
Start Mixing	0:00	1	0:00	0:00
Addition of Water + ½ Superplasticizer	2:00	1	2:00	4:00
First Speed Increase	4:15	4	4:15	6:15
Second Speed Increase	6:00	5	6:00	8:00
Turning Point	11:00	5	11:00	20:00
Addition of ½ Superplasticizer	12:00	5	12:00	22:00
Addition of Fibers	14:00	3	14:00	24:00
Reduce Speed	16:00	1	16:00	27:00
Stop Mix	18:00	1	18:00	30:00

Figure 3-2: Turning Point of UHPC

Several issues with the prescribed procedures developed during the mixing process including internal temperature and mixing times. During mixing, it is suggested by Lafarge North-America that the material's internal temperature remain below 86°F to ensure the longest pot life of the material. However, several of the batches exceeded this temperature during mixing and attained mix temperatures up to 95°F. There is no known way of controlling this internal temperature; rather it is an implicit measure. This was not viewed as a significant problem however, as consistency of the material rheology and compressive strengths were still achieved.

Another concern was that mixing time increased for batches made at later times in the research program. Previous research (Graybeal 2006a) indicated that mix times increased as premix age increased. As the premix used for this testing aged from two to eleven months, the corresponding mixing time was also longer. Table 3.2 indicates typical and adjusted timing. The typical mix procedure called for a total mixing time of 18 minutes and for the time from the

addition of water to the turning point to be approximately 8-9 minutes. However, for the older

premix the total mix time increased to nearly 30 minutes and the average time from the addition

of water to the turning point averaged 15-16 minutes.

While specific reasons for the delay in mix time were not investigated, all of the older

premix bags used for specimen batching had 1 in. or larger sized clumps of the premix material

present before mixing. The premix clumping may have inhibited the ability of the water and

superplasticizer to adequately wet all of premix in the shorter mixing time used previously.

Also, as the beginning of the mix procedure was adjusted to break apart these clumps, the time

between the addition of water and the turning point is considered a better comparison than

contrasting total mix times. The increase in mix time may lead to higher water evaporation and

therefore poor rheological properties. However, in spite of these changes, the UHPC material

obtained mix properties, compressive strengths, and durability properties comparable to that of

other research.

After mixing was completed, the rheology of the UHPC mix was tested for consistency.

An adjusted ASTM C 1437 *Standard Test Method for Flow of Hydraulic Cement* method was

used so that the recommendations outlined in Ductal® reference T006 (*Operating Procedure –

Flow Test*) were followed (20 impacts compared to the ASTM specified 25 impacts). UHPC was

first placed on the impact table in a short steel cone which was then lifted off slowly to allow the

concrete to flow evenly about the table. Four measurements of the diameter of the flow were

taken at equally spaced locations (Figure 3-3), and then the impact table was dropped 0.5 in.,

twenty times. The same four diameter dimensions of the UHPC flow were measured again and a

domain classification of the mix assigned according to Table 3.3. All of the batches mixed were

classified under Domain B, so all specimens were cast according to Ductal® reference T002

Cylinder and Prism Preparation for Domain B mixes.

Figure 3-3: Impact Table Measurement of UHPC's Flow

Table 3.3: Flow Domain Classifications of Freshly Mixed UHPC

	Domain A Stiff	Domain B Fluid	Domain C Highly Fluid
Average Flow Measurements after 20 blows	< 200 mm	200 mm - 250 mm	> 250 mm

3.3   Casting Specimens

Cylinders and beams were cast on a vibrating table capable of reproducing the specified

0.020 in. amplitude set by Ductal® reference T006. Cylinder molds were held on the table and

filled in two equal lifts. Beam molds were placed on the table and filled from one end, and the

mix was allowed to flow to the opposite end to fill the mold. After the molds were filled, they

remained on the vibrating table for an additional 30 seconds to consolidate the mix. Upon

removal from the table, the cylinders were sealed with a fitting cap, and an acrylic plastic top

sealed with weather-strip covered the beam molds. These sealed tops prevented moisture loss

from the fresh specimens. The specimens were placed on a bench in the casting room and allowed to remain at ambient conditions for three days until being demolded.

During batching, mineral oil was used to prevent the concrete specimens from sticking to the steel prism molds as well as the plastic cylinder molds. In the plastic cylinder molds, however, overuse of mineral oil resulted in more air bubbles appearing on the sides of specimens. Moreover, when no mineral oil was used to lubricate the forms, the sides of de-molded cylinders had a smooth, almost glassy, finish. Specimens with both types of surface conditions were tested, yet the phenomenon appeared to have had no effect on the material properties analyzed.

3.4   Curing Regimes

The curing regime was a primary variable in this study. Specimens were either air cured at ambient laboratory conditions (Air), or thermally treated (TT). Air-cured specimens for testing at 3-days were demolded two to three hours before testing to allow ample time to prepare and test the three day specimens in the allotted time by ASTM C 39 which was 3 days ± 2 hours. Air-cured specimens tested at later ages were also demolded at this time and placed on a laboratory shelf in ambient conditions until being tested.

The TT-cured specimens were subjected to a 48-hour, 100% humidity, steam treatment at 194°F upon demolding at 3-days. The thermal treatment began with a 6-hour ramp up period to 194°F and 100% humidity followed by a 48-hour hold at the elevated temperature and relative humidity. At the end of this time, the environment was allowed to ramp down to lab conditions over 6 hours by opening the outer lid of the cure chamber (Figure 3-4). All specimens were removed after the 60 hour cure process and allowed to return to ambient temperature before end grinding or testing occurred. Specimens destine for delayed thermal treatment (DTT) or doubly-

delayed thermal treatment (DDTT) were demolded at 3-days and placed on a laboratory shelf in ambient conditions until starting the thermal curing process at days 10 and 24, respectively.

Figure 3-4: Michigan Tech's UHPC Thermal Treatment Cure Chamber

3.5 Specimen Preparation and Test Procedures

ASTM and AASHTO standards were used as a baseline for investigating the properties of UHPC. However, several sections of the procedures were adjusted in an effort to maintain the integrity of the curing practices. Also, due to the unique nature of UHPC, a clear understanding of how the specimens were handled and tested is necessary to properly interpret and apply the results. Therefore, it is essential that the materials, equipment, specimen preparation, and testing procedures are outlined so that these tests may be reproduced and properly understood. Recommended specimen preparation and testing procedures for UHPC are summarized below for each experimental test conducted.

3.5.1 Compressive Strength

<u>Specimen Preparation – Compressive Strength</u>

The traditional methods of preparing the ends of cylinders for compressive testing by using unbonded caps (neoprene pads) or sulfur caps greatly exceeded the allowable stress of 12.0 ksi stated ASTM C 1231 and C 617, respectively, and therefore could not be used for testing UHPC. Currently, the best alternative is to grind the ends of the cylinders using a surface grinder. Figure 3-5 shows the Reid surface grinder used to prepare specimens for this research. Specimens were prepared one day before their scheduled testing time with the exception of the three day Air-cured cylinders as they were demolded and end-ground a few hours before testing.

Figure 3-5: Reid Surface Grinder

Cylinders were held in place using a v-shaped jig which kept the specimens perpendicular to the grinding wheel. After several passes of the wheel, the ends were checked for perpendicularity using the procedure set forth by Ductal® reference T009 *Operating Procedure Cylinder End Preparation*. The cylinder end planeness limit of 1° corresponds to the limit set by ASTM C 39 which states that neither end of the cylinder can depart from

42

perpendicularity by more than 0.5°. End perpendicularity was measured using a digital dial gage

as seen in Figure 3-6 utilizing the referenced procedure (Peuse 2008). All cylinders were ground

within the 1° tolerance with the initial grinding.

Figure 3-6: End Perpendicularity Set-up

Specimen Testing – Compressive Strength

     ASTM C 39 – *Standard Test Method for Compressive Strength of Cylindrical Concrete*

Specimens was used as the baseline for compression testing.   However, testing a 6 x 12 in.

UHPC cylinder after thermal treatment would potentially require a compression machine to have

a capacity of approximately 800 kips. A machine of this size is not typically used in the precast

industry or testing laboratories.   Research by Kollmorgen (2004) and Graybeal (2005) showed

that the size effect of 3 x 6, 4 x 8 or 6 x 12 in. cylindrical specimens was not statistically

significant regarding the compressive strength.   Hence, the smaller 3 x 6 in. cylinder was

chosen, affording a test machine capacity of about 250 kips which is readily available in testing labs and at precast plants in the United States. Tests performed on 3 x 6 in. cylinders were conducted on a Baldwin CT 300 (Figure 3-7). This hydraulic load frame has a capacity of 300 kips and was operated by manual controls. Data was externally collected by DASYLab Version 8.0 (2004).

Figure 3-7: Baldwin CT 300 Compression Testing Machine

A slight modification to ASTM C 39 was made to make the testing of UHPC more practical, namely the increase of the load rate applied to the specimen. The current standard sets the load rate at 35 ± 7 psi per second which would dictate that a specimen of UHPC could take up to 15 minutes to break. This lengthy time period would be unacceptable for the time required to break specimens for production use. Ductal® reference T001-*Operating Procedure Compressive Test* suggests a load rate of 150 psi per second which reduces the length of a test to approximately three minutes and also falls within the allotted time requirement of ASTM C 39. Additionally, Graybeal and Hartmann (2003) conducted research showing there was no

significant difference in UHPC compressive strength when changing the load rate from the ASTM standard to the recommended UHPC load rate. For this reason, and the fact that previous research completed at Michigan Tech used the manufacturer prescribed load rate, a load rate for compression testing of 150 psi per second was used. Load data was recorded at 5 Hz until ultimate failure of the specimen.

3.5.2 Modulus of Elasticity and Poisson's Ratio

<u>Specimen Preparation – E_c and ν</u>

The modulus of elasticity and Poisson's ratio were conducted on 3 x 6 in. cylindrical specimens. Specimen ends were prepared as described for compression testing one day before their scheduled testing time with the exception of the three day Air-cured cylinders as they were demolded and end-ground a few hours before testing. All specimens remained in the laboratory at ambient conditions after demolding until the time of testing, with the exception of the time that thermal treatment was applied.

<u>Specimen Testing – E_c and ν</u>

The testing process followed ASTM C 469 – *Standard Test Method for Static Modulus of Elasticity and Poisson's Ratio of Concrete in Compression*, except the load rate was increased to 150 psi per second as mentioned for the compression testing. Additionally, companion compression cylinders were not tested to determine the maximum applied load (0.40 $f`_c$), rather a background study determined the appropriate maximum load level as 40 percent of the average compressive strength based on age and curing regime of cylinders made during trial batches of UHPC. This variation from breaking a companion specimen was permitted because of the high predictability and low coefficient of variation (COV) of the compressive strength results based on previous work conducted by Kollmorgen (2004) and Graybeal (2005).

A combined unbonded compressometer and extensometer equipped with two digital indicators, which measured the transverse and tangential displacements. The set up is shown in Figure 3-8. Load, transverse and tangential displacement, and time were recorded by DASYLab Version 8.0 at a rate of 5 Hz. The specimens were loaded 150 psi per second until the predetermined maximum load based on curing regime and age. The specimens were completely unloaded at approximately the same rate and the gauges zeroed. This process occurred three times for each specimen, following the ASTM procedure. The initial loading was used to seat the gauges and the data disregarded. Data from the second and third loading was averaged and reported as the results for the specimen.

Figure 3-8: Compressometer and Extensometer

3.5.3 Flexural Strength

Specimen Preparation – Flexure

Testing was conducted on 2 x 2 x 11.25 in. beam specimens, and not conducted on the preferred size of 4 x 4 x 14 in. as suggested by ASTM C 1018. This smaller prism was used for

testing because, as Graybeal (2005) pointed out, UHPC elements subject to flexural forces are not likely to be 4 in. thick, and it was desired to compare the results of this study with Graybeal's (2005) and Kollmorgen's (2004) results. Additionally, the ASTM specifies that the cross section need only be three times the fiber length which was satisfied with the 2 x 2 in. cross section. No additional preparation was performed and all specimens remained in the laboratory at ambient conditions after demolding until the time of testing, with the exception of the thermal treatment duration.

Specimen Testing – Flexure

ASTM C 1018 *Standard Test Method for Flexural Toughness and First-Crack Strength of Fiber-Reinforced Concrete (Using a Beam with Third Point Loading)* was used to determine the first-crack strength and flexural toughness of Ductal[®]. This test consists of loading a small prism at the third points, to create a constant moment region, and recording the load and deflection so the data can be analyzed to give the flexural cracking stress, toughness, and approximate flexural strength of the fiber reinforced concrete. Testing of beam specimens was conducted on a 55 kip MTS load frame with Test Star II controls and Test Ware data acquisition.

When conducting this test, special attention needs to be given to the requirements of ASTM C 1018 as it specifically calls for a testing configuration which can maintain the net midspan deflection using a closed-loop servo-controlled testing machine. Controlling the rate of deflection is the key to this test because if the test was conducted under load control, the post-crack portion of the curve would not be suitable for analysis. The loading apparatus must allow the net midspan deflection to be recorded and to control the rate of deflection. The ASTM outlines two possible configurations, and the method used in this research uses a rectangular jig to hold LVDTs that are averaged to determine net deflections as shown in Figure 3-9.

Figure 3-9: ASTM 1018 Loading Configuration

This configuration loaded the specimens at the third points of the span and created a simple support condition as outlined in ASTM C 78 *Standard Test Method for Flexural Strength of Concrete (Using Simple Beam with Third-Point Loading)* where the specification for the loading apparatus is given. The deflection measuring jig was secured to the prism at the neutral axis of the prism, directly above the support points. This allowed the jig to remain stationary as the prism deflected. Two LVDT's with strokes of ± 0.20 in. were used to measure the midspan deflection from each side of the prism relative to the bar which was epoxied to the top surface of the prism. The two LVDT's signals were electronically averaged before being read by the testing software which controlled the closed-loop control system. The midspan deflection rate was chosen to be 0.003 in. per minute because ASTM C 1018 specifies that the first crack deflection be reached in 30 to 60 seconds.

3.5.4 Rapid Chloride Penetration

For the rapid chloride penetration testing, ASTM C 1202 – *Electrical Indication of Concrete's Ability to Resist Chloride Ion Penetration* was followed for both the specimen

48

preparation and testing. The testing standard requires that specimens be vacuum saturated with water and tested for electrical conductance. The electrical conductance is measured by applying a 60-volt potential across a specimen that is mounted to a test cell with sodium chloride and sodium hydroxide solutions for 6-hours. During that time the current passing is recorded, and used for calculating the total charge in coulombs passing.

Specimen Preparation – RCPT

Preparation consisted of vacuum treating and impregnating the UHPC specimens with water prior to the actual testing for chloride ion penetration. Despite UHPC's highly impermeable nature and the likelihood that it was never fully saturated through the specimen depth, ASTM C 1202 was still followed to allow for a qualitative comparison between UHPC and other concretes.

The specimens were initially cast in a 4 in. diameter by 3 in. high cylinder and, therefore, two-days prior to testing the specimens were cut down to the required 2 in. height using a kerosene cooled saw. The kerosene remaining on the surface of the UHPC specimens was then evaporated off in an oven at 122°F for approximately two hours and then cooled to room temperature over another two hours. A water cooled saw was specified in the ASTM method, however, due to UHPC's low permeability most of the kerosene was believed to be on the surface and therefore evaporated in the oven drying process. After the specimens had cooled, they were sealed on their side surface using Enviro-Tex self leveling epoxy mix and allowed to cure for at least 12 hours (Figure 3-10). Specimens were then placed in a plastic container inside a vacuum desiccator, and a vacuum was applied over the specimen for a total of four hours (Figure 3-11). At three hours into the vacuuming process, de-airated water was introduced to cover the specimen while the vacuum was maintained for the final hour. After this time, the

specimens were removed from the chamber and allowed to sit with the water covering them for 18 hours (± 2 hours). Water was then drained and the container sealed to maintain an environment at 95% humidity until testing. To provide proper time for preparation, all of the specimens were cut and epoxy coated on day 26 and vacuum treated on day 27, such that testing could begin on 28-day old specimens.

Figure 3-10: Epoxy-coated UHPC Specimens for RCPT

Figure 3-11: ASTM C 1202 Specimen Preparation Setup

Specimen Testing – RCPT

After the specimen preparation was completed, the prepared UHPC samples were then tested following the ASTM C1202 procedures. A 60-volt potential was induced across the test cells and specimen by a Kepco power supply (Figure 3-12). For 6-hours the current passing through the specimen was monitored and recorded by an Agilent 34970A Data Acquisition unit, and later would be used to calculate the total charge passing in coulombs. To replicate field situations where the exposed surface of a UHPC beam would be smooth and finished, the bottom cylinder surface (un-cut and finished) of the sample was placed facing the 3% sodium chloride (NaCl) solution, while the saw cut side of the sample was placed facing the 0.3 N (0.3 normality) sodium hydroxide (NaOH) solution.

50
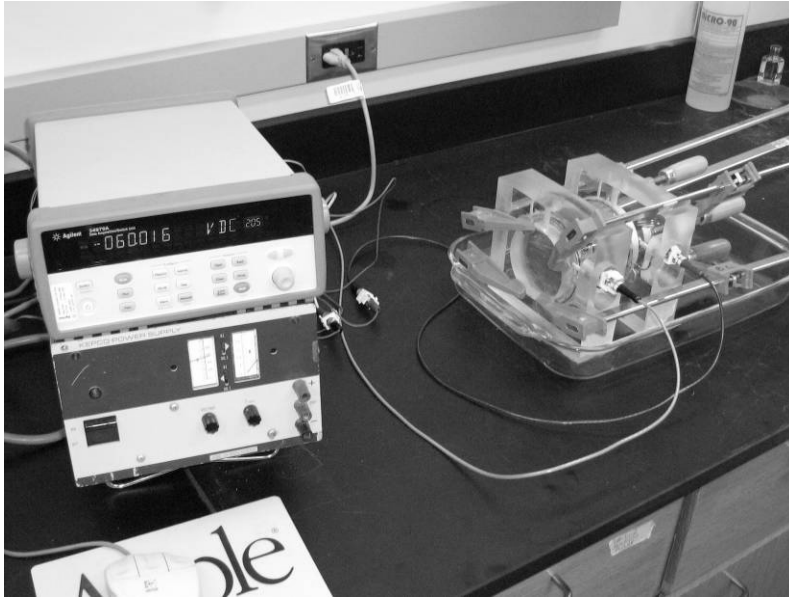
Figure 3-12: UHPC Specimen Undergoing ASTM C 1202 Testing

Care was taken to ensure that the test cells did not leak and that no short circuit was created due to the steel fiber reinforcement. If a short circuit was created, the specimen could overheat leading to erroneous results and the boiling off of the solutions. While initially the creation of a "short" circuit was a concern, no short circuiting occurred because of the random distribution and the short nature of the steel fibers. Occasionally, when more than one specimen was tested in a day, two cells were clamped together and a 60-volt potential was applied across both specimens. The data acquisition unit recorded the current passing for each individual specimen.

At the conclusion of the test, the data was compiled and a total charge passing was calculated by integrating the area under the current (amperes) versus time (seconds) curve. The integration was performed by using the trapezoidal rule (as suggested by the ASTM standard) and the current passing at 30-minute intervals (Equation 3.1). However, the total charge passed was based on a 3.75" diameter specimen according to ASTM standards and, therefore, Equation

3.2 was used to adjust the value obtained from Equation 3.1. Using this adjusted total charge

passed, Table 3.4 was then used to evaluate the chloride ion penetrability of the UHPC specimen.

$$Q = 900(I_0 + 2I_{30} + 2I_{60} + ... + 2I_{300} + 2I_{330} + I_{360})$$ Equation 3.1

where:

Q = charge passed (coulombs)

I_0 = current (amperes) immediately after voltage is applied

I_t = current (amperes) at t min after voltage is applied

$$Q_s = Q_x \times \left(\frac{3.75}{x} \right)^2$$ Equation 3.2

where:

Q_s = charge passed (coulombs) through a 3.75-in.

   diameter specimen

Q_x = charge passed (coulombs) through a x in. diameter specimen

x = diameter (in.) of the nonstandard specimen

Table 3.4: Chloride Ion Penetrability Based on Charge Passed (ASTM C 1202)

Charge Passed (coulombs)	Chloride Ion Penetrability
> 4,000	High
2,000 - 4,000	Moderate
1,000 - 2,000	Low
100 - 1,000	Very Low
< 100	Negligible

3.5.5 Freeze-Thaw Cyclic Testing

Freezing and thawing testing was performed in accordance with ASTM C 666 – *Resistance of Concrete to Rapid Freezing and Thawing* standards. Eight cycles were completed per day by means of freezing in air and thawing in water. Approximately every 32 cycles the fundamental transverse frequency, length change, and mass were observed and recorded. Specimens were tested until failure or 300 freeze-thaw cycles, whichever came first. Only one minor variation was adapted for the testing of UHPC specimens as noted below.

Specimen Preparation – Freeze/Thaw

The freeze-thaw specimens were cast in 3 x 4 x 15.5 in. beam molds with 1-1/4 in. stainless steel gauge studs embedded 1 in. into the ends of the specimen, leaving 1/4 in. of the gauge studs exposed on each end. This produced specimens with a nominal length of 16 in. (length between the two exposed ends of the gauge studs) and a gauge length of 13.5 in. (length between the embedded ends of the two gauge studs). After demolding and curing for 27-days and prior to testing, the UHPC specimens were cooled to the thaw temperature of the freeze-thaw test machine by placing them in a 41°F water bath for at least 16 hours. Soaking of the specimens according to ASTM C 666 in a lime bath for 48-hours was not performed to avoid impacting the curing regimes. This may have allowed some UHPC freeze-thaw specimens to be inadequately saturated. However, due to the high impermeability of UHPC, it is unlikely that any of the specimens would have become fully saturated in 48-hours.

Specimen Testing – Freeze/Thaw

There are two methods specified in ASTM C 666 for determining the freeze-thaw durability of a concrete – Procedure A and Procedure B. In Procedure A, the specimens are

frozen and thawed in water, while in Procedure B the specimens are frozen in air and thawed in water. The current freeze-thaw testing machine at Michigan Tech is designed for Procedure B.

Testing for freeze-thaw durability was performed in an 80-specimen Scientemp freeze-thaw chamber (Figure 3-13). As a chamber of this size contained too many slots to be completely occupied by UHPC specimens during testing, a large number of NSC "dummy" specimens were made to maintain a full-load and proper heating/cooling rates in the machine. Furthermore, three UHPC control specimens were cast with type-T thermal couples embedded to monitor and control the temperature in the chamber. Prior to using any specimen slot, these control specimens were rotated to ensure each specimen slot's freeze-thaw temperature cycle conformity to the ASTM C 666 requirements.

Figure 3-13: MTU 80-specimen Freeze-Thaw Chamber (Procedure B)

During testing, the specimens' fundamental transverse frequency, mass, and length change were evaluated at regular intervals. The fundamental transverse frequency was measured according to ASTM C 215 – *Fundamental Transverse, Longitudinal, and Torsional Frequencies of Concrete Specimens* and involved striking the end of the UHPC specimen with a precision

54

weighted steel impact hammer and measuring the dynamic response of the specimen with an accelerometer. A 2 in. thick Styrofoam pad was used to dampen any outside frequency interference, and a fast-Fourier transform method in DASYLab (ver. 8.0 2004) calculated the specimen's fundamental transverse frequency (Figure 3-14). An average fundamental transverse frequency of the specimen was determined from three strikes with the impact hammer. Using this average fundamental transverse frequency, the relative dynamic modulus (RDM) of the UHPC specimen was calculated as the ratio between the fundamental transverse frequency of a specimen after *n* cycles and the fundamental transverse frequency of the specimen immediately prior to testing. The specimen's mass was also recorded to the nearest 0.01 lbs using a calibrated scale.
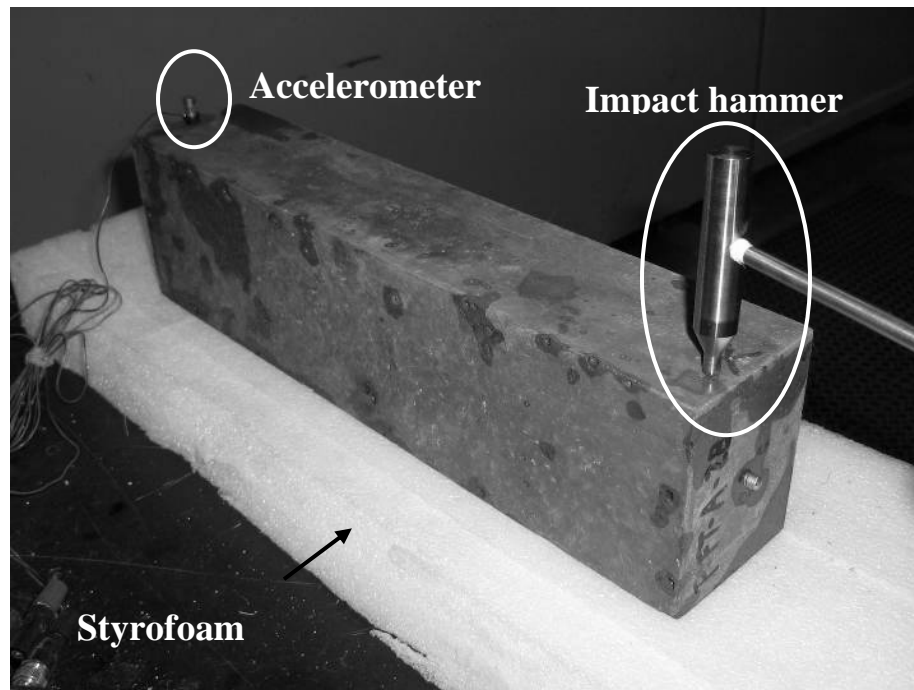
Figure 3-14: Testing the Fundamental Transverse Frequency of an UHPC Specimen

While defining failure of a freeze-thaw specimen based on a length increase of 0.10% is one option according to ASTM C 666, the 2001 Michigan Test Methods (MTM 115) specifically

use this length change parameter as the test for specimen failure. Therefore, the length change of each specimen was measured using equipment specified in ASTM C 490 – *Use of Apparatus for the Determination of Length Change of Hardened Cement Paste, Mortar and Concrete*. Specimens were measured horizontally by holding the specimen against the base of the length comparator measuring the relative length on the dial gauge (Figure 3-15). The horizontal measuring method was employed due to Note 1 in ASTM C 490, which indicates the need to use a horizontal comparator to measure specimens with cross sections larger than 9 in.^{2}. However, because the length measurement was only used for a relative comparison between specimens a vertical measurement may also be sufficient. A standard rod was used to zero the length comparator before each test to guarantee that each measurement was made relative to a standard length.
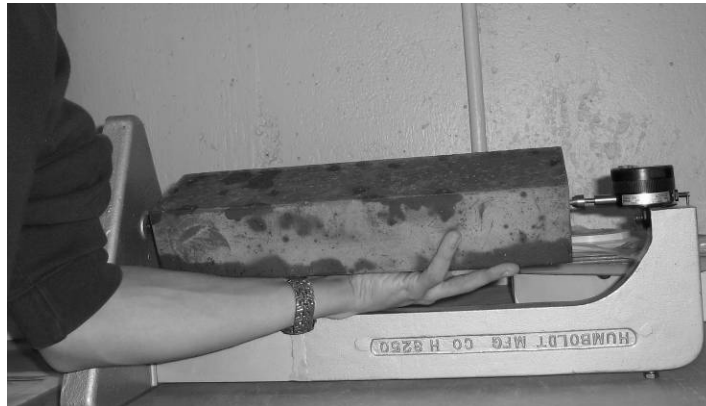
Figure 3-15: Length Change Measurement of an UHPC Freeze-Thaw Specimen

One freeze-thaw cycle was completed every 3-hours and the first measurements of initial RDM, length, and mass were taken at 24-hours (8 cycles) after the specimens began cycling. Repeat measurements were then taken at 96 hour intervals (32-cycles) until testing was complete (300 cycles or specimen failure, which ever occurred first). Specimens were removed during the thaw cycles at approximately 40°F, so that accurate length comparisons could be made.

56

Graybeal (2006a) observed that untreated UHPC specimens actually experienced as much as a 10% increase in their relative dynamic modulus and a 0.2% mass gain after 300 cycles. Therefore, two additional beams were cast in each batch (six in total) to investigate the impacts of water absorption and additional hydration of unhydrated cement particles on the RDM and mass of the UHPC specimens in the freeze-thaw chamber. To simulate the wetting and drying of the specimens undergoing Procedure B freezing and thawing cycles without temperature change, these extra "side-study" specimens were cycled every 24 hours between air and water in a water bath kept at ambient temperature.

3.5.6 Coefficient of Thermal Expansion

The coefficient of thermal expansion for concrete was determined following a modified version of AASHTO TP-60-00 – *Coefficient of Thermal Expansion of Hydraulic Cement Concrete (2004)*. Modifications to both specimen preparation and testing procedures were made due to equipment specifications and in the interest of maintaining the integrity of UHPC curing regimes. The standard process according to AASHTO TP-60-00 requires that specimens be saturated with water prior to testing, placed into a test frame and submerged in a thermally regulated water bath, and then subjected to heating and cooling cycles until an accurate CTE measurement is obtained. Detailed changes to specimen preparation and testing for UHPC are described below.

Specimen Preparation – CTE

Typically, specimen preparation for CTE testing involves saturating the concrete specimen in a limewater bath for a minimum of 48-hours prior or until a mass change of less than 0.5% is observed (whichever comes last). However, due to the extremely low water-cement ratio in UHPC, some cement particles do not become fully hydrated even after the curing regime

is applied. Because the curing regime is one of the variables being investigated through this research, it is important that the UHPC specimens do not absorb water that can react with unhydrated cementitious particles. Therefore, the standard preparation of submerging specimens in a limewater bath for 48-hours prior to testing was not employed. Instead, specimens were preserved in the unsaturated condition by coating them with an epoxy sealant.

After curing for 26 days under the specified curing regime, the 4 x 8 in. cylinder specimens were cut to size (4 x 7 in. cylinder) by removing the top 1 in. of the specimen using a kerosene saw. The specimens were oven-dried at 122°F and then measured for perpendicularity. To measure perpendicularity, 8 marks were made around the circumference of the cut side of the cylinder and a 12 in. (±0.0005 in.) micrometer was used to measure the specimen length at these 8 points. The bottoms of the specimens were not cut due to the already smoothly formed surface from the base of the mold. Nevertheless, some problems with perpendicularity arose on some specimens. However, because the bottom of the cylinder rested on three steel support buttons in the frame and was not in contact with the linear variable differential transformer (LVDT), it was not considered harmful to the length change measurements.

Following the perpendicularity measurements, the UHPC specimens were completely coated with epoxy (Figure 3-16) except for the locations on each end where the steel support buttons of the test frame and the LVDT tip came into contact with the specimen. This allowed for direct contact between the specimen and LVDT frame support buttons as well as the LVDT transducer. After the epoxy application was complete, the epoxy was allowed to cure for at least 12 hours.

Figure 3-16: Epoxy-coating CTE Specimen

Specimen Testing – CTE

UHPC CTE testing utilized Pine Instrument Company's AFCT1A Coefficient of Thermal Expansion of Portland Cement Concrete Measurement System. The components of this system included a 25-gallon water bath with a temperature stability of ±0.2°F over a temperature range of 41°F to 160°F (Figure 3-17). The specimen test frame was calibrated in accordance with manufacturer's instructions and utilized a 1 in. stroke linear variable differential transformer with a resolution of 0.0002 in. All of the equipment and programming was designed in agreement with the FHWA Procurement Specification (Appendix B). While the majority of the FHWA Specification follows AASHTO TP 60-00, some differences exist. The main variation was the measurement tolerance of the specimens that was stipulated by the FHWA specification to be 0.00005 in. rather than the 0.00001 in. as specified by the AASHTO TP 60-00 specification. Also, when determining if a specimen had reached thermal equilibrium, measurements were taken every 5 minutes over a half-hour period for the FHWA procedure rather than every 10 minutes as noted by AASHTO. Additionally, the specimen measuring frame used a correction factor procedure different from that outlined in AASHTO TP 60-00 *Appendix X.2*. The

correction factor procedure in the procurement specification provides for a two-point calibration that allows a greater range of specimen lengths to be tested in a given frame (Pine 2006). Overall, these changes were necessary for testing using the equipment available.

Figure 3-17: Pine CTE Specimen Test Frame and Water Bath

After a specimen had been prepared, mass and length were recorded prior to placing it in the water bath (Figure 3-18) for testing. The CTE values of UHPC were obtained by taking the average CTE of the specimen during a heating segment, 50°F to 122°F, and a cooling segment, 122°F to 50°F. One test cycle (one heating segment and one cooling segment) lasted approximately 24 hours. However, several specimens required longer than one test cycle to meet the AASHTO specification for successive CTE values (difference of no more than 0.5 micro strain/°F between successive CTE values). These tests were continued until the AASHTO specification was attained.

Figure 3-18: UHPC Specimen in Water Bath Undergoing CTE Testing

(This page intentionally left blank)

4.0   Results and Discussion

Several properties of UHPC were investigated during this research project. Compressive

strength, modulus of elasticity, Poisson's ratio, flexural characteristics, rapid chloride

permeability (RCPT), freeze-thaw resistance (F/T), and coefficient of thermal expansion (CTE)

of an ultra-high performance concrete were tested with differing curing conditions and at

different ages to examine how these factors influence each of the properties. Table 4.1 lists the

total number of specimens tested for each UHPC property studied under several curing regimes.

Table 4.1: Experimental Test Matrix - Specimens Tested per Curing Regime

Curing Regime[†]	Specimen Age at Testing (days)	Number of Specimens Tested						
		Compressive Strength	Modulus of Elasticity	Poisson's Ratio	1st Flexure Cracking	RCPT	F/T	CTE
Air-cured	3	6	4	4	-	-	-	3
	7	6	6	6	-	-	-	4
	14	6	6	6	-	-	-	3
	28	6	6	6	12	4	4	3
	28 – NF[‡]	6	6	5	3	-	-	-
TT (Thermal Treatment)	7	6	6	6	-	3	-	3
	14	6	6	6	-	-	-	-
	28	6	6	6	12	4	4	3
	28 - NF	5	5	5	3	-	-	-
DTT (delayed TT)	14	6	6	6	-	-	-	-
	28	6	6	6	12	-	-	-
	28 - NF	5	5	5	3	-	-	-
DDTT	28	5	5	5	-	-	-	-

[†]Curing Regime summary:
        Air-cured = ambient lab conditions 72°F, 30-50% relative humidity
        TT = Thermal treatment of 194°F, 100%RH for 48 hours beginning at age 3-days, ambient cure otherwise
        DTT = Delayed thermal treatment beginning at age 10-days
        DDTT = Doubly-delayed thermal treatment beginning at age 24-days
[‡]N.F. = refers to UHPC specimens cast without fibers

The resulting data from these tests was recorded, synthesized, and analyzed and the

summary data presented herein (additional data can be found in Appendix A). Calculating

sample mean values revealed the central tendencies of the data, while the standard deviation and

coefficient of variation (COV) were used to assess dispersion tendencies. The COV is the standard deviation divided by the mean which shows the relative variability of a sample set.

A statistical analysis was conducted to compare the effects thermal treatment on the properties of UHPC. Many options exist for testing several sample sets of data at the same time, for example an analysis of variance (ANOVA). However, this test can only tell if one or more sample group is statistically different, and does not locate which sample is different. Because the focus of the study was to determine how the different curing regimes performed compared to each other, the ANOVA was not an acceptable approach. When comparing data from two populations (e.g. – comparing TT-cured UHPC freeze-thaw specimens to Air-cured freeze-thaw specimens) a series of statistical F-tests and t-tests were performed to test the null and alternate hypotheses on the sample sets from each curing regime and age, as well as each property conducted. Complete details of the hypothesis testing and results can be found in Peuse (2008) and Misson (2008). A summary of those results are provided here. Test results are also compared to results in currently published literature.

4.1 Compression Strength

A total of 75 3x6 in. cylindrical specimens were tested for compressive strength. Table 4.2 shows the mean and COV for the compressive testing based on curing regime and age. Test data recorded for each specimen is tabulated in Appendix A (Tables A.1, A.2, A.3).

4.1.1 Results

Table 4.2 summarizes the compressive stress test results for various curing regimes and ages tested.

64

Table 4.2: Compressive Stress Test Results

Curing Regime	Specimen Age at Testing (days)	Number of Specimens (Sample Size)	Sample Mean (ksi)	Sample COV (%)
Air-cured	3	6	14.4	3.8
	7	6	19.9	1.8
	14	6	22.3	3.2
	28	6	23.9	2.2
	28 - NF	6	24.9	3.0
TT (Thermal Treatment)	7	6	30.3	2.9
	14	6	30.1	4.6
	28	6	31.1	1.3
	28 - NF	5	31.9	6.2
DTT (delayed TT)	14	6	29.7	3.5
	28	6	29.9	2.2
	28 - NF	3	31.6	3.7
DDTT	28	5	29.4	3.2

The data shows that the COV for all compressive specimens was very low and is consistent with the COV shown in ASTM C 39. ASTM C 39 reports an expected within-test COV of 2.4 percent for samples prepared from the same sample of concrete and tested at the same age. These results were based on over 1200 test reports on 6 x 12 in. cylinders with compressive strengths of 2000 psi to 8000 psi. Obviously the strength of UHPC is outside the tested range and specimens tested came from different batches, but in general the COV for the UHPC is similar to the expected value in ASTM C 39. The referenced standard also gives an acceptance range of 7.8 percent for 3 individual cylinders which is based on two times the standard deviation and thereby correlates to a COV of 3.9 percent in which all but two curing regimes and ages fall under. In addition, Peuse (2008) compared intra-batch results as well as inter-batch results to find no significant error was introduced by using one specimen per batch.

Figure 4-1 is a graphical representation of the mean compressive stress results for each age and curing regime. The error bars plotted above and below the mean values show ± one standard deviation for the respective specimen ages and curing regimes.
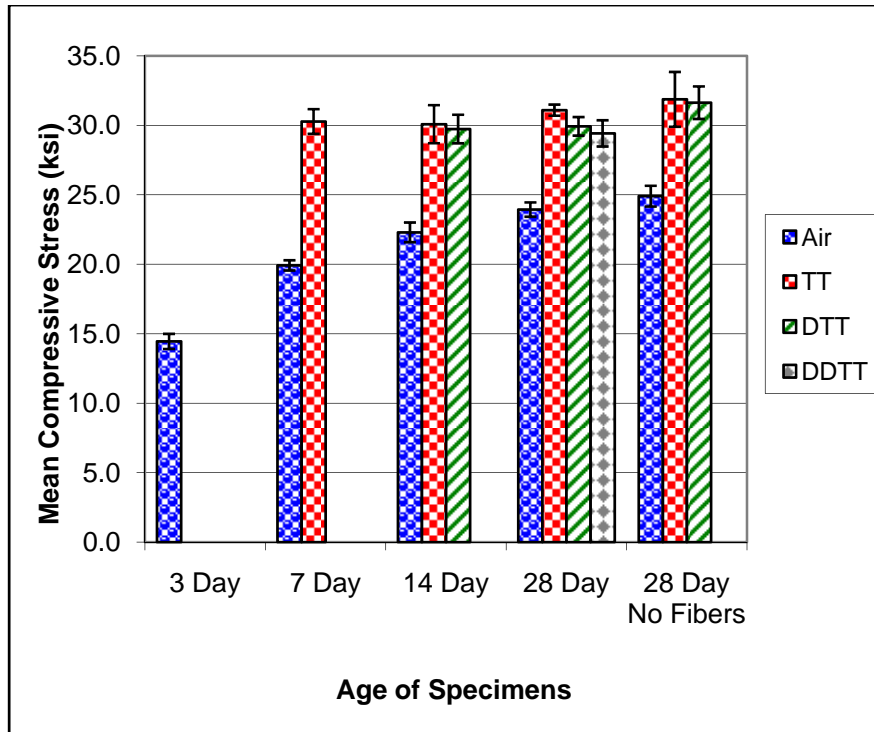
Figure 4-1: Mean Compressive Results for All Ages and Curing Regimes

It should be noted that a typical specimen failure was characterized as a shear failure by ASTM C 39. The failure plane extended from the top corner to the opposite bottom corner and the two pieces of the specimen experienced fiber pullout and fiber breakage. Specimens tested without fibers were very explosive, leaving most of the specimens in small pieces.

4.1.2 Statistical Analysis and Discussion

The main focus of this research was determining the impact that age at thermal treatment had on several properties of an ultra-high performance concrete, including after thermal treatment was complete. For example, is the compressive strength of a cylinder which underwent thermal treatment from 3-6 days the same on day 7 as it is on days 14 and 28? The compressive stress of 3 x 6 in. cylinders under the four curing regimes of air-curing, thermal treatment, delayed thermal treatment, and double delayed thermal treatment at various ages were

compared first within each curing regime and then later to each other to analyze the effect each curing regime has on compressive strength.

Hypothesis testing for pairings within curing regimes were initially run through an F-test to determine if the population variance for the two curing regimes were equal. Pairings were then compared using a t-test with the null hypothesis (Ho) equating the population means and the alternate hypothesis suggesting that they were unequal. Details of the statistical testing can be found in Peuse (2008). Table 4.3 summarizes the statistical results from hypothesis testing for comparison within each curing regime. Air-cured specimens continued to cure over the 28 day duration and all pairings were found to be not equal. Section 4.1.3 discusses strength growth with time. Air-cured specimens represent all of the thermally treated specimens up to the time of thermal curing, e.g. TT specimens were not tested at an age of 3 days because thermal treatment had not yet begun. The DDTT thermal curing occurred during days 24-27 which meant that only 28 day specimens were tested for this curing regime and no hypothesis testing was possible.

Table 4.3: Statistical Results for Compressive Strength Testing

Age of Specimen Pairings (days)	Reject or Failed to Reject the Null Hypothesis (t-test)	Population Mean
Air-cured Specimens		
3 vs 7	Reject Ho	Not Equal
3 vs 14	Reject Ho	Not Equal
3 vs 28	Reject Ho	Not Equal
7 vs 14	Reject Ho	Not Equal
7 vs 28	Reject Ho	Not Equal
14 vs 28	Reject Ho	Not Equal
TT – Thermal Treatment		
7 vs 14	Failed to Reject Ho	Equal
7 vs 28	Failed to Reject Ho	Equal
14 vs 28	Failed to Reject Ho	Equal
DTT – Delayed Thermal Treatment		
14 vs 28	Failed to Reject Ho	Equal

The purpose of conducting the hypothesis testing within the curing regimes was to determine if the data had equal population variance and the same population mean. If all the age groups (i.e. 7, 14, and 28 day) from a particular curing regime had the same population mean, then all the data could be put together to make a larger sample set for each curing regime. These larger sample sets could then be used to compare the curing regimes to one another. The results showed that the Air-cured specimens did not have the same population mean, and therefore could not be combined to form a larger sample set. Specimens tested at 28 days were chosen to represent the Air curing regime because the sample set had the highest compressive strength. Specimens undergoing TT and DTT did have the same population mean in their respective data set. Therefore, data from each age group of TT and DTT were combined into two data sets, one for TT and one for DTT. Table 4.4 shows the organization for the combined hypothesis testing.

Table 4.4: Combined Compressive Stress Results

Curing Regime	Specimen Age at Testing (days)	Sample Size	Combined Sample Mean Compressive Stress (ksi)	Combined Sample COV (%)
Air	28	6	23.9	2.2
TT	7, 14, 28	18	30.5	3.3
DTT	14, 28	11	29.8	2.6
DDTT	28	5	29.4	3.2

As with the individual curing regimes, hypothesis testing all combinations were initially run through an F-test to determine if the population variance for the two curing regimes were equal. The same combinations underwent hypothesis testing using a t-test with the null hypothesis equating the population means and the alternate hypothesis suggesting that they were unequal. For tests which include the Air curing regime, the null hypothesis was rejected and the population means were not equal. However, the remaining pairings showed that the null hypothesis was not to be rejected and that all three thermal treatment curing regimes shared the same population mean. Table 4.5 is a summary of the results of the hypothesis testing based on curing regime.

Table 4.5: Statistical Results for Combined Compressive Strength Testing

Curing Regime Pairings	Reject or Failed to Reject the Null Hypothesis (t-test)	Population Mean
Air vs TT	Reject Ho	Not Equal
Air vs DTT	Reject Ho	Not Equal
Air vs DDTT	Reject Ho	Not Equal
TT vs DTT	Failed to Reject Ho	Equal
TT vs DDTT	Failed to Reject Ho	Equal
DTT vs DDTT	Failed to Reject Ho	Equal

Hypothesis testing indicated that specimens which had undergone thermal treatment, regardless of when, had the same population mean. Therefore, the mean compressive stress of

specimens undergoing thermal treatment independent of age is 30.1 ksi, which is an increase of 25 percent over the mean of Air-cured specimens at 28 days which is 23.9 ksi. The valuable conclusion of this statistical analysis is that for compressive strength measured after thermal treatment has been applied, there is not a great difference in when thermal treatment occurs. This would have a large benefit to the precasting industry if elements could be cast individually on different days but cured together at some time in the future.

Previous work completed by Kollmorgen (2004) and Graybeal (2005) showed similar compressive strengths and COV on 3 x 6 in. cylinders. Kollmorgen (2004) reported an average compressive strength prior to thermal treatment (3 day air-cured) which was 40 percent lower than results seen in this research and had a COV of 15 percent. However, the average compressive strength of thermally treated specimens (7 day, 14 day, and 28 day) ranged from only 3.3 to 4.6 percent lower than results reported by this research. The COV varied from 3.9 to 4.0 percent. Graybeal (2005) reported 28 day compressive strengths for air, steam, and delayed steam cured specimens which were 23.6, 10.0, and 17.1 percent lower than what observed in this research program, respectively. COV ranged from approximately 3 to 6 percent for Graybeal's reported data.

4.1.3 Air-Cured Compressive Strength Growth over Time

Previous sections have shown that once UHPC receives a thermal treatment its compressive strength properties vary little. However, it was also shown that until UHPC receives a thermal treatment its strength increases with time much like traditional NSC or HPC. Determining how quickly and to what ultimate capacity UHPC will increase in strength under ambient conditions is an important factor for the design and use of UHPC.

Graybeal (2005) tested specimens with four curing treatments for compressive strength, modulus of elasticity, and linearity of the response over time. The mean results of the compressive strength over time for specimens cured under ambient conditions can be seen along with the mean results of Air-cured specimens for this research in Figure 4-2.
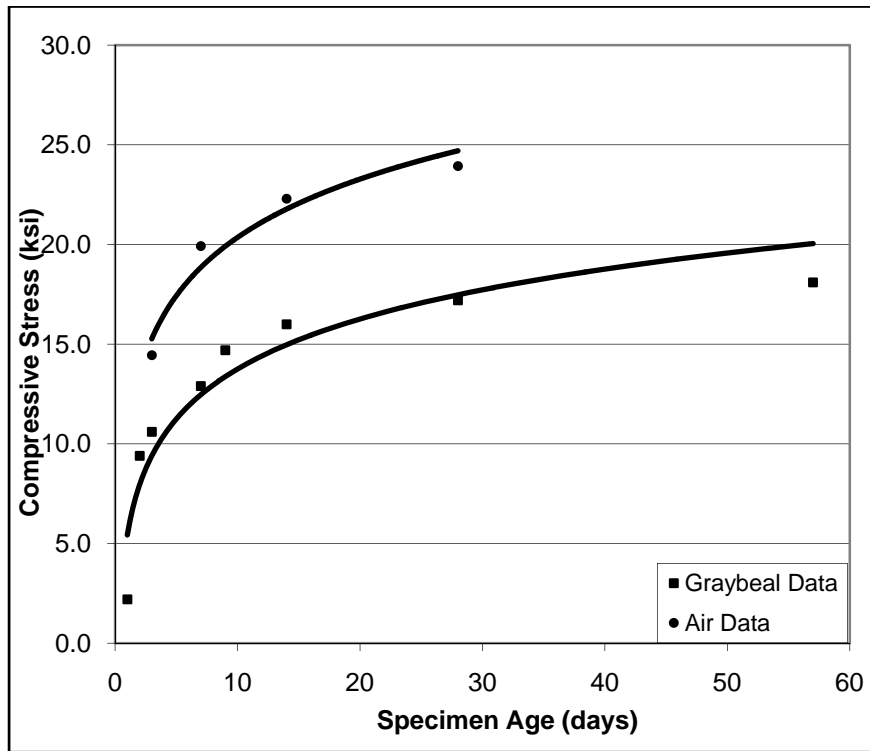
Figure 4-2: Compressive Stress Gain over Time for Air-Cured Specimens

Both sets of data present the classic asymptotic shape of the compressive strength approaching some ultimate limit. In fact both data sets seem to have very similar curves, but the data from this research has a greater compressive strength. Graybeal's (2005) data appears to be approaching 20 to 22 ksi while this research data appears to approach 25 to 27 ksi. There are several possibilities which could cause this difference in results. The first is the age at which specimens were demolded. Recall that specimens were demolded after 3 days for this research program and 24 hours for work conducted by Graybeal (2005). As part of the material study on

71

UHPC, Graybeal (2005) investigated the impact of age at demolding had on compressive strength. The results showed that by leaving the specimens in the molds to 48 hours, an increase in 28 day compressive strength of 5 ksi was seen in specimens receiving ambient curing. A second possibility is the age of premix at the time of mixing. Both Kollmorgen (2004) and Graybeal (2005) noted that the older the premix was the longer it took to mix each batch, and Graybeal (2005) saw that older premix took longer to set. If the premix was old and specimens had just enough strength to survive demolding and then were exposed to ambient conditions, the specimens would likely dry out before using all available water for hydration, and would result in lower strength (Graybeal 2005). The age of premix used for specimens in the compressive strength specimens was approximately 2 to 4 months. A third possibility would be different constituents or their proportions in the premix. The exact constituents and their proportions is not know as this is a proprietary UHPC and the premix comes blended. Finally, the ambient curing conditions could be different in each laboratory. Mixing, casting, and curing of specimens for this research were conducted in the basement of Benedict Laboratory at Michigan Tech during June, July, and August. Although the temperature and relative humidity did not vary excessively during these months (~70°F, 30-50% RH), they were not controlled. It is possible that UHPC curing in higher relative humidity could use the more readily available water vapor continue hydration. None the less, data clearly shows that UHPC continues to gain strength while curing at ambient conditions.

4.2   Modulus of Elasticity and Poisson's Ratio

A total of 73 3x6 in. cylindrical specimens were tested to investigate the effects of age at thermal treatment on modulus of elasticity and Poisson's ratio. Both properties could be measured simultaneously on any given specimen, and specimen preparation and testing

procedures were discussed in Chapter 3. In general, the process followed ASTM C 469 –

Standard Test Method for Static Modulus of Elasticity and Poisson's Ratio of Concrete in

Compression, except the load rate was increased to 150 psi per second. Test data recorded for

each specimen is tabulated in Appendix A (Tables A.1, A.2, A.3).

4.2.1 Results

Table 4.6 summarizes the mean and COV for the modulus of elasticity and Poisson's

Ratio based on curing regime and age. Two specimens which were Air-cured and compression

tested at 3 days were not tested for modulus of elasticity and Poisson's ratio because of

difficulties with the data acquisition system.

Table 4.6: Modulus of Elasticity and Poisson's Ratio Test Results

Curing Regime	Specimen Age at Testing (days)	Number of Specimens (Sample Size)	Mod. of Elasticity Sample Mean (ksi)	Mod. of Elasticity Sample COV (%)	Poisson's Ratio Sample Mean	Poisson's Ratio Sample COV (%)
Air-cured	3	4	6,910	0.6%	0.198	2.7
	7	6	7,520	1.9	0.205	2.0
	14	6	7,865	0.8	0.206	1.3
	28	6	7,863	1.8	0.205	4.2
	28 - NF[‡]	6	7,696	1.2	0.200	1.7
TT (Thermal Treatment)	7	6	8,056	1.6	0.206	2.2
	14	6	8,215	1.3	0.206	2.4
	28	6	8,114	0.7	0.205	2.1
	28 - NF	5	7,889	1.1	0.203	2.5
DTT (delayed TT)	14	6	8,177	1.5	0.205	2.6
	28	6	8,161	0.6	0.207	4.4
	28 - NF	3	7,741	2.2	0.200	1.1
DDTT	28	5	8,098	1.0	0.203	1.0

This table shows data with a very low COV and is very similar to previous results with

this type of UHPC (Kollmorgen 2004; Graybeal 2005). It is because of this low variability that

statistically significant results can be determined with low sample sizes.

Figure 4-3 shows a typical stress-strain graph for the calculation of modulus of elasticity. This particular specimen was thermally treated from Batch 1 and tested at 14 days.
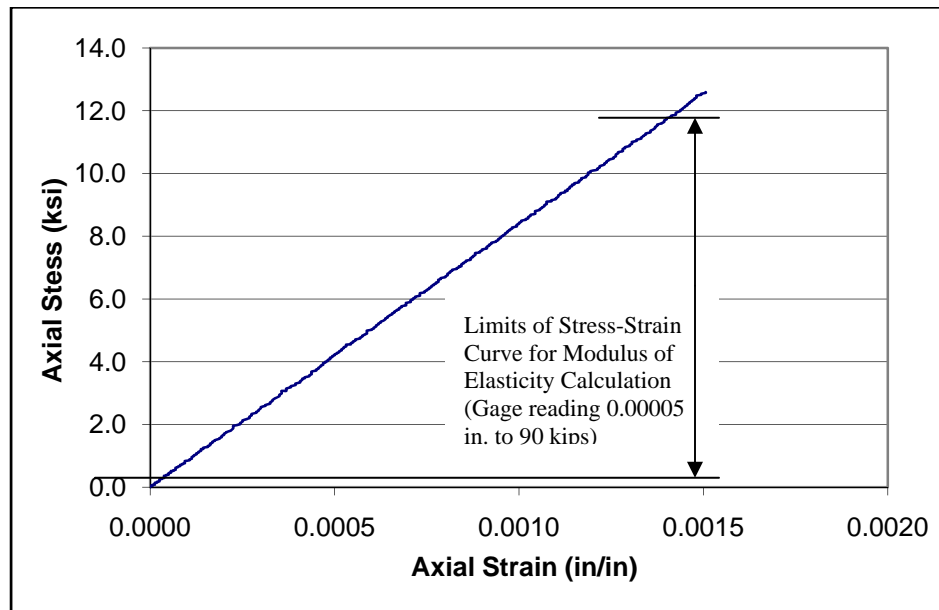
Figure 4-3: Typical Stress-Strain Curve for Calculating the Modulus of Elasticity

Figures 4-4 and 4-5 show the mean modulus of elasticity and Poisson's ratio results, respectively, for each age and curing regime. The error bars indicate ± one standard deviation from the mean.
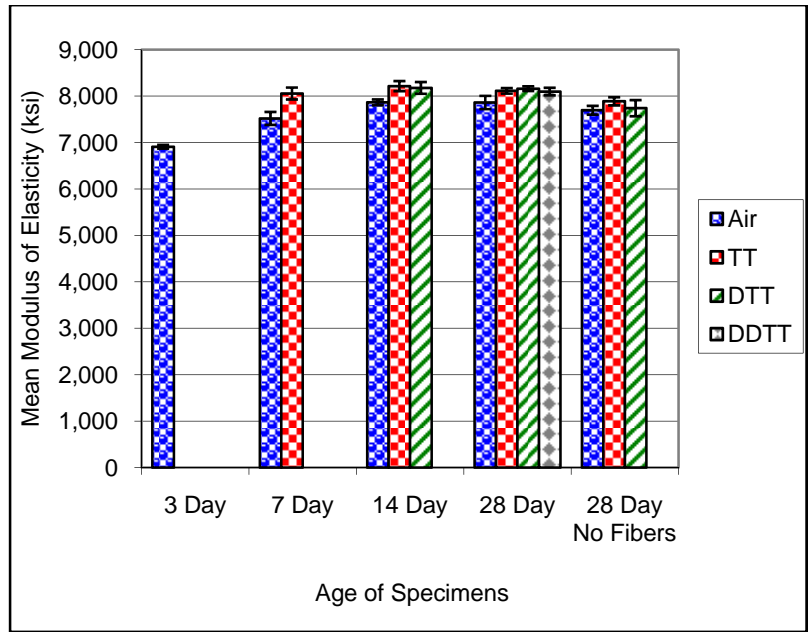
Figure 4-4: Mean Modulus of Elasticity Results for All Ages and Curing Regimes
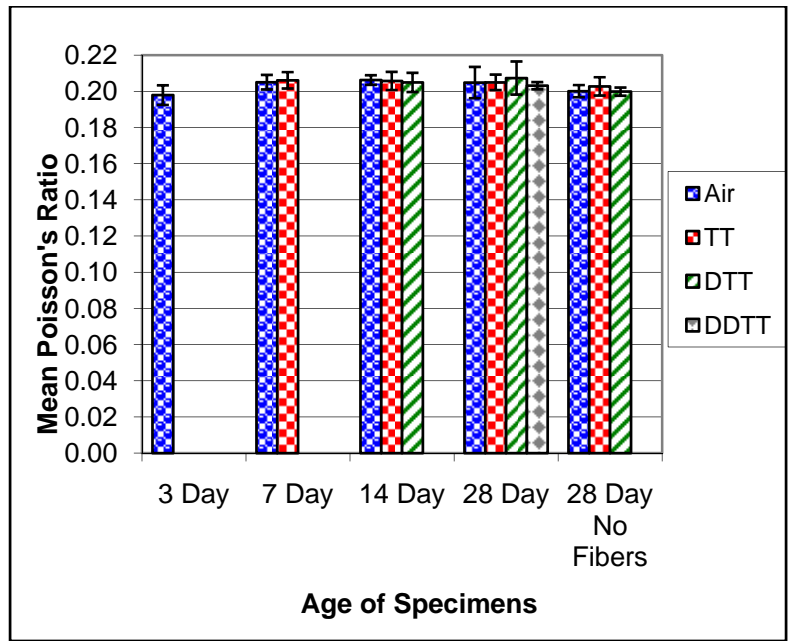
Figure 4-5: Mean Poisson's Ratio Results for All Ages and Curing Regimes

The obvious trend which can be seen in the Table 4.6 and Figure 4-4 is that the modulus value increases with time for the Air-cured specimens. The modulus value increases over 950

ksi or 13.8 percent from 3 to 28 days. This is to be expected because of the increase in

compressive stress that was noted in the previous section. TT results only vary 159 ksi or about

2 percent independent of age. DTT mean modulus of elasticity values showed a difference of

only 20 ksi from 14 to 28 days. In fact, when comparing all means of specimens undergoing

thermal curing at any age the range in modulus values was from 8056 to 8215 ksi. A less

noticeable trend in the data is that the modulus of elasticity decreased when the fibers were

removed from the mix. Poisson's Ratio for all curing regimes and ages were consistently

between 0.20 and 0.21, which is in line with typical concrete and the value given by AFGC

(2002).

4.2.2   Statistical Analysis and Discussion

Statistical analysis, similar to compressive stress testing, was conducted for modulus of

elasticity and Poisson's Ratio comparing first within each curing regime and then later to each

other for each property to analyze the effect of each curing regime. Table 4.7 shows the results

of the hypothesis testing on all specimens for modulus of elasticity.

Table 4.7: Statistical Results for Modulus of Elasticity Testing

Age of Specimen Pairings (days)	Reject or Failed to Reject the Null Hypothesis (t-test)	Mod. of Elasticity Population Mean
Air-cured Specimens		
3 vs 7	Reject Ho	Not Equal
3 vs 14	Reject Ho	Not Equal
3 vs 28	Reject Ho	Not Equal
7 vs 14	Reject Ho	Not Equal
7 vs 28	Reject Ho	Not Equal
14 vs 28	Failed to Reject Ho	Equal
TT – Thermal Treatment		
7 vs 14	Failed to Reject Ho	Equal
7 vs 28	Failed to Reject Ho	Equal
14 vs 28	Failed to Reject Ho	Equal
DTT – Delayed Thermal Treatment		
14 vs 28	Failed to Reject Ho	Equal

Air-cured specimens continued to gain stiffness over the first 14 day duration and all pairings were found to be not equal. However, once thermally treated, the Modulus was achieved and remained constant independent of when thermal treatment was applied. Air-cured specimens represent all of the thermally treated specimens up to the time of thermal curing, e.g. TT specimens were not tested at an age of 3 days because thermal treatment had not yet begun. The DDTT thermal curing occurred during days 24-27 which meant that only 28 day specimens were tested for this curing regime and no hypothesis testing was possible. Section 4.2.3 discusses the relationship between concrete strength and stiffness (modulus of elasticity).

The purpose of conducting hypothesis testing on all curing regimes was to determine if the specimens tested at different ages had the same population mean. The t-tests have shown that the 14 and 28 day Air-cured sample sets had the same population mean, and that all TT specimens shared the same population mean, and all DTT specimens shared the same population

mean. The data sharing the same population mean was further combined and hypothesis testing

was completed. Table 4.8 shows the combined values.

Table 4.8: Combined Modulus of Elasticity Results

Curing Regime	Specimen Age at Testing (days)	Sample Size	Combined Sample Mean Mod. of Elasticity (ksi)	Combined Sample COV (%)
Air	14, 28	12	7,864	1.3
TT	7, 14, 28	18	8,129	1.5
DTT	14, 28	11	8,168	1.1
DDTT	28	5	8,098	1.0

The F-test showed that all the combinations of curing regimes had an equal population

variance for the modulus of elasticity results. Conducting a t-test was the next step which

produced results showing that the population mean of the Air-cured specimens was different than

TT, DTT, and DDTT. Table 4.9 shows the results of the t-test.

Table 4.9: Statistical Results for Combined Modulus of Elasticity Testing

Curing Regime Pairings	Reject or Failed to Reject the Null Hypothesis (t-test)	Population Mean
Air vs TT	Reject Ho	Not Equal
Air vs DTT	Reject Ho	Not Equal
Air vs DDTT	Reject Ho	Not Equal
TT vs DTT	Failed to Reject Ho	Equal
TT vs DDTT	Failed to Reject Ho	Equal
DTT vs DDTT	Failed to Reject Ho	Equal

When the specimens that received thermal curing were compared, all three combinations

showed that the population mean was equal for all curing regimes. This is the same result

obtained from the compressive hypothesis testing. For specimens receiving thermal treatment at

any age the mean modulus of elasticity is 8150 ksi, which is an increase of 3.8 percent over the

combined Air-cured value of 7850 ksi. It is interesting to note that the compressive strength of

Air-cured specimens continued to increase from day 14 to 28 but the modulus value appears to have reached a plateau by 14 days. A similar result was noted by Graybeal (2005) as the data showed the compressive strength increasing to 8 weeks after casting but the stiffness and peak strain at failure curtailed at 4 weeks after casting.

All curing regimes were compared to determine the effects that the different curing regimes had on the Poisson's ratio. Table 4.10 shows the results of the hypothesis testing on all specimens for Poisson's ratio tests.

Table 4.10: Statistical Results for Poisson's Ratio Testing

Age of Specimen Pairings (days)	Reject or Failed to Reject the Null Hypothesis (t-test)	Poisson's Ratio Population Mean
Air-cured Specimens		
3 vs 7	Failed to Reject Ho	Equal
3 vs 14	Failed to Reject Ho	Equal
3 vs 28	Failed to Reject Ho	Equal
7 vs 14	Failed to Reject Ho	Equal
7 vs 28	Failed to Reject Ho	Equal
14 vs 28	Failed to Reject Ho	Equal
TT – Thermal Treatment		
7 vs 14	Failed to Reject Ho	Equal
7 vs 28	Failed to Reject Ho	Equal
14 vs 28	Failed to Reject Ho	Equal
DTT – Delayed Thermal Treatment		
14 vs 28	Failed to Reject Ho	Equal

Similar to compression stress and modulus of elasticity results and based on the above analysis, Poisson's ratio hypothesis testing results were combined for curing regimes and compared for statistical differences. Results are summarized in Tables 4.11 and 4.12.

Table 4.11: Combined Poisson's Ratio Results

Curing Regime	Specimen Age at Testing (days)	Sample Size	Combined Sample Mean Poisson's Ratio	Combined Sample COV (%)
Air	3, 7, 14, 28	22	0.204	3.0
TT	7, 14, 28	18	0.206	2.1
DTT	14, 28	11	0.206	3.6
DDTT	28	5	0.203	1.0

Table 4.12: Statistical Results Poisson's Ratio Testing

Curing Regime Pairings	Reject or Failed to Reject the Null Hypothesis (t-test)	Population Mean
Air vs TT	Failed to Reject Ho	Equal
Air vs DTT	Failed to Reject Ho	Equal
Air vs DDTT	Failed to Reject Ho	Equal
TT vs DTT	Failed to Reject Ho	Equal
TT vs DDTT	Failed to Reject Ho	Equal
DTT vs DDTT	Failed to Reject Ho	Equal

Results show none of the null hypotheses were rejected and all six pairings show that all curing regimes come from the same population mean. Even if there was a slight difference in the population mean (a few thousandths), caution would have to be exercised in stating that a difference was evident because Poisson's ratio is reported and used in equations to two decimal places. So if a difference shows up in the third or fourth decimal place, it has no practical application. Based on this analysis, data for the UHPC specimens (Air-cured and all thermally cured specimens independent of age at curing) have a mean Poisson's ratio of 0.21.

Kollmorgen (2004) reported specimens tested before thermal treatment having modulus values 5.1 percent less than those presented in this research. These specimens had a high COV at 20 percent. Following thermal treatment and independent of age at testing a mean value of 9210 ksi was presented which is over 13 percent greater than the results for TT at 28 days and

the COV was 7.1 percent. These results were based on the utilization of three cylinder sizes and LDTs as presented in Chapter 3. Poisson's ratio results, for specimens tested before and after thermal treatment, ranged from 0.16 to 0.22 with a mean of 0.19 and COV of 13.3 percent.

Graybeal (2005) presents modulus of elasticity results for air, steam, and delayed steam cured specimens as 6200 ksi, 7650 ksi, and 7300 ksi respectively. When comparing these results to those presented herein based on 28 day means, Graybeal's (2005) results are 21.1 percent, 5.7 percent, and 10.6 percent lower than Air-cured, TT, and DTT results. COV for the three curing treatments were very low ranging from 2 to 3 percent. The modulus of elasticity values were calculated over the ranges of 10 to 40 percent of the ultimate capacity of each specimen. It was noted that cylinders which underwent thermal curing reached 80 to 90 percent of their ultimate capacity before deviating from a linear elastic behavior by 5 percent. This shows UHPC as exhibiting nearly linear behavior to high stress levels.

While an in depth investigation on Poisson's ratio was not conducted by Graybeal (2005), a background study completed for determining an acceptable load rate indicated consistent Poisson's ratio results of 0.19 for thermally cured specimens and compares well with research results presented herein.

4.2.3 Compressive Stress and Modulus of Elasticity Relationship

The modulus of elasticity of concrete is an important parameter and, therefore, a simple yet acceptably accurate way to predict this property is necessary. As discussed in Chapter 2, there are several different models which relate the compressive strength of UHPC to its modulus of elasticity. It is not the intent of this research to propose a relationship, but rather to determine if published equations predict the modulus of elasticity given the compressive strength for the data collected herein. All specimens which were determined to have the same population mean

were used in the relationship of modulus of elasticity and compressive strength. For example, TT specimens at 7, 14, and 28 days had the same population mean so all specimens were averaged and included in the following figure. However, Air-cured specimens at 3, 7, 14, and 28 days had different population means and means are shown separately. Figure 4-6 shows the experimental data plotted with the different prediction equations for modulus of elasticity based on compressive strength.
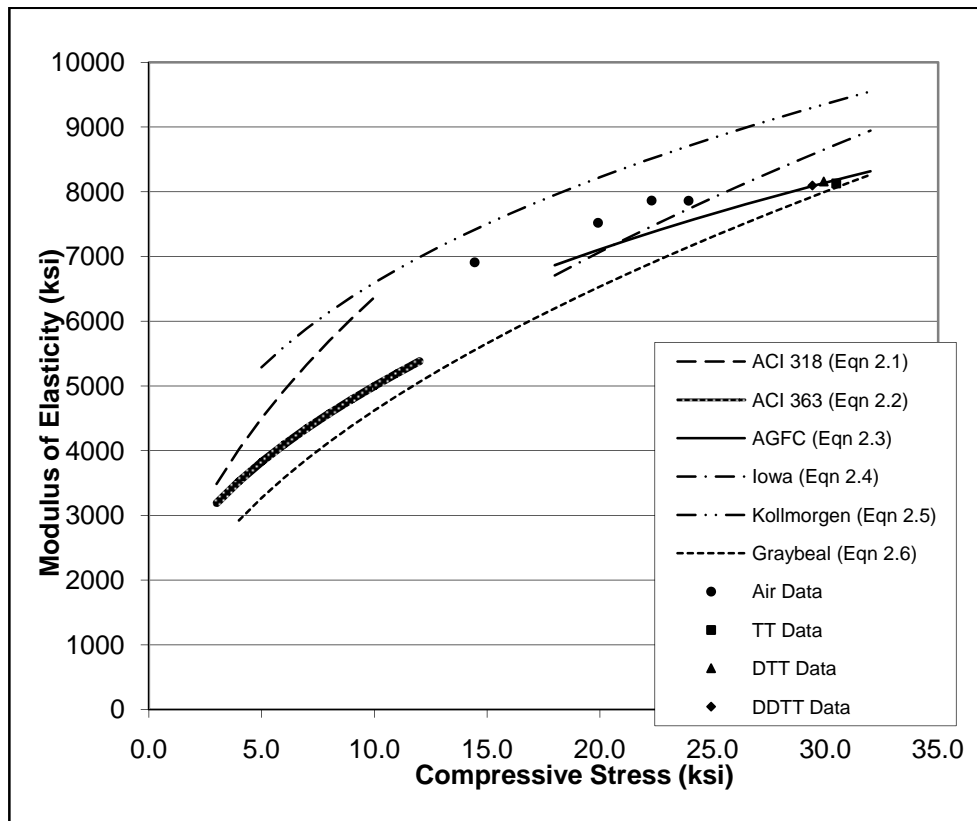
Figure 4-6: Regression Model for Modulus of Elasticity vs. Compressive Strength

The predictive relationships vary significantly and none are a great match for all the data gathered during this research. The sum of squares of the residuals was calculated for each equation to determine the best fit for the data. The results showed that the sum of squares of the residuals was minimized when the AFGC (2002) model was used. The value of the sum of

squares of the residuals was less than half of the next smallest value which was the Iowa model. Just minimizing the sum of squares of the residuals does not guarantee a good fit. The coefficient of determination which shows the goodness of fit and was calculated to be 0.34, which is not a good fit. However, when the Air-cured specimens were removed from the analysis, the coefficient of determination increased to 0.98 which is an excellent fit. Recall that the AFGC (2002) equation requires the specimens to undergo a thermal treatment, so limiting the analysis to the thermally treated specimen is warranted. However, this does not address the problem of determining the modulus of elasticity for UHPC air-cured under ambient conditions.

Figure 4-7 presents the mean results (based on age at testing) of specimens cured under ambient conditions and tested for compressive stress and modulus of elasticity. The results are summarized with data from Kollmorgen (2004) and Graybeal (2005).
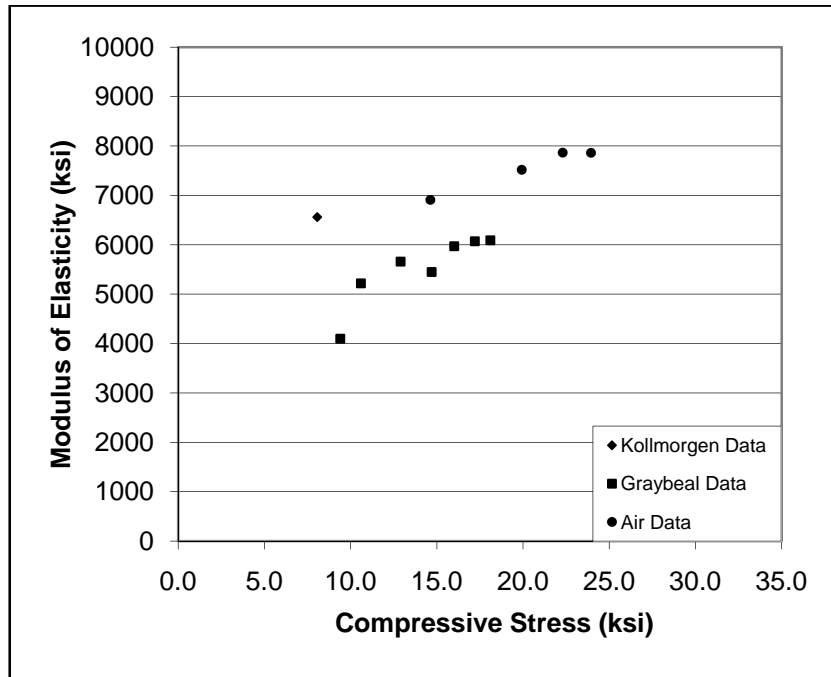
Figure 4-7: Mean Values of Compressive Stress and Modulus of Elasticity for Air-Cured Specimens

The mean Air-cured results for this research program fall in between the average results presented by Kollmorgen (2004) and Graybeal (2005). This is the same trend observed in Figure 4-6 where Kollmorgen's equation over predicts the modulus of elasticity, and Graybeal's equation under predicts the results over their appropriate ranges of compressive stress. At the time of this report Graybeal's (2005) raw data was not available to compile all the results from the individual specimens and complete a regression model to determine an appropriate equation for Air-Cured specimens. Further testing and/or analysis should be completed to determine the relationship of compressive stress to modulus of elasticity for specimens cured under ambient conditions. Therefore, <u>data collected from this study shows the AGFC (2002) model to most accurately predict the modulus of elasticity based on compressive strength of thermally treated specimens, independent of age at thermal treatment application</u>.

4.3   Flexural Strength Testing for First Cracking

Flexural testing was conducted at 28 days on 2 x 2 x 11.25 in. prisms that underwent three curing regimes; Air-cured, thermal treatment, and delayed thermal treatment. ASTM C 1018 *Standard Test Method for Flexural Toughness and First-Crack Strength of Fiber-Reinforced Concrete (Using a Beam with Third Point Loading)* was used to determine the first-crack strength and flexural toughness of specimens. A total of 36 prisms were cast with fibers and 9 were cast without fibers (Table 4.1) to see the effect that fibers had on the first crack flexural stress. One specimen, Air-cured, was rejected because of a break outside of the acceptable region. Additionally, three specimens had breaks within 5% of the constant moment region and their values were reduced as outlined in ASTM 1018.

The first-crack flexural stress is used as an indicator of the maximum tensile stress for UHPC. ASTM C 78 *Standard Test Method for Flexural Strength of Concrete (Using Simple*

84

Beam with Third-Point Loading) presents the equation for modulus of rupture (R), or cracking stress, for beams with third-point loading.

$$R = \frac{P*L}{b*d^2} \quad \text{(psi)}$$

Equation 4.1

Where: P = Load at first crack;

L = Span length;

b = Average specimen width;

d = Average specimen depth.

However, Graybeal (2005) points out that it has been widely observed that cracking stress is an over estimate of the actual tensile capacity of UHPC. This discrepancy has been attributed to depth and gradient effect set up by bending. To obtain the actual tensile cracking stress (f_{ct}), AFGC (2002) recommends the flexural cracking stress be corrected with the use of Equation 4.2 which correlates the values back to a 100 x 100 mm (approximately 4 x 4 in.) prism.

$$f_{ct} = R*\frac{2.0*\left(\frac{d}{d_o}\right)^{0.7}}{1+2.0*\left(\frac{d}{d_o}\right)^{0.7}}$$

Equation 4.2

Where: f_{ct} = corrected first-crack flexural stress;

d_o = reference depth of 100 mm.

4.3.1 Results

Table 4.13 lists the results of the flexural testing for the curing regimes of Air, TT, and DTT for specimens with and without fibers. Test data recorded for each specimen is tabulated in Appendix A (Tables A.4, A.5, A.6). Equation 4.2 was applied to the first-crack flexural stress to calculate the corrected first-crack flexural stress or cracking tensile stress. The tensile strength

listed in the table for TT and DTT are slightly below the range of values for tensile strengths

reported by manufacturers.

Table 4.13: Flexural Stress, Deflection and Maximum Load Results

Curing Regime	Specimen Age and fibers (days)	Sample Size	Sample Mean First-Crack Flexural Stress	Sample COV First-Crack	Sample Mean Corrected First-Crack	Sample COV (%) Corrected First-Crack
Air	28	12	1.34	10.9	0.74	10.9
	28 –NF	3	1.50	9.5	0.83	9.5
TT	28	12	1.91	8.0	1.06	8.0
	28 – NF	3	2.03	6.7	1.13	6.7
DTT	28	12	2.12	9.1	1.18	9.1
	28 – NF	3	2.18	6.4	1.21	6.4

Curing Regime	Specimen Age and fibers (days)	Sample Size	Sample Mean First-Crack Deflection (in.)	Sample COV (%)First-Crack Deflection	Sample Mean First-Crack Load (kips)	Sample COV (%) First-Crack Load
Air	28	12	0.00179	8.9	1.23	8.1
	28 –NF	3	0.00205	4.2	1.36	7.4
TT	28	12	0.00240	7.4	1.70	7.3
	28 – NF	3	0.00275	6.8	1.82	5.5
DTT	28	12	0.00273	6.2	1.93	7.0
	28 – NF	3	0.00307	7.0	1.98	6.4

Curing Regime	Specimen Age and fibers (days)	Sample Size	Sample Mean Max. Load Deflection (in.)	Sample COV (%) Max. load Deflection	Sample Mean Max. Load (kips)	Sample COV (%) Max. Load
Air	28	12	0.0452	14.8	4.21	9.1
	28 -NF	3	-	-	-	-
TT	28	12	0.0498	14.8	4.83	5.9
	28 - NF	3	-	-	-	-
DTT	28	12	0.0430	27.3	4.55	8.6
	28 - NF	3	-	-	-	-

The flexural strength for fiber reinforced concretes is often difficult to calculate because

of the extensively cracked section and load carrying fibers. However, for convenience ASTM C

1018 allows the flexural strength to be calculated using Equation 4.1 by replacing the cracking

load with the ultimate load. As Graybeal (2005) points out this result does not have any physical

meaning, but is used for comparison purposes. The mean flexural strength for Air-cured, TT, and DTT are 4.58 ksi, 5.44 ksi, and 4.99 ksi respectively. The results for flexural strength, like those for tensile strength, are at the lower end of their respective range of values as reported by the supplier. The results of the flexural testing show the largest COV for the mechanical properties tested for this research. However, the COV presented is only slightly higher than the one-sigma limit of 7 percent presented in ASTM C 1018 for first crack flexural stress.

Figure 4-8 shows the mean values and ± one standard deviation from the mean for the corrected first-crack flexural stress for specimens with and without fibers.
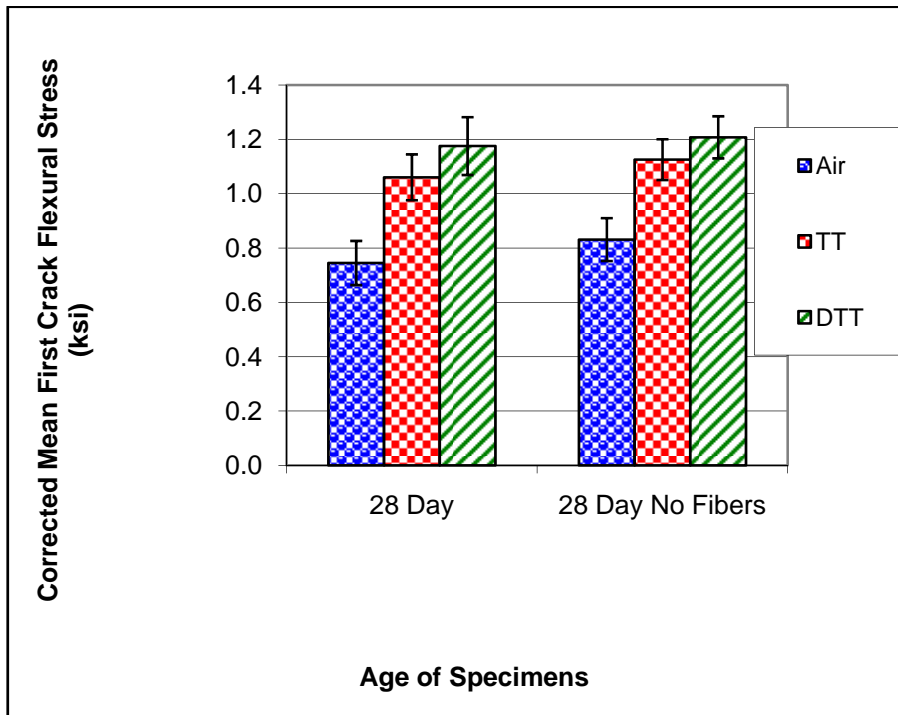
Figure 4-8: Mean First-Crack Flexural Stress for All Curing Regimes

4.3.2 Statistical Analysis and Discussion

One of the more interesting observations, made from Table 4.13 and Figure 4-8, is that the samples without fibers seem to have a larger first-crack stress than the specimen cast with

fibers. This can be explained looking at the nature of the material from a homogeneous standpoint. The fibers are geometrically the largest material in the mix and create irregularities in the mix along the interface of the fibers and the paste. When looking at the small scale, fibers create a non-homogeneous mixture and cause disruptions in the matrix and allow microcracking to propagate more readily through the specimen than through the homogenous matrix without fibers. Hence the lower first-cracking stress in UHPC with fibers. However, the difference in first-cracking stress is very small and, as Mindess et al. (2003) points out, the purpose of the fibers is to bridge the crack and provide post-crack ductility.

Flexural testing only had the three curing regimes of Air-cured, Thermal Treatment, and Delayed Thermal Treatment. Additionally, flexural specimens were only tested at 28 days, and are not compared within each curing regime. Unlike traditional unreinforced concrete, UHPC's first crack was not its last crack because of the fiber reinforcement. Therefore, the corrected first crack strength and the maximum load could be analyzed to see the effects of the three curing regimes. Recall that the corrected first crack strength is based on the SETRA procedure for adjusting data to a normalized size of 100 mm x 100 mm (nominally 4 x 4in.) (AFGC 2002). Similar to previous analyses, Table 4.14 displays the pairings and results of the hypothesis testing for first-crack flexural strength.

Table 4.14: Corrected First-Crack Flexural Strength Hypothesis Testing

Curing Regime Pairings	Reject or Failed to Reject the Null Hypothesis (t-test)	Population Mean
Air vs TT	Reject Ho	Not Equal
Air vs DTT	Reject Ho	Not Equal
TT vs DTT	Reject Ho	Not Equal

Hypothesis testing results for flexural strength are different than the compression and modulus of elasticity testing where only the Air-cured specimens had a different population mean, and Poisson's ratio results where all population means were equal. UHPC's ability to continue to carry load after the element has cracked is one of the properties which make it desirable for structural elements. However, flexural first cracking strength appears to be influenced by the curing regime.

As previously noted Kollmorgen (2004) conducted flexural testing utilizing ASTM C 78 and did not correct the first-crack flexural stress. The mean first crack stress for thermally treated 2 x 2 x 11.25 in. prisms at 28 days was 3.1 percent greater than results of this research with a COV of 17 percent. The mean maximum load for the same specimens was 5.4 percent lower and with COV of 8.0 percent.

When comparing the corrected first-crack data to results presented by Graybeal (2005), using the same specimen size and testing configuration data, results were 73 percent, 35 percent, and 10 percent greater than the Air-cured, TT, and DTT mean values, respectively, for this research. No COV or standard deviation was reported for the mean values. Average peak load values were 170 to 200 percent greater than the first crack load. Mean peak load values for this research program were 340 percent, 280 percent, and 240 percent greater than the first-crack load for Air-cured, TT and DTT, respectively. Large differences in testing results indicate that ASTM procedures are not necessarily applicable to UHPC for flexural strength and further study is warranted.

4.3.3 Flexural Toughness

Post-crack ductility is measured by the toughness that a fiber reinforced concrete exhibits. Figure 4-9 is a graphical representation of a flexural elastic-plastic material, and

displays the areas under the load deflection curve used to calculate the reference toughness

indices. The toughness indices for plain concrete, elastic-plastic material, and observed ranges

for fibrous concrete are presented in Table 4.15. Figure 4-10 is a typical load deflection curve

for all specimens.
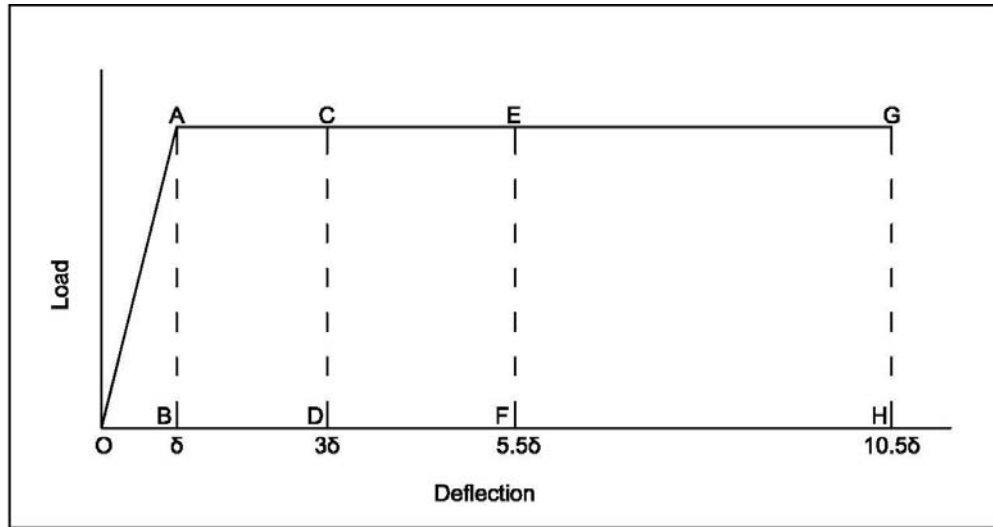
Figure 4-9: Load Deflection Curve for Elastic-Plastic Material (ASTM C 1018 Figure X1.1)

Table 4.15: Typical Toughness Values (ASTM C 1018 Figure X1.1)

Area Basis[A]	Index Designation	Deflection Criteria[†]	Values of Toughness Indices		
			Plain Concrete	Elastic-Plastic Material	Observed Range for Fibrous Concrete
OACD	I_5	3δ	1.0	5.0	1 to 6
OAEF	I_{10}	5.5δ	1.0	10.0	1 to 12
OAGH	I_{20}	10.5δ	1.0	20.0	1 to 25

[A] Indices calculated by dividing this area by the area to the first crack OAB.
[†] δ is the deflection at first-crack.

90
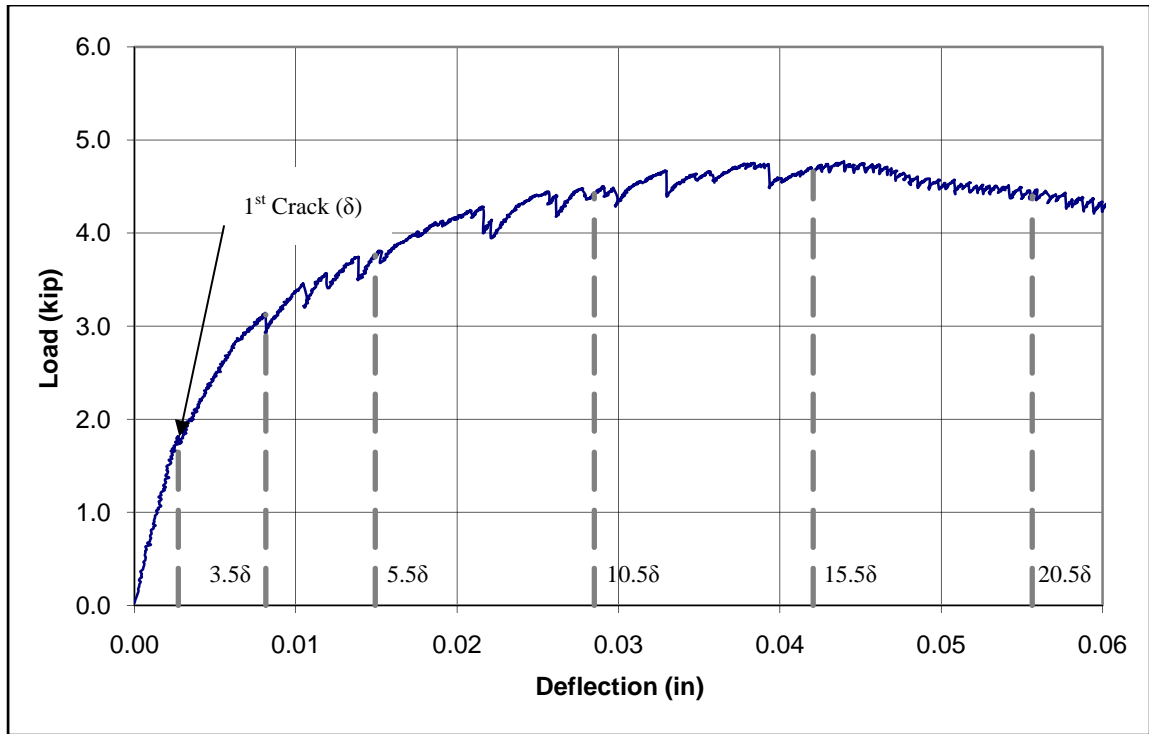
Figure 4-10: Typical Load Deflection Curve for Flexural Specimens

Toughness is an indication of the energy absorption capabilities of a material. Toughness indices are calculated at set intervals of the first-crack deflection and provide a means to compare the toughness of different materials. However, it is important to compare identical specimen sizes and loading configurations as the toughness indices are not independent of specimen dimension (Mindess et al. 2003). The toughness indices are a measure of how the material responds versus the standard, a linear elastic material up to first crack followed by perfectly plastic material behavior. For example, the index designation I_5 is the area under the load deflection curve, up to 3 times the deflection at first-crack, normalized by dividing the aforementioned area by the area under the curve up to the first-crack. More specifically, it is the area of the polygon OACD divided by the area of the triangle OAB, as seen in Figure 4-9. Additional toughness indices beyond those listed in Table 4.15 can be calculated in the same

manner. Toughness Indices I_{30} and I_{40} were calculated at a deflection of 15.5δ and 20.5δ, respectively, for this research to compare to data published by Graybeal (2005). Also, in research conducted by Chen et al. (1995) the toughness indices I_5, I_{10}, and to a lesser extent I_{20} were not particularly sensitive to fiber addition rate or fiber type.

A second relative parameter evaluated from ASTM C 1018 is the residual strength factor, which is has a standard value of 100 over two consecutive toughness indices values, for an elastic-plastic material. For example, $R_{5,10}$ is calculated as $20(I_{10} - I_5)$ and $R_{20,30}$ is $10(I_{30} - I_{20})$. The residual strength factors represent the average level of strength retained after first crack as a percentage of the first-crack strength. Plain concrete has a residual strength factor of zero.

The experimental results for flexural toughness indices and residual strength factors for specimens with and without fibers are shown in Table 4.16.

Table 4.16: Experimental Toughness Indices and Residual Strength Factors

Curing Regime	Test Age	Sample Size	Corrected Mean First-Crack Flexural Stress (ksi)	Toughness Indices				
				I_5	I_{10}	I_{20}	I_{30}	I_{40}
Air	28	12	0.74	6.8	17.6	44.7	74.9	107.0
	28 –NF	3	0.83	1.0	1.0	1.0	1.0	1.0
TT	28	12	1.06	6.5	16.1	39.5	65.1	92.8
	28 – NF	3	1.13	1.0	1.0	1.0	1.0	1.0
DTT	28	12	1.18	6.3	15.4	36.6	58.7	85.0
	28 – NF	3	1.21	1.0	1.0	1.0	1.0	1.0

Curing Regime	Test Age	Sample Size	Corrected Mean First-Crack Flexural Stress (ksi)	Residual Strength Factors			
				$R_{5,10}$	$R_{10,20}$	$R_{20,30}$	$R_{30,40}$
Air	28	12	0.74	217	271	302	320
	28 – NF	3	0.83	0	0	0	0
TT	28	12	1.06	193	234	256	273
	28 – NF	3	1.13	0	0	0	0
DTT	28	12	1.18	182	212	224	241
	28 – NF	3	1.21	0	0	0	0

The toughness indices I_5 and I_{10} for Air-cured, TT, and DTT show results at the upper end or slightly above the observed values listed in Table 4.15 for fiber reinforced concrete.

However, the remaining toughness indices, $I_{20,}$ I_{30} and I_{40} show substantially higher values than those presented by ASTM C 1018. The residual strength factors show average levels of strength retained from 240 to 320 percent of the first crack strength. They continue to increase to $R_{30,40}$ which captures the load deflection curve behavior over the deflection range of 15.5 to 20.5 times the cracking deflection. This is consistent with the specimen's load carrying capabilities increasing from first crack to the point of maximum load. The high toughness indices and residual strength factors indicate that this UHPC is highly ductile, a desirable property in almost all concrete applications.

The toughness indices presented by Graybeal (2005) are approximately 12 to 40 percent lower than those presented in Table 4.16. Likewise Graybeal's (2005) residual strength factors are 16 to 46 percent lower than the observed results. The differences in the results may be partially explained by the following. Recall that the toughness indices are normalized by dividing the area under the load deflection curve at a given deflection by the area under the curve up to the first crack. Results provided by Graybeal (2005), with a 2 x 2 in. cross section with a 9 inch span, for the first-crack flexural stress were 10 to 73 percent higher than the observed values presented in this research. Because the area under the load deflection curve is triangular to first-crack, a greater flexural stress will result in a larger area and ultimately smaller toughness indices.

Kollmorgen (2004) calculated toughness using a procedure outlined by AFGC (2002) which calculates toughness at the first crack, ultimate load, and a deflection limit of 0.030 in. based on a 2.0 x 2.0 x 11.25 in. specimen. The toughness values have units of in-kips, and are not directly comparable to results from this study. Kollmorgen (2004) suggests that the values

be normalized by dividing by the toughness at first-crack or the toughness of specimens without fibers.

Specimens cast without fibers were included in this study to provide guidance as to the impact the fibers had on the first-crack stress, and as previously noted the fibers have a tendency to reduce the first-crack stress. Testing specimens without fibers would allow toughness values, which were the summation of the area under the load deflection curve, to be normalized for comparison between different fiber addition rates and fiber types. Jamet et al. (1995) calculates the effective toughness of fibers at different addition rates by subtracting the toughness of the unreinforced high strength concrete from the toughness of the fiber reinforced high strength concrete. By removing the toughness of the unreinforced matrix the effects of fiber addition rates, fiber types, and interactions with different mix designs could be examined. Because only one fiber addition rate, one fiber type, one mix design, and one specimen geometry were utilized in the presented research, analyzing the effect of the different fiber addition rates or fiber types was not possible.

4.4   Rapid Chloride Penetration Test

UHPC specimens of three unique age/curing regime applications were tested for chloride penetration according to ASTM C 1202: 7-day thermally treated, 28-day air-treated, and 28-day thermally treated. These curing regimes were applied as described in Section 3.4 and the specimen age refers to the age of the specimen when tested. Following curing and specimen preparation, the chloride ion penetrability was measured by the total charged passed in coulombs over a 6-hour period.

4.4.1 Results

Initially, three specimens for each age/curing regime were tested. However, additional specimens were available for 28-day Air and 28-day TT cured specimens and were included in the analysis. Test data recorded for each specimen is tabulated in Appendix A (Tables A.7, A.8). Additionally, one of the 7-day TT specimens was tested on day 8 and yielded a total charge passing of 10 coulombs. As this was within the standard deviation for 7-day TT specimens, it was also included in the analysis. Results from these tests are summarized in Table 4.17. While the standard deviation and COV values in Table 4.17 seemed high upon initial observation, the ASTM C 1202 standard specifies a 42% COV value for a single operator on concrete samples from one batch.

Table 4.17: Michigan Tech Rapid Chloride Penetration Summary Data

| Curing regime | Age at testing (days) | No. Specimens | Charge Passed (coulombs) | | | Chloride Ion Penetrability |
			Average	Standard Deviation	COV (%)	
Air	28	4	75	15	20	Negligible
TT	7	3*	10	1.5	15	Negligible
TT	28	4	15	3.5	24	Negligible

*one specimen tested at 8 days

4.4.2 Discussion

All of the UHPC specimens tested exhibited chloride ion penetration values in the negligible range (< 100 coulombs passed). Nonetheless, the values for the TT-cured specimens were lower than the Air-cured specimens. Correspondingly, a t-test statistical analysis demonstrated that the amount of charge passed for the thermally treated specimens was statistically lower than the air cured specimen results (Misson 2008). In addition, this data was congruent with other research data (Bonneau et al. 1997) that reported very high resistance

(negligible penetration) to ionic transport in steam treated UHPC specimens, and somewhat

higher post-thermal treatment resistances (Graybeal 2006a). Comparatively, the 28-day TT-

cured UHPC specimens tested herein had an average total charge passing equal to Graybeal's

(2006a) 28-day steam treated specimens with a 95% confidence interval (Table 4.18). Another

statistical analysis on thermally treated specimens tested herein revealed that ionic movement in

thermally treated UHPC was independent of whether the specimen is 7-day or 28-day within a

95% confidence interval.

Table 4.18: Graybeal (2006a) Rapid Chloride Penetration Summary Data

| Curing regime | Age at testing (days) | No. Specimens Tested | Charge Passed (coulombs) | | | Chloride Ion Penetrability |
			Average	St. Dev.	COV (%)	
Steam	28	3	18	1	6	Negligible
Untreated	28	2	360	2	1	Very Low
Untreated	56	3	76	18	24	Negligible
Tempered Steam	28	3	39	1	3	Negligible
Tempered Steam	56	3	26	4	15	Negligible
Delayed Steam	28	3	18	5	28	Negligible

However, the charge passed by the 28-day Air-cured specimens were lower than the

results reported by Graybeal (2006a), who reported an average of 360 coulombs passing for 28-

day untreated UHPC specimens. One possible reason for the difference may be the different

preparation methods used (kerosene saw vs. water cooled saw) where the kerosene may inhibit

ion migration. Graybeal also used an accelerator in mixing. Nevertheless, a statistical

comparison confirmed that Graybeal's (2006a) 56-day untreated specimens and the 28-day Air

(untreated) specimens tested herein were equivalent, having an average of 76 coulombs passing

and a standard deviation of 18 compared to 75 coulombs passing and a standard deviation of 15

for the 28-day old specimens from this study, respectively. Further testing may be needed to

evaluate the differences and similarities between the Air-cured UHPC specimens at different ages.

Visual observation of the UHPC specimens after testing revealed that the specimens experienced some corrosion of the steel fibers (Figure 4-11). These stains appeared to be limited to the surface of the UHPC directly in contact with the sodium chloride solution and no other distress was visible. All of the specimens tested exhibited similar staining patterns. This observation was similar to that observed in previous research (Graybeal 2006a).

Figure 4-11: Surface Staining of UHPC Specimen after ASTM C 1202 Test

It should be noted that the ASTM C 1202 test does not specifically measure any one type of ion movement and instead measures the bulk flow of ions through the specimen (Stanish et al. 2000). Also, the method does not measure permeability as is sometimes understood, but again measures the ionic movement through the specimen. Finally, in materials containing high amounts of silica fume (like UHPC), the test method tends to indicate a lower chloride movement rate than would normally be expected (Perenchio 1994; Mindess et al. 2003), but no

correlation between movement rate and silica fume quantity has been investigated to date for applicability to UHPC.

4.5   Freeze-Thaw Cyclic Testing

Freezing and thawing testing was performed in accordance with ASTM C 666 – *Resistance of Concrete to Rapid Freezing and Thawing* standards. This test procedure involves the rapid freezing and thawing of concrete by means of freezing in air, and thawing in water. Eight cycles were completed per day, and approximately every 32 cycles the fundamental transverse frequency, length change, and mass were observed. Specimens were tested until failure or 300 freeze-thaw cycles, whichever came first. Only one minor variation was adapted for the testing of UHPC specimens and as outlined in Section 3.5.5.

4.5.1   Results

Freeze-thaw testing following ASTM C 666 Procedure B (freezing in air, thawing in water) was performed on four 28-day Air cured and four 28-day TT-cured UHPC specimens to monitor UHPC's resistance to freeze-thaw damage. Deterioration due to freeze-thaw (cracking, spalling, or disintegration) was observed mechanically through the monitoring of a specimen's relative dynamic modulus (RDM), length change, and mass change (Table 4.19). Decreases in a specimen's RDM indicated disruptions to the transfer of vibrations through the material due to microcrack formation, while increases in length was a sign of cracks and microcracks creating void space in the specimen, and decreases in mass signified spalling or disintegration of material. These three tests were performed every 32 freeze-thaw cycles (96 hours) and the RDM test was performed on all eight specimens, while the length and mass change was recorded for six of the specimens. Occasionally, due to equipment malfunction, these parameters were recorded at

98

periods greater than 32 cycles but never at an interval of more than 36 cycles. Also, on some occasions the specimens were stored in the frozen condition until the equipment was functional again. The effects of water absorption on the RDM and mass of the six additional side-study UHPC specimens (three air cured and three thermally treated) were also analyzed (specimens denoted by "SS").   Length change was not documented on these side study specimens.

Table 4.19: Effects of Freeze-Thaw Cycles on UHPC

Curing and (Testing) Regime[+]	No. Spec.	Average RDM at end of cycling (%)	COV (%)	Avg. Length Change (%)	COV (%)	Avg. Mass Change (%)	COV (%)
Air (F-T)	4	101.57	0.32	0.0004*	20.4	0.54*	5.5
TT (F-T)	4	100.27	0.12	0.00014*	14.4	0.08*	44.0
Air (SS)	3	101.91	0.50	N.A.	N.A.	0.22	28.66
TT (SS)	3	100.10	0.50	N.A.	N.A.	0.06	0.54

*Note: Only three of the F-T specimens were tested for length change and mass change

[+]F-T for freeze-thaw cycles, SS for side-study wet-dry cycles

4.5.2 Discussion

Failure of a specimen undergoing freeze-thaw cycles as stated by ASTM C 666 has been reached when the specimen's relative dynamic modulus of elasticity reaches 60% of its initial modulus, or if a 0.10% expansion in length of the specimen is attained. However, all of the UHPC freeze-thaw specimens maintained their integrity and exhibited an increase in RDM (< 2%) as testing continued. Table 4.19 shows the summary data for the specimens tested (data is listed in Appendix A, Figures A.9, A.10, A.11). UHPC freeze-thaw specimens showed only a small increase (< 1%) in mass and negligible (< 0.01%) change in length. The side-study specimens (which underwent wet-dry cycles without temperature changes) demonstrated similar increases in RDM and mass. Lastly, the increases for the Air cured F-T specimens (RDM - 1.57

%; Mass – 0.54%) were significantly higher than the increases for the thermally treated F-T specimens (RDM - 0.27%; Mass – 0.08%).

Figure 4-12 displays the correlation between the increase in RDM for the freeze-thaw and side-study specimens. After 300 cycles, all eight freeze-thaw UHPC specimens had higher RDM's than at the beginning of testing, suggesting that the specimens did not deteriorate at all, but rather continued to hydrate. The similar increases also indicated that the increase in RDM from both testing regimes was due to the effects from cycling the specimens in and out of water. The Air-cured side-study specimens' RDM increased with a similar trend as the Air-cured freeze-thaw specimens. However, the increase of the TT-cured specimens was small in comparison to the Air-cured specimens. This can be primarily attributed to the greater amounts of unhydrated cement particles in the Air-cured specimens that can become hydrated in the presence of water.
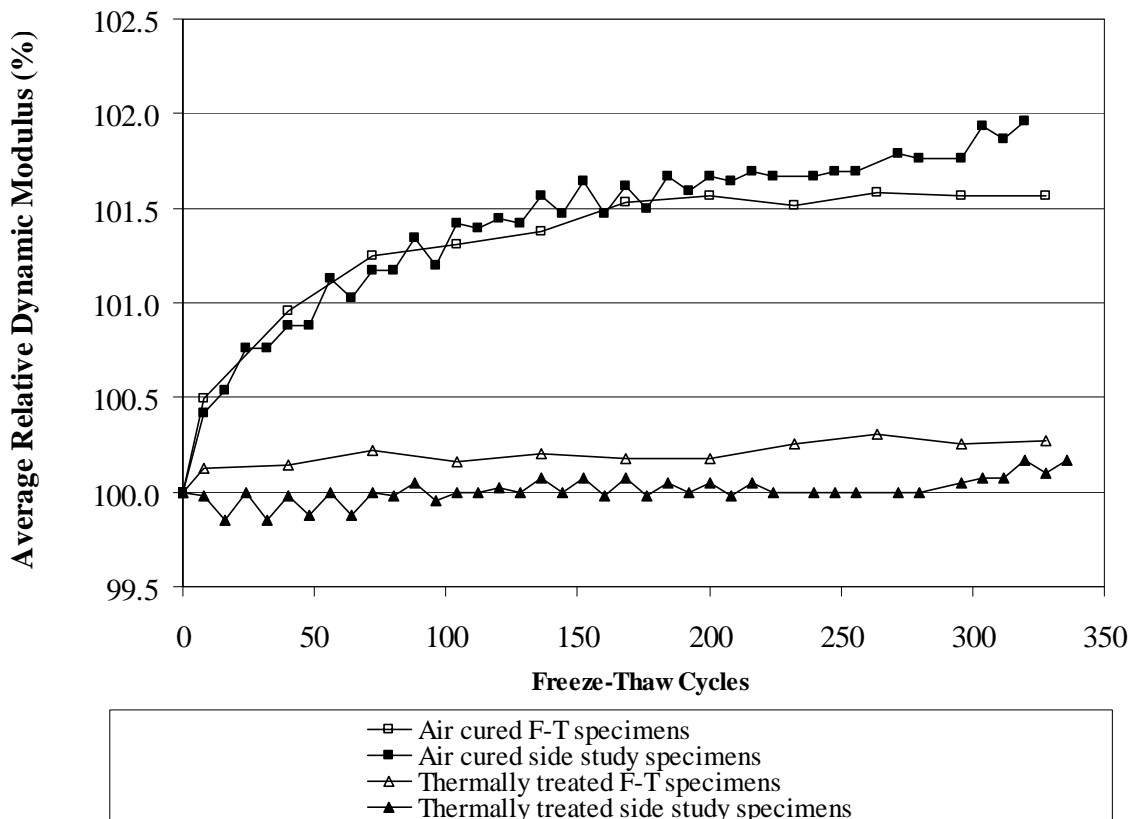
Figure 4-12: Effects of Freeze-Thaw Cycling on the Average Relative Dynamic Modulus of UHPC Samples

Testing by others (Graybeal 2006a; Lee et al. 2005) also reported a similar phenomenon

for freeze-thaw specimens. In both studies, specimens undergoing freeze-thaw cycles increased

in RDM, and Graybeal also reported that the specimens also showed a mass increase. Lee

demonstrated that reactive powder concrete (a precursor to UHPC) cubes increased in

compressive strength after 300 cycles of freeze-thaw testing, and further testing by Graybeal

(2006a) revealed that untreated UHPC specimens immersed in a water bath (without wet/dry

cycles) also increased in compressive strength. These studies suggest that the submersing of

UHPC in water can increase both compressive strength and RDM, even when being exposed to a

harsh freeze-thaw environment. The data in Figure 4-12 supports this as the side-study

specimens exhibited similar changes in RDM and mass as the specimens undergoing freeze-thaw cycling. The overall increase in RDM (1.57 % for Air-cured specimens) in this study was different than in other research (approximately 10% for untreated specimens) (Graybeal 2006a). However, Procedure B (freezing in air, thawing in water) was used in this study rather than Procedure A (freezing in water, thawing in water) which was used in Graybeal's study. Lengthier exposure of the UHPC specimens to water during Procedure A may allow for a greater probability of water reacting with unhydrated cement particles.

Although little visual damage was noted, small microcracks were observed on the surfaces of the freeze-thaw specimens upon removal from the freeze-thaw chamber, especially the air cured specimens (Figure 4-13). These cracks were only evident while the surfaces of the specimens were wet, and quickly disappeared from view once the specimens dried. Despite the visual observation of cracking in the specimens, the RDM values for all of the specimens were greater than 100 upon the completion of testing.

Figure 4-13: Cracks in Air Cured UHPC Specimens Following Freeze-Thaw Testing

An analysis of the fundamental transverse frequencies recorded provided further evidence

of the low variability of UHPC. Figure 4-14 shows the change in mean resonant frequencies of

UHPC freeze-thaw and side study specimen as testing was performed. The tight range of the

initial resonant frequencies revealed that the air-cured and thermally treated specimens

undergoing freeze-thaw cycles were within 8 Hz of their identically treated side-study

specimens. These resonant frequencies (2720-2770 Hz) were also very close to the frequencies

observed by Graybeal (2400 – 2600 Hz). The somewhat higher frequencies (5% - 15%) in this

testing were likely due, in part, to the shorter length dimension (3% shorter) of the specimens

due to the length change studs (3 x 4 x 15 ½ in. with two ¼ in. of exposed studs as opposed to 3

x 4 x 16 in.). Also note that the initial fundamental resonant frequency of the Air-cured

specimens is lower than that of the TT-cured specimens, an observation also noted by Graybeal

(2006a). However, precise absolute length measurements were not recorded prior testing, so

further comparison of the resonant frequencies is beyond the scope of this project.
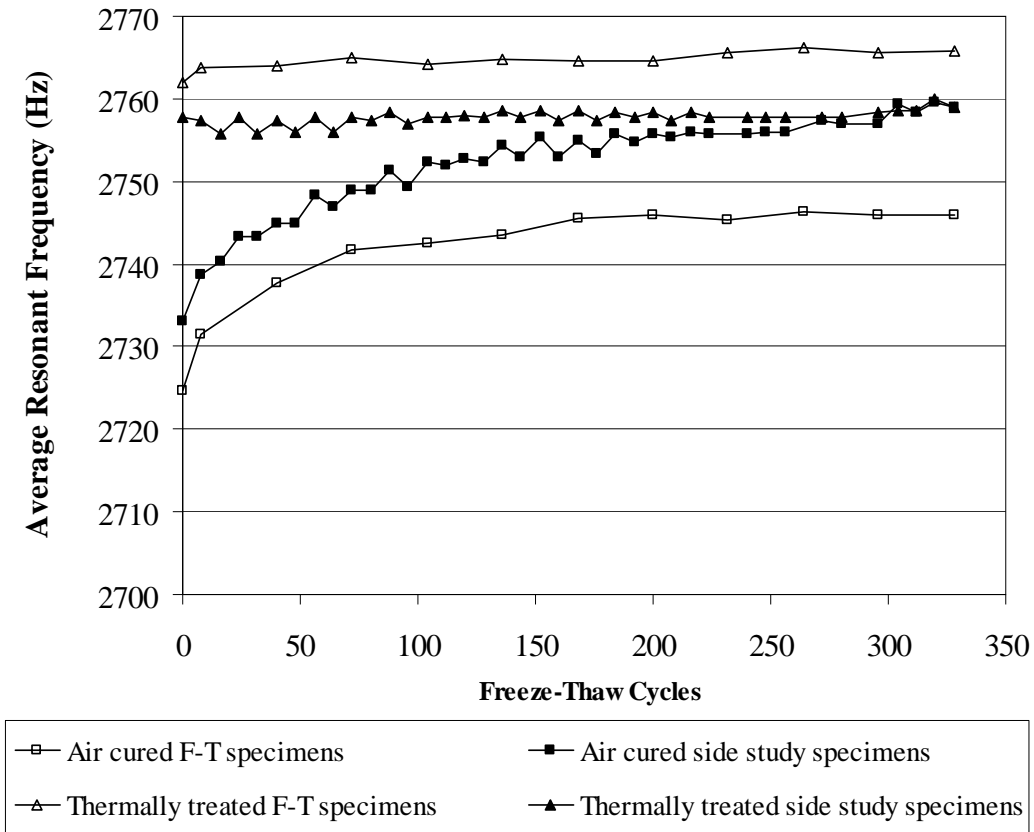
Figure 4-14: Average Resonant Frequencies of UHPC Freeze-Thaw and Side-Study Specimens

The UHPC specimens were stored in ambient conditions in the lab after freeze-thaw testing was completed. Approximately six months after testing was completed, additional resonant frequency testing revealed that the UHPC specimens displayed frequency responses not initially observed upon the completion of the testing. First, a noticeable decrease in the resonant frequencies of the Air-cured freeze-thaw specimens, -1.29%, was observed (Table 4.20). The thermally treated specimens subjected to freeze-thaw cycling also experienced a decrease in their resonant frequencies over time, though not as substantial (-0.34%) (Figure 4-15). However, a similar decrease was not observed in the side study specimens for either curing regimes (Figure

4-16). The decrease in resonant frequency suggests that damage to the UHPC specimens from freeze-thaw cycling may be greater than that observed immediately after testing was completed.

Table 4.20: Change in Resonant Frequency of UHPC Specimens after Testing Completed

Curing Regime	Testing Regime	Specimen ID	Resonant Frequency at end of testing (Hz)	Resonant Frequency 6 months after testing (Hz)	% change	Average change (%)
Air	F-T	M-FT-A-28	2729	2715	0.51	
Air	F-T	P-FT-A-28	2756	2693	2.29	-1.29
Air	F-T	R-FT-A-28	2744	2725	-0.69	
Air	F-T	S-FT-A-28	2749	2703	-1.67	
TT	F-T	M-FT-TT-28	2762	2754	-0.29	
TT	F-T	P-FT-TT-28	2766	2757	-0.33	0.34
TT	F-T	R-FT-TT-28	2769	2756	-0.47	
TT	F-T	S-FT-TT-28	2767	2759	-0.29	
Air	SS	P-FT-SSA-28	2771	2781	0.36	
Air	SS	R-FT-SSA-28	2742	2751	0.33	0.34
Air	SS	S-FT-SSA-28	2761	2770	0.33	
TT	SS	P-FT-SSTT-28	2754	2759	0.18	
TT	SS	R-FT-SSTT-28	2748	2756	0.29	0.23
TT	SS	S-FT-SSTT-28	2772	2778	0.22	
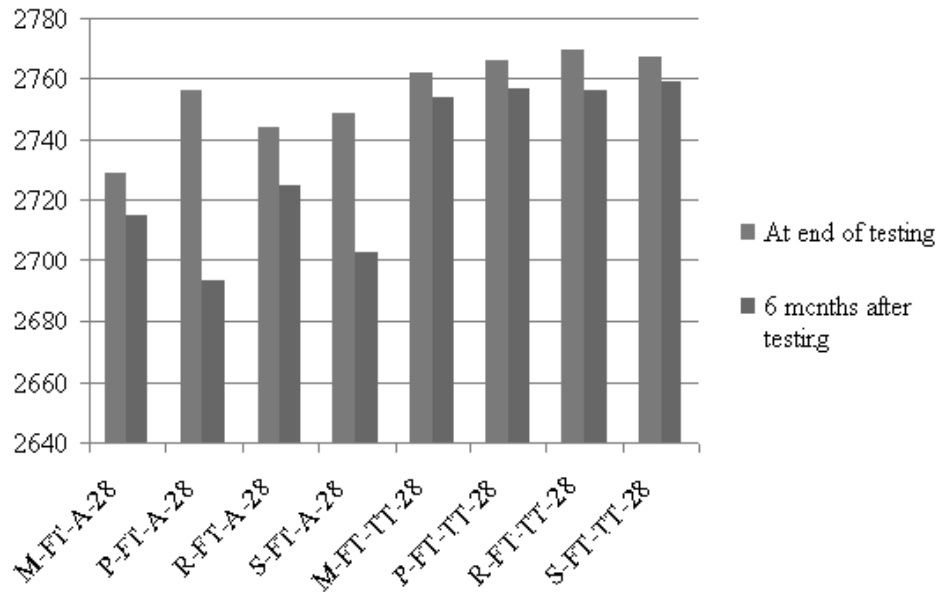
Figure 4-15: Resonant Frequencies of UHPC Specimens after Freeze-Thaw Testing
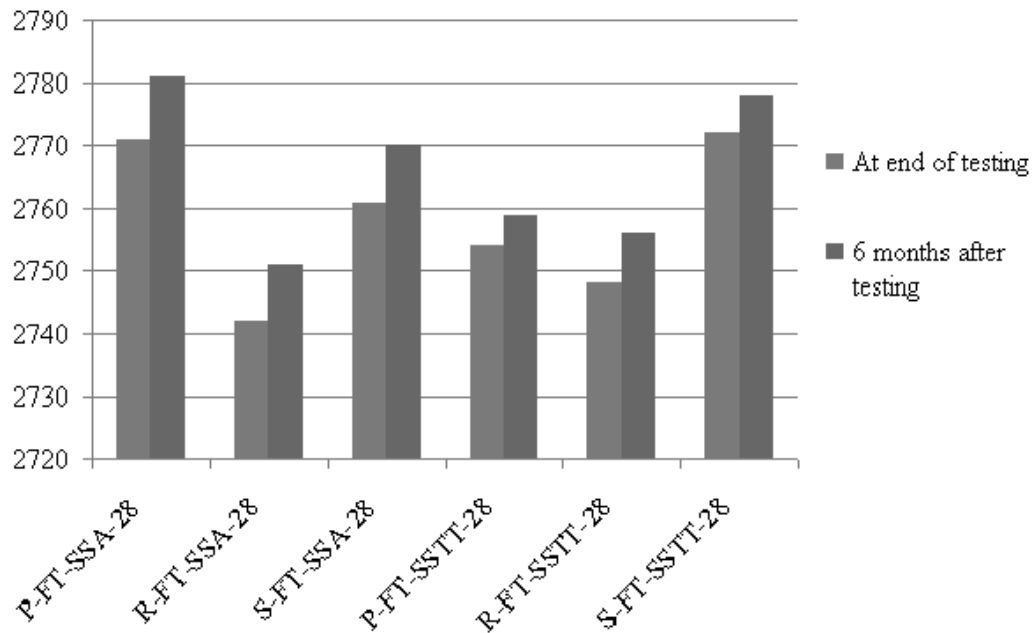
Figure 4-16: Resonant Frequencies of UHPC Specimens after Side-Study Testing

Further evidence that frequency responses were different than those initially observed after testing was the change in the shape of the frequency distribution curves for the air cured freeze-thaw specimens. During freeze-thaw testing and immediately after testing, the curves used to determine the transverse resonant frequency of the beams were bell shaped for all specimens (freeze-thaw and side-study) as shown by the curve in Figure 4-17 of a side-study specimen. However, after testing had been completed and the specimens were stored for several months at ambient lab conditions, the curves for the Air-cured freeze-thaw specimens exhibited the more skewed shape depicted in Figure 4-18. This change in shape indicates a change in the distribution of frequencies acquired from the impact resonance test and may indicate a change in material behavior.

106
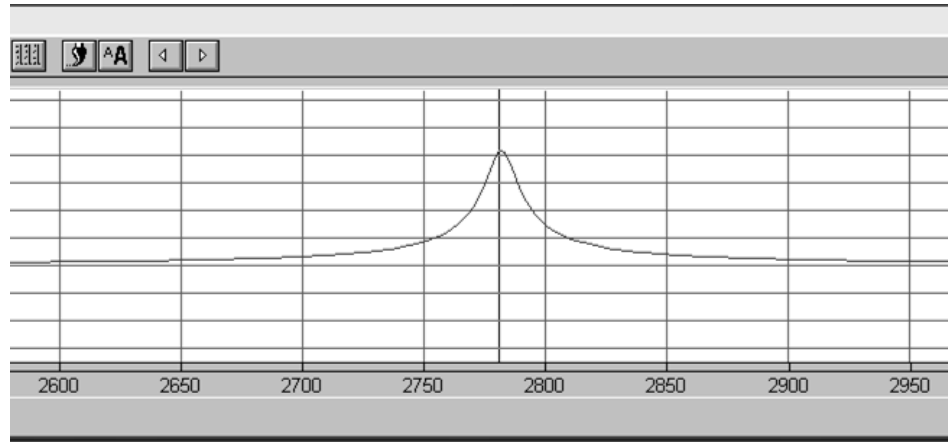
Figure 4-17: Typical Bell Shaped Resonant Frequency Output of Air-cured UHPC Specimen (Frequency in Hz)
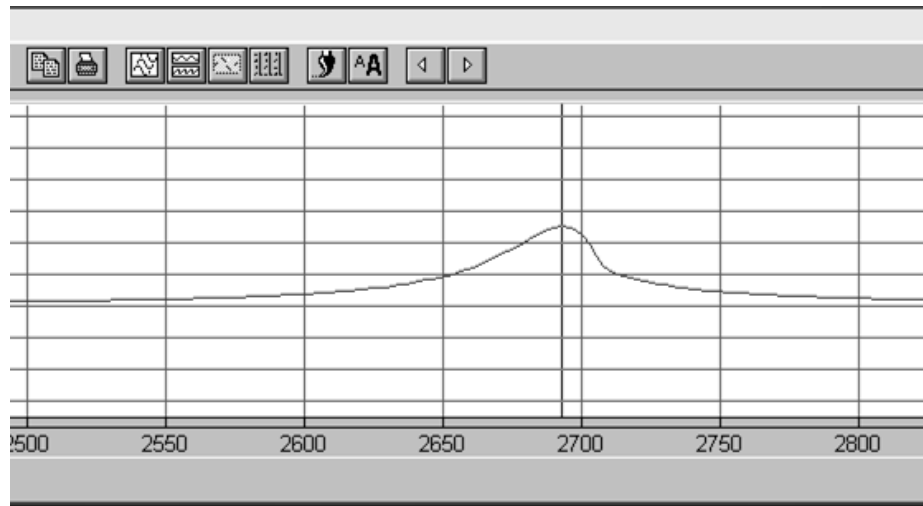
Figure 4-18: Typical Skewed Resonant Frequency Output of an Air-cured UHPC Specimen Six Months after Freeze-Thaw Testing (Frequency in Hz)

Overall, these test results indicate that the UHPC specimens underwent some form of autogenous healing similar to what Jacobsen and Sellevold (1996) observed in HPC freeze-thaw specimens. Increases in RDM and mass during freeze-thaw cycling were both indicators that additional hydration may be taking place within the specimens. Additionally, UHPC specimens outside of freeze-thaw cycling had improved RDM values similar to those in the freeze-thaw

chamber. However, this healing appears to have limited long term impact as RDM values decreased just months after testing was completed.

4.6   Coefficient of Thermal Expansion

The coefficient of thermal expansion for concrete was determined following a modified version of AASHTO TP-60-00 – *Coefficient of Thermal Expansion of Hydraulic Cement Concrete*. Modifications to both specimen preparation and testing procedures were made due to equipment specifications and in the interest of maintaining the integrity of UHPC curing regimes. The standard process according to AASHTO TP-60-00 requires that specimens be saturated with water prior to testing, placed into a test frame and submerged in a thermally regulated water bath, and then subjected to heating and cooling cycles until an accurate CTE measurement is obtained.

4.6.1 Results

Coefficient of thermal expansion testing was performed on Air-cured UHPC specimens ranging from 3-days in age to 28-days and on 7-day and 28-day TT-cured specimens. These curing regimes were applied upon specimen demolding, and the specimen age refers to the age of the specimen when tested (Chapter 3). A total of 22 specimens were tested. Typically, CTE tests began on the day of the stated specimen age (e.g – a specimen tested for 7-day CTE values began testing on day 7) and lasted 24-36 hours. However, due to one operable test frame and tests that ran longer than 1-day, three of the specimens were not tested on their appropriate test day. Therefore, additional specimens were cast for each of the missed testing times such that sample size of at least three test specimens was available for each curing regimes. The data for the three specimens not tested on their appropriate test day is not included in this section, but is

included in Appendix A for reference. Data for individual CTE tests are listed in Appendix A (Tables A.12, A.13).

All of the UHPC specimens were kept unsaturated during testing through the use of an epoxy coating to avoid the potential hydration effects of water on unhydrated cement particles in the cement matrix. Further motivating this decision was UHPC's low permeability that would create an increased likelihood of unequal degrees of saturation in each specimen. This reasoning follows previous CTE research conducted on UHPC specimens (Graybeal 2006a). However, moisture content does affect the CTE values of normal strength concrete specimens (Mindess et al. 2003), and therefore this data does not represent the CTE values of saturated or partially saturated UHPC specimens.

A summary of the CTE values for unsaturated UHPC specimens is presented in Table 4.21. For unsaturated 28-day TT-cured specimens, the average CTE was $8.16 \times 10^{-6}/°F$, and the CTE value for unsaturated 28-day Air-cured specimens had an average CTE value of $7.74 \times 10^{-6}/°F$. Values for the thermally-treated 7-day specimens ($8.20 \times 10^{-6}/°F$) were similar to the TT-cured 28-day specimens and comparatively higher than the Air-cured 7-day specimens ($7.62 \times 10^{-6}/°F$). Also, a statistical t-test confirmed that regardless of specimen age, TT-cured UHPC specimens had a statistically higher CTE value than the Air-cured specimens.

Table 4.21: Coefficient of Thermal Expansion (CTE) Test Summary

Curing regime	Specimen age at testing (days)	No. samples tested	Average CTE value (/°F)	St. Dev (/°F)	COV (%)
Air	3	3	7.53E-06	0.08E-06	1.1
Air	7	4	7.62E-06	0.11E-06	1.0
Air	14	3	7.69E-06	0.13E-06	1.8
Air	28	3	7.74E-06	0.15E-06	1.9
TT	7	3	8.20E-06	0.06E-06	0.7
TT	28	3	8.18E-06	0.15E-06	2.1

4.6.2 Discussion

The results demonstrate that the age of a specimen at testing plays a more significant role in Air-cured UHPC specimens than in TT-cured specimens. The averages of the data in Table 4.21 indicate an increasing CTE value as the Air-cured specimens age (see Figure 4-19). Figure 4-19 shows the CTE values for the Air-cured UHPC specimens and their respective standard deviations. Yet after performing a statistical t-test on the Air-cured data, only the 3-day and the 7-day specimens were statistically smaller (88 percent and 78 percent confidence, respectively) than the next testing age (7-day and 14-day, respectively). That is, the 3-day air specimen exhibited a statistically lower CTE (88% confidence) than the 7-day Air-cured specimen, and the 7-day Air-cured specimen exhibited a statistically lower CTE (78% confidence) than the 14-day Air-cured specimen. However, the 14-day Air-cured specimen's CTE value was not statistically lower than the CTE value for the 28-day Air-cured specimen.
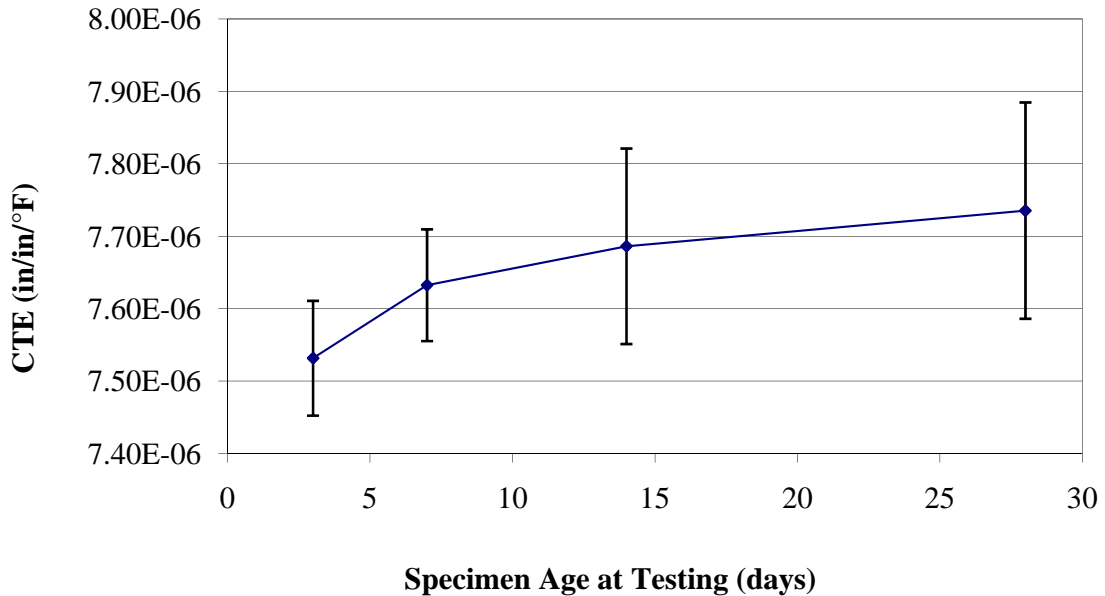
Figure 4-19: Average CTE Values for Air-cured UHPC Specimens

Conversely, the 28-day TT-cured specimens showed little change from the 7-day

specimens (Table 4.21). In fact, a two-sample t-test (95% confidence interval) determined that

TT-cured UHPC specimens maintained the same CTE value whether tested at 7-days or at 28-

days. Again, this supports the assertion that thermally steam treating UHPC "locks" in

properties so that specimen properties change little post-treatment.

The UHPC CTE values are slightly higher than the values typically reported for normal

and high strength concretes which tend to have CTE values of approximately 4.1-7.3 x 10^{-6}/°F

(FHWA 2006). However, a closer look at the factors that influence the CTE of a concrete

reveals that CTE values obtained for UHPC are reasonable. By and large the CTE of a concrete

is most greatly influenced by the CTE of its coarse and fine aggregates, but UHPC has no coarse

aggregate. Instead, UHPC consists mostly of fine sand (41%) and portland cement (29%).

Therefore, the CTE value for UHPC should fall between the range of a 1:6 cement/natural silica

sand mortar (6.7 x 10^{-6}/°F) (Mehta and Monteiro 2006) and saturated portland cement pastes (10

to 11 x 10^{-6}/°F). Equation 2.1 reveals an expected CTE value for UHPC of approximately 8.5 x

10^{-6}/°F. Therefore, the CTE value of UHPC is not unexpectedly high.

The CTE values measured in this testing vary from published data (Table 4.22). The

Japanese recommendations (JSCE 2006) suggest a CTE value of 7.5 x 10^{-6}/°F for steam treated

UHPC samples while Graybeal's thermally treated specimens (Graybeal 2006a) had a CTE value

of 8.7 x 10^{-6}/°F. Measured CTE values (8.16 x 10^{-6}/°F) appear larger than Japan's data and

smaller than Graybeal's data. No statistical tests were performed to compare the data because of

differing specimen ages at the time of testing. However, the COV values for Graybeal's data and

the data presented in this report are similar, showing that both test sets have tight fitting data and

little variation of CTE values between specimens. Some explanations for the variations in data

include slightly different batching and curing procedures, the influence of admixtures used by

others, and the different ages of the specimens at the time of testing.

Table 4.22: Comparison of Some Published UHPC CTE Data

Curing regime	Specimen Age (days)	Average CTE Value (in/in/°F)	St. Dev (in/in/°F)	COV (%)
Michigan Tech CTE Data				
Air	28	7.74E-06	1.5E-07	1.9
TT	28	8.16E-06	1.7E-07	2.1
Graybeal CTE Data (Graybeal 2006a)				
Air	> 60 days	8.17E-06	2.2E-07	2.7
TT	> 60 days	8.67E-06	1.7E-07	1.9
Japan CTE Data (JSCE 2006)				
TT*	N.A.	7.50E-06	N.A.	N.A.

*TT – Definition of exact procedure unknown at the time of publishing

4.6.3 Study of water absorption

To provide alternative methods for sealing UHPC specimens prior to CTE testing, a study was performed to determine the sealing properties of two types of sealant – concrete driveway sealant and epoxy sealant. The objective of the study was to determine whether concrete driveway sealant would provide a simpler and more effective method of preparing UHPC specimens prior to CTE testing. For that reason, a driveway concrete sealant was used to coat the UHPC specimens that were used to shakedown the CTE equipment. The shakedown involved testing the repeatability of the equipment following the same testing procedures previously outlined. However, the UHPC specimens coated in driveway concrete sealant exhibited a mass increase of approximately 0.4% throughout the shakedown. Therefore, epoxy sealant was employed during testing and a side study to examine the effect of water absorption on the weight and length of specimens coated in epoxy was developed. During testing it was found that specimens coated in epoxy only increased 0.02% in mass during a typical CTE test (Table A.13 – Appendix A) or approximately a gram of water absorbed by each specimen. For that reason, epoxy was determined to be an adequate sealant. Application of concrete driveway

113

sealer was a simpler process than epoxy application, but it provided less adequate protection against water absorption. A more detailed study to account for minute length changes due to water absorption in UHPC was beyond the scope of this project.

5.0   Conclusions of the Experimental Studies

The purpose of this research was to determine the impact that age of thermal treatment had on the mechanical properties of compressive strength, modulus of elasticity, Poisson's Ratio, and flexural strength and toughness of an ultra-high performance concrete. Four different curing regimes were used to measure the impact on the mechanical properties, Air-cured, Thermal Treatment, Delayed Thermal Treatment, and Double Delayed Thermal Treatment (Air, TT, DTT, and DDTT, respectively). Additionally, a UHPC using two curing regimes was compared for resistance to rapid chloride penetration and freeze-thaw, and to determine the coefficient of thermal expansion. A summary of the tests conducted was listed previously in Table 4.1. Results and discussion were also provided in Chapter 4. This chapter summarizes the major conclusions of the experimental studies.

In general, the following conclusions can be made. Specific conclusions for each test type are listed below in separate sections.

1. UHPC durability properties researched herein exceed those of normal strength concretes and high performance concretes.

2. Mixing time increases as the age of the premix of UHPC increases, however material properties do not show significant changes.

3. UHPC test results are repeatable between different laboratories when comparing to Graybeal's work at the FHWA Turner-Fairbank Laboratory (2005), although the research reported herein is much expanded over the preliminary studies conducted at FHWA.

5.1 Compression Strength

1. Compressive strength testing showed that there was no difference in the compressive stress after thermal treatment was applied. The mean compressive stress for all TT, DTT, and DDTT cylinders was 30.1 ksi. The compressive stress was independent of age at which thermal treatment was applied as well as the age at which the specimen was tested following thermal treatment. This could have a large impact on how UHPC is used in industry, by allowing a precaster to cast several elements over a period of time and then thermally treat them simultaneously, allowing more flexibility in the casting and curing sequence.

2. Air-cured specimens showed an increase of strength with age and at 28 days had a compressive stress of 23.9 ksi. The Air-cured specimens appear to be asymptotically approaching a maximum compressive stress of 25 to 27 ksi.

5.2 Modulus of Elasticity and Poisson's Ratio

1. Modulus of elasticity was scarcely impacted by the four curing regimes. The Air-cured specimens at 14 and 28 days, which were shown to have the same population mean, had a mean modulus of elasticity of 7850 ksi. Like the compressive stress samples, the three curing regimes of TT, DTT, and DDTT had the same population mean and a combined modulus of elasticity of 8150 ksi. By conducting thermal curing, the modulus value was only increased by 3.8 percent where the compressive stress increased by 25.9 percent over air curing based on 28 day information.

2. Modulus of elasticity data for this research is best predicted by the model proposed by AFGC (2002) which is:

$$E_c = 262,000 * \left(\sqrt[3]{f`_{ATT}} \right) \text{ (psi)} \qquad\qquad \text{Equation 2.3}$$

116

Where: $f\hat{}_{ATT}$ = Compressive stress of UHPC after thermal treatment.

Like the compressive stress, having the same modulus value independent of when the thermal cure was applied or when the specimen was tested would be a measurable benefit not only to the precast industry but the design industry as well because the casting and curing of the material is flexible.

3. The four curing regimes had no impact on Poisson's ratio as all specimens, independent of age or curing regime, had the same population mean. The mean value for all samples was 0.21 which is slightly greater than 0.20, the commonly accepted value for normal strength concrete. Again, by having Poisson's ratio independent of when thermal curing is applied makes the manufacturing process much more flexible.

5.3 Flexural Strength Testing for First Cracking and Toughness

1. One age (28 days) and three curing regimes were considered for flexural testing, Air, TT, and DTT. Data was corrected for specimen size as discussed in Section 4.3. Unlike compression and modulus, all curing regimes had different population means for corrected first crack stress. The sample means for corrected first crack stress are as follows: Air 0.76 ksi, TT 1.06 ksi, and DTT 1.18 ksi. The difference between TT and DTT does not coincide with the compression and modulus trends were specimens which received thermal curing had the same population means, which would slightly complicate the production process; however this could be easily overcome by using the conservative value for calculations.

2. Flexural toughness and residual strength factors are significantly enhanced by the use of fibers. Fibers provide post-crack ductility.

5.4   Rapid Chloride Penetration Test

1. Rapid chloride penetration resistance of UHPC is superior to NSC and HSC regardless of curing regime. All UHPC specimens, whether Air-cured or TT-cured had negligible chloride ion penetrability.

2. Thermally treating UHPC specimens enhances its chloride penetration resistance by limiting ionic movement to even lower levels than that of Air-cured specimens.

3. 7-day and 28-day thermally treated specimens exhibited statistically similar total charge passing results, indicating that specimen age does not play a major role in thermally treated UHPC chloride ion resistance.

5.5   Freeze-Thaw Cyclic Testing

1. UHPC demonstrated a high resistance to freeze-thaw damage (100+ durability factor and less than 0.01% length change) with no large cracking or spalling of the material regardless of curing regime.

2. Air-cured and TT-cured UHPC specimens increased in both relative dynamic modulus and mass during freeze-thaw testing at rates similar to companion UHPC specimens undergoing wet-dry cycles. The greatest increases documented were in the Air-cured specimens, but were still less than 2.0%.

3. UHPC exhibits signs of autogenous healing that leads to increased RDM and mass gain when submerged in water, even while undergoing freeze-thaw testing. However, the long term impact of healing decreased just months after testing was completed as noted by the resonant frequency of UHPC specimens declining.

5.6   Coefficient of Thermal Expansion

1. A coefficient of thermal expansion of $8.2 \times 10^{-6}/°F$ is recommended for UHPC once it has been thermally treated regardless of age.

2. Coefficient of thermal expansion values were tested on unsaturated UHPC specimens and increased with age in Air-cured UHPC specimens, although the only statistically significant changes occurred before specimens aged 14-days. TT-cured specimens maintained CTE values regardless of age.

3. 28-day TT-cured UHPC specimens had a statistically higher CTE value than 28-day Air-cured specimens ($8.18 \times 10^{-6}/°F$ and $7.74 \times 10^{-6}/°F$, respectively).

4. UHPC has a coefficient of thermal expansion value slightly higher than NSC. However, this value can be estimated based on the volumetric proportions and CTE values of UHPC constituent materials.

5. Epoxy coating performed better than concrete driveway sealer when sealing test cylinders for maintaining water saturation levels in UHPC specimens.

(This page intentionally left blank)

6.0   Preliminary Life Cycle Costs of a UHPC Superstructure

A preliminary life cycle cost analysis comparing the initial and long term costs of UHPC and normal strength concrete (NSC) bridges has been performed. Two scenarios were evaluated for the UHPC superstructure; scenario one involving a UHPC bridge of only UHPC girders and an NSC cast-in-place deck and scenario two involving a UHPC bridge of UHPC girders and deck panels. The Mars Hill Bridge in Wapello County, Iowa served as model for these scenarios and is composed of UHPC girders and NSC deck and sub-structure. It should be noted that the Mars Hill Bridge did not use UHPC in an optimized section, which could lead to excessively higher costs. However, it is currently the only bridge in the U.S. that is built using UHPC. A cost estimate was also performed for the control bridge, a bridge using a NSC superstructure with correspondingly larger beams for the constant bridge span and width.

6.1   Bridge Components

The control and similar UHPC bridges were divided into three components: superstructure, deck, and sub-structure. The superstructure consisted of the three I-beams and the sub-structure included the abutments and footings. All three model bridges were a 110 ft. single-span with a width of 24.5 ft. (Moore 2006) to accommodate two lanes of traffic. Precast, prestressed concrete I-beams and a NSC deck, typical of current MDOT construction practices, were assumed for the control bridge. The NSC deck was a nine inch, cast-in-place (CIP) concrete slab. The UHPC model bridges used a modified 45-inch Bulb Tee girders. Modifications were a two inch reduction in the lower flange and web width and a one inch reduction in the upper flange (Moore 2006). The abutments were assumed to be equal to the bridge width, 12.5 ft. high and have a width of 3.0 ft. while footings were assumed to be 3.5 ft.

121

high and have a width of 8.5 ft. The NSC deck of UHPC scenario one was the same as the

control bridge. While the original Wapello County Bridge used an 8 in. deck, costs were

adjusted to a 9 in. deck for comparison to MDOT standard practice. For scenario two, the deck

was assumed to be four inch thick, precast UHPC deck panels, with a similar width and span of

the control bridge, topped with a water-proofing membrane and asphalt wearing surface.

6.2   Construction

RS Means data were used to find the unit cost of each bridge component and activity,

which are described in Tables 6.1 and 6.2. Reference numbers are provided for further

information (RS Means 2005).

Table 6.1: Bridge Component Unit Costs

Item	Unit	Cost	Reference Number (RS Means 2005)
Abutment	Cubic Yard	$345	02800-02850-205-1050
Approach Railing	Linear Foot	$119	02800-02850-205-4000
Concrete Deck	Cubic Yard	$298	02800-02850-205-1000
Prefabricated I-beam	Each (100-120 ft span)	$16,000	02800-02850-205-1620
Footing	Cubic Yard	$298	02800-02850-205-1000
Parapet	Cubic Yard	$585	02800-02850-205-1150
Reinforcing,(Epoxy Coated)	Ton	$3,550	02800-02850-205-2100
Sidewalk	Square Foot	$17.55	02800-02850-205-1230

Table 6.2: Construction Activities Unit Costs

Item	Unit	Cost	Reference Number
Machine Excavation for Abutments	Cubic Yard	$10.80	02300-02315-462-6050
Mobilization and Demobilization Up to 25 miles (Dozer, loader, backhoe)	Each	$305	02300-02305-250-0100
Additional 5 mile haul distance	+ 5 mi. Each	10%	02300-02305-250-2500
Mob. & Demob. Truck-mounted Crane	Each	$120	02300-02305-250-2000

122

The total cost of each component and activity for the control bridge was then calculated

using assumed quantities and the above unit costs. Total costs for the approach railings,

parapets, and sidewalks were added to the cost of the deck. The information obtained from RS

Means was cross checked against information from recent Michigan bids available through

MERL (Michigan Engineers' Resource Library, a database of Michigan bid items that allows

project managers and engineers to make road and bridge project estimates). An estimated cost of

$432,000, taken from the Mars Hill Bridge, was used as a guide for the UHPC structures

(Endicott 2006). Given that Scenario 1 represented the Mars Hill Bridge, the application of a

3.0% inflation rate per year was the only modification to the cost of the UHPC structure so as to

compare in 2007 dollars. The added cost of a UHPC deck, as opposed to a NSC deck, was

included in the cost of the UHPC structure in scenario two, along with the 3.0% inflation rate per

year. Table 6.3 contains the estimated construction costs for the control and UHPC bridges.

Table 6.3: Estimated Construction Costs

Bridge Component	Control Bridge (NSC Girders and Deck)	Scenario 1 (UHPC girders, NSC Deck)	Scenario 2 (UHPC Girders, UHPC deck panels)
Deck, railing, parapet	$33,000	$33,000	$82,000[†]
Sub-structure	$40,000	Not Available	Not Available
Superstructure	$48,000	Not Available	Not Available
Reinforcing, Epoxy Coated	$107,000	Not Available	Not Available
Activities	$4,000	Not Available	Not Available
Design (10% of costs)	$23,100	Not Available	Not Available
Total (Control in 2005 $, Scenario 1 & 2 in 2006 $)	$255,000	$434,000*	$483,000
Total (2007 $) Control-3.4% inflation average 2005-2007 UHPC-3% inflation 2006-2007	$273,000	$447,000	$497,000

*Reported cost adjusted to 9 in. deck from 8 in. deck, all other costs estimated.

[†] Includes waterproofing membrane and asphalt wearing surface.

6.3   Maintenance

Bridge maintenance was assumed according to the MDOT Bridge Preservation Timeline for a concrete deck with epoxy coated rebar and prestressed concrete beams (MDOT 2007b). Unit costs were obtained from the Ohio Department of Transportation's *Preventative Maintenance* page, as this information was readily available (Ohio LTAP 2007). Maintenance unit costs can be seen in Table 6.4.

Table 6.4: Unit Costs of Maintenance Activities

Activity	Unit	Cost
Beam End Rehab	CF	$50.00
BIT Overlay	SF	$15.00
Deck Patch	SF	$100.00
Joint Replace	LF	$40.00
Overlay (Deep and Shallow)	SF	$35.00
Sub Repair: Diagonal Cracking	LF	$20.00
Sub Repair: Deteriorated Concrete	SF	$45.00

The MDOT Bridge Preservation Timeline stipulates regular Capital Scheduled Maintenance (CSM) throughout the life of the bridge to prevent deterioration of the structure. Capital Scheduled Maintenance, as defined in the CSM Manual, includes superstructure washing, vegetation control, spot painting, joint repair/replacement, concrete coating/sealing, minor concrete patching and repair, concrete crack sealing, approach pavement relief joints, and slope paving repair (MDOT 2007a). Given that it is difficult to assume an average value for these tasks, an annual deck maintenance cost was utilized in place of the CSM. The annual deck maintenance cost includes washing, flushing, patching, and sealing. An annual cost of $0.20 per square foot for Michigan bridges was obtained from a questionnaire sent to several DOT's, consultants, and contractors pertaining to procedures and costs of concrete bridge decks (Lopez-

124

Anido 1998). Michigan was one of twelve DOT's that participated in the survey, and the price stated above reflects the individual response of MDOT.

The Bridge Preservation Timeline obtained from MDOT suggests a 90 year design life for the control bridge, at the end of which an evaluation of the bridge is made and replacement of the superstructure or bridge is decided, along with additional rehabilitation needs (MDOT 2007b). It was assumed that the deck and I-beams of the control bridge would need replacement at the end of the 90 year design life. Additional rehabilitation needs included sub-structure repair of diagonal cracking and deteriorated concrete.

A design life of 180 years was chosen for the UHPC structures because UHPC is expected to outperform traditional structural concrete by at least twice as much. This assumption is based on results of mechanical and durability tests of the material performed herein. The Bridge Preservation Timeline was followed for all NSC components of the UHPC structures and a modified preservation timeline was used for the UHPC components. Tables 6.5 and 6.6 compare the NSC and UHPC maintenance of the bridge girders and deck.

Table 6.5: Bridge Girder Maintenance

Control		UHPC	
Year	*Maintenance*	*Year*	*Maintenance*
40	Beam end rehab		
90	Beam replace	90	Beam end rehab
130	Beam end rehab		

Table 6.6: Bridge Deck Maintenance

Control Deck		UHPC Deck	
Year	*Maintenance†*	*Year*	*Maintenance†*
12	DP & JR		
25	DP & JR		
40	DO & JR	45	JR
52	DP & JR		
65	SO & JR		
80	BIT Overlay		
90	Deck Replace	90	JR
102	DP & JR		
115	DP & JR		
130	DO & JR	130	JR
142	DP & JR		
155	SO & JR	155	JR
170	BIT Overlay		

†*DP = Deck Patch, JR = Joint Replace, DO = Deep Overlay, and SO = Shallow Overlay*

The UHPC structure in scenario two was also expected to not require annual deck maintenance. It was assumed that little maintenance would be needed for a UHPC deck, in comparison to a NSC deck, and the maintenance schedule was reduced to regular joint replacements.

6.4   Preliminary Life Cycle Costs

The cost-benefit analysis for each bridge included the construction and maintenance costs over a 180 year period. An analysis period of 180 years was chosen because it is the first incidence point of the control and UHPC structures, or the first point at which both structures are at similar maintenance needs. Maintenance costs and repair costs over the 180 year design life were reduced to a net present value (NPV) based on a seven percent discount rate and a three percent inflation rate. Equation 6.1 details the method of reduction to *NPV* where *r* is the real discount rate and *n* is the difference in years from the present to future date.

126

$NPV = (present\ \$) / (1+r)^n$ Equation 6.1

Table 6.7 summarizes the construction and maintenance costs for the control and UHPC bridges for the 180 year common time increment.

Table 6.7: Costs of Control and UHPC Bridges, 2007 $

Activity	Control Bridge (NSC Girders and Deck)	Scenario 1 (UHPC girders, NSC Deck)	Scenario 2 (UHPC Girders, UHPC deck panels)
Construction	$273,000	$447,000	$497,000
Maintenance	$71,000	$69,000	$4,000
Total (3% inflation/year & 7% discount rate)	$344,000	$516,000	$501,000
Incremental increase (%)	(baseline)	50.0%	45.6%

It is interesting to note that the control bridge still provides the lowest cost bridge over the 180 year period, which includes a total deck replacement. This is easily explained by the cost of the UHPC material. The cost per cubic yard of the UHPC used in the experimental study for this research project was around 20 times more expensive than the cost per cubic yard of typical concrete ($2000/yd versus $100/yd). However, if this cost were to drop, UHPC usage may become more advantageous in life cycle cost assessments. Figure 6-1 depicts the change in the cost of scenario two, given a change in the cost per yard of UHPC. The changing cost for scenario two was found by taking the current unit cost of UHPC and assuming quantities for the bridge deck and beams, based on their dimensions. When calculating the price for the beams a 10% design cost was added, along with 5% for additional charge that may be unforeseen. These unforeseen charges were not assumed to include plant modifications needed for UHPC or transportation costs for the bridge components. Based on Figure 6-1, for it to be advantageous in

scenario two the target cost would be about $1,750 per yard, or about a 12.5% decrease over

current prices.
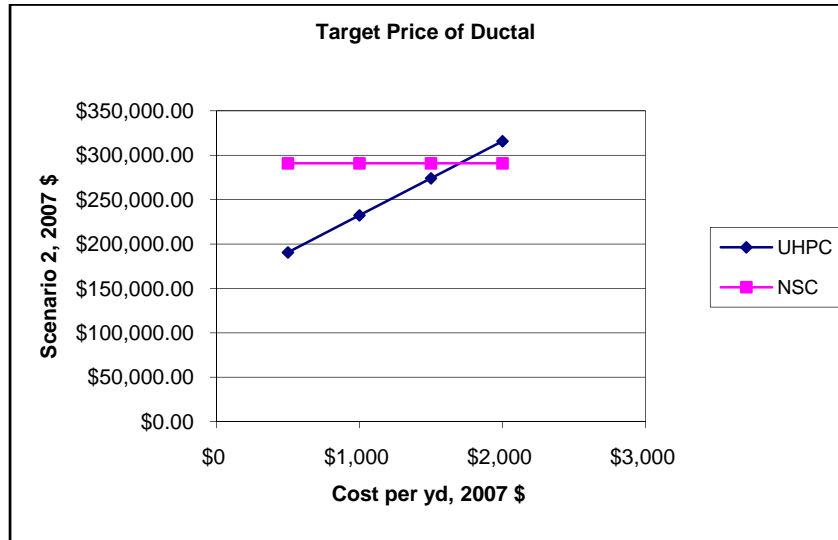
Figure 6-1: Target Cost of UHPC

6.5   Conclusion of the Preliminary Life Cycle Cost Analysis

The preliminary life cycle cost analysis shows that the control bridge will cost $172,000

less than a UHPC bridge constructed of UHPC girders and a NSC deck, and $157,000 less than a

UHPC bridge constructed of UHPC girders and UHPC deck panels, over a 180 year design life.

However, the analysis performed only accounted for the construction and maintenance costs and

does not incorporate additional user costs or benefits of either bridge. Also, the model bridge

chosen incurred increased costs due to transportation of the bridge components. Furthermore,

the UHPC bridge design and actual costs considered did not take full advantage of UHPC by

using an optimized cross-section. After finding the target cost of UHPC it was apparent that if

the unit cost of the UHPC material were to drop about 12.5%, life cycle costs may be less over

the 180 year design life. This would entail that the transportation cost, cost of modifying the

128

current plant, and any additional charges would not raise the cost of UHPC above the stated target cost. It is acknowledged that the initial costs of a current NSC control bridge is much lower, but the reduced maintenance of the UHPC bridges, in particular for the bridge model using the UHPC deck panels, is significantly less over time.

Additional costs and benefits to note relating to the user are the delays due to construction or maintenance, bridge safety, and the effects of deterioration on the performance of the bridge. The assumed maintenance of the UHPC bridges in this report can only be considered a rough estimate; further observation of UHPC structures will be needed for a better assumption.

Also, UHPC is a new material to the construction market, and little is known about the potential optimization of UHPC components and the future cost of the material after product familiarization has occurred. Component optimizations in this report are conservative estimates and may not truly reflect the capabilities of UHPC. As more UHPC structures are implemented, the limits of the material will be better understood and design of the components will improve. The future cost of the product is also hard to forecast, however, current prices may be higher due to research costs, low material production, and the cost of precast plants to modify current technologies to fit the needs of UHPC.

6.6   Future Work

A thorough cost-benefit analysis is needed to gain more insight on the feasibility of UHPC bridges in Michigan. This analysis would include the user costs and benefits listed above, as well as other costs or benefits that may be pertinent, and a risk analysis to assess the sensitivity of the outcome to input variation. The risk analysis could be as simple as fluctuating the discount or inflation rates or as complicated as applying computer simulation of weighted

129

input variables. Monte Carlo Simulation is one method of computer simulation that could be utilized (Walls and Smith 1998).

Eventually a detailed life cycle analysis is needed for UHPC structures. This analysis would include the environmental impact of the structure, costs and benefits of the structure, and sustainability of the materials used. As more UHPC structures are built, it is important that the proper data and observations are made throughout their lives, so that the life cycle analysis can be simplified.

7.0   Recommendations, Implementation and Future Work

Recommendations are made for adapting current test procedures to properly evaluate UHPC properties. Implementation activities and suggestions for future work are also included in this chapter.

7.1   Recommendations for UHPC Testing Procedures

While ASTM and AASHTO Standards are accepted for normal strength concretes, usually up to about 10,000 psi, these procedures may not always be applicable for assessing UHPC performance. As such, the spirit of ASTM and AASHTO standards were followed for testing UHPC but some modifications were necessary. This chapter summarizes information on modifications to the testing procedures used.

7.1.1 Compression Testing

Base Procedure: ASTM C 39

Procedure Modifications for UHPC:

- The load rate was increased from 35 psi per second to 150 psi per second.

- 3 x 6 in. cylinders were used instead of 4 x 8 in. or 6 x 12 in. cylinders

7.1.2 Modulus of Elasticity and Poisson's Ratio

Base Procedure: ASTM C 469 using Compressometer-Extensometer

Procedure Modifications for UHPC:

- The load rate was increased from 35 psi per second to 150 psi per second.

- Instead of breaking a companion cylinder and determining 0.40 $f`_c$ from that test, specimens were loaded to a predetermined load based on curing regime and age at time of testing.

7.1.3 Flexural Strength Testing for First Cracking and Flexural Toughness

Base Procedure: ASTM C 1018

Procedure Modifications for UHPC:

- The midspan deflection rate was chosen as 0.003 in. per minute independent of curing regime tested.

- The test was carried out to 20.5 times the first crack deflection so a greater number of toughness indices and residual strength factors could be calculated.

7.1.4 Rapid Chloride Penetration Test

Base procedure: ASTM C 1202

Procedure Modifications for UHPC: None

Preparation Notes:

- Specimens were cast in a 4 in. diameter x 3 in. high cylinder and one day before treating were cut down from the top to 4 in. diameter x 2 in. high a day before treating. The bottom surface of the cylinder should not be cut due to the fact that the finished surface of UHPC will normally be exposed.

- Specimens may never be fully saturated during preparation. Further research is needed to discover whether or not vacuum preparation actually saturates specimens.

132

Testing Notes:

- Finished bottom of specimens shall be exposed to the NaCl solution to simulate finished surface of UHPC. Both ends may be cut, but the significance must be checked.

7.1.5 Freeze-Thaw Cyclic Testing

Base procedure: ASTM C 666, Procedure B

Procedure Modifications for UHPC: None

Preparation Notes:

- The time that UHPC specimens should be soaked in water prior to testing should be determined based on a balanced evaluation of the need to maintain curing regime integrity versus the need to have a saturated specimen for freeze-thaw cycling.

Testing Notes:

- The optional length change test should not replace the RDM test due to the potential for autogenous healing of UHPC specimens while undergoing freeze-thaw cycling.

- Length change tests should be performed vertically to allow for easier handling of the specimens while maintaining accuracy.

- Visual inspection should be carefully performed to monitor for minute micro-cracking and erosion of the outer surface.

- Future freeze-thaw testing of UHPC should test the specimens for several months after testing is complete to monitor for changes in RDM.

7.1.6 Coefficient of Thermal Expansion

Base procedure: AASHTO TP 66-00

Procedure Modifications for UHPC:

- Do not soak the UHPC samples in a lime bath prior to testing. This may hydrate additional cement particles and change the properties of the UHPC sample. Instead, samples must be coated in an epoxy resin to allow for testing in the unsaturated state. Samples must be completely coated in epoxy except for the points where the LVDT will be in contact with the sample and where the support frame buttons are in contact with the sample.

Preparation Notes:

- (Not performed during this research, but suggested for future testing) Specimens shall be cast in a 4 x 8 in. cylinder mold and then cut to 4 x 7 in. Both ends of the sample should be cut 1/2 in. to ensure a plane surface of contact for both the LVDT and the support frame buttons.

Testing Notes: None

7.2   Draft U.S. Design Recommendations for UHPC

Ultra-High Performance Concrete (UHPC) is one of the latest advances in concrete technology and it addresses the shortcomings of many concretes today. UHPC is typically defined as a concrete achieving high compressive strength in excess of 25,000 psi (sometimes greater than 30,000 psi) with exceptional durability performance. As such, innovative solutions can be created for long-term applications.

The purpose of these draft design recommendations is to begin the development of a design code for using the material in the U.S. bridges. Recommendations are based on testing conducted at Michigan Technological University and reported herein. Tests were conducted on

Ductal®, the only UHPC currently available in the U.S. market at the time of testing.   Steel fiber reinforcement (8×10^{-3} in. φ by 0.50 in. length) was provided at a rate of 2% by volume.

Typical recommendations would include three parts: (I) material characterization, (II) design and analysis of UHPC structures, and (III) durability. While several sections of the recommendations are outlined below, only those sections with applicable results from the research study herein are drafted. Other sections are noted as "future sections".

Part I – Material Characteristics

Characterization of material behavior is necessary to design systems using UHPC. Recommended testing procedures for UHPC material and durability characterization were listed previously in Section 7.1.

Part I.1 – Mixing and Placing

The concrete mix is batched in a laboratory within manufacturer recommended procedures to attain design characteristics for the proposed application. Trial batching at a plant should be conducted to ensure that all parties are familiar with the material prior to casting final elements. UHPC must be covered throughout the casting process and immediately after casting to avoid moisture evaporation that can lead to reduced hydration and excessive surface shrinkage.

Part I.2 – Effects of Thermal Treatment

Some UHPC applications benefit from a thermal curing, while other applications may not be able to allow for curing other than in ambient conditions. The main benefits of thermal curing are:

- Increased compressive and tensile strengths
- Improved durability
- Apparent reduced creep and shrinkage after curing

- Increased time to maturity so as to eliminate waiting for a 28-day or longer cure time

Thermal treatment is defined as a 100% humidity steam treatment at 194°F for 48 hours. Thermal treatment begins with a 6 hour ramp up period, 48 hours at the specified humidity and temperature, followed by a 6 hour ramp down period. Ambient air-curing is typically considered as 72°F at 30-50% humidity.

Part I.2.x – UHPC Maturity (future section)
Comments: UHPC maturity to be defined by the set time, such that thermal treatment is applied only after the set to avoid the potential of DEF (delayed ettringite formation).

Part I.3 – Compressive Strength
Compressive behavior is characterized most often by ultimate strength. Test specimens are typically 3x6 in. cylinders cast vertically or horizontally. Horizontal casting allows for parallel ends and eliminates the need for end grinding as neoprene pads and high-strength sulfer capping are not appropriate for UHPC's high strengths.

The ultimate compressive strength of thermally treated UHPC can be expected to achieve 25-30 ksi independent of when thermal curing is applied. The ultimate compressive strength of ambient cured UHPC is time dependent and shall be measured for specific applications. If no other information exists at the design stage, a preliminary design compressive strength of 24 ksi at 28-days can be assumed.

Part I.3.x – Compressive Strength Gain with Time (future section)

136

Part I.4 – Tensile Strength

Tensile behavior has been characterized in two stages: an elastic stage and a post-cracking stage. The fiber strength and disbursement can strongly influence the tensile capacity of a UHPC member. A direct tensile test is considered the most accurate measure of tensile strength, however no such test has proved successful for UHPC in the U.S. to date. The flexural tensile strength at first cracking can be compared to current U.S. design standards for mild steel reinforced concrete sections. As additional test results become available, tensile behavior of thin slabs may be different than beam elements.

Part I.4.x – Direct Tensile Strength (future section)
Part I.4.x – Splitting Tensile Strength (future section)

Part I.4.x – Flexural Tensile Strength

The flexural tensile strength of UHPC at first cracking is dependent on the curing method applied. Testing should be conducted to verify results for the intended curing method. Full size specimen testing may be needed for thin slab applications. If no other information is known in the early design stages, a first crack flexural strength of 0.75 ksi can be assumed for ambient curing at 28-days, and 1.05 ksi for thermally cured specimens.

Part I.4.x – Post-cracking Behavior (future section)

Part I.5 – Modulus of Elasticity

Part I.5.1 – Static Modulus of Elasticity

The following relationship can be used to estimate the modulus of elasticity for UHPC elements (AFGC 2002):

$$E_c = 262,000 \times (\sqrt[3]{f'_c}) \qquad \text{(psi)}$$

where: f'_c = compressive strength of UHPC (psi).

If in the initial design stages and information is unknown, the modulus of elasticity for thermally cured fiber reinforced specimens can be estimated as 8150 ksi. For ambient cured specimens, an estimate of 7800 ksi after 14-days can be assumed.

Part I.5.2 – Dynamic Modulus of Elasticity (future section)

Part I.6 – Poisson's Ratio

Poisson's ratio for UHPC can be generally assumed to be 0.21 within the elastic range.

Part I.7 – Thermal Characteristics

Part I.7.1 – Coefficient of Thermal Expansion

A value of $8.2 \times 10^{-6}/°F$ can be assumed as the coefficient of thermal expansion for UHPC that has been thermally cured. This value should be reduced to $7.7 \times 10^{-6}/°F$ for 28-day ambient cured UHPC elements.

Part I.7.x – Thermal Conductivity, Thermal Diffusivity, Specific Heat (future section)

Part I.8 – Shrinkage Behavior (future section)

Part I.8.x – Early Age Behavior
Part I.8.x – Post Thermal Treatment Behavior

Part I.9 –Creep Behavior (future section)

Part I.9.x – Early Age Behavior
Part I.9.x – Post Thermal Treatment Behavior

Part I.10 – Fatigue Strength (future section)

Part I.11 – Impact Strength (future section)

138

Part II – Structural Analysis and Design

Part II.1 – Loads

Loading for UHPC elements does not vary from loadings applied to normal strength concrete members.   Applied loadings and induced stresses due to loadings shall be calculated in accordance with accepted methods and the current edition of the AASHTO Bridge Design Specifications.

The unit weight of UHPC shall be assumed to be 155 pcf.

Part II.2 – Serviceability and Ultimate Limit States (future sections)

This section should include discussions for serviceability and ultimate limit states, capacities, and general detailing. The following outline is proposed and can be adjusted as research becomes available to support findings:

- General detailing – cover, spacing, beveling
- Serviceability – deflections, cracking, vibration
- Moment capacity and strain compatibility
- Shear capacity – one-way beam shear, punching shear, interface (horizontal) shear
- Torsional capacity
- Fatigue resistance
- Buckling of slender members
- Anchorage – bond strength, and confinement steel for bursting zones
- Connection details

Part III – Durability

Part III.1 Chloride Ion Ingress

UHPC has demonstrated superior resistance to chloride ion ingress (negligible penetrability) regardless of curing method.

Part III.2 – Freeze/Thaw Resistance

UHPC has demonstrated a high resistance to freeze-thaw damage (100+ durability factor and less than 0.01% length change) with no large cracking or spalling of the material regardless of curing method.

Part III.3 – Carbonation (future section)

Comment: Carbonation has been found to be negligible (Japan 2006)

Part III.4 – Chemical Attack (future section)
Part III.5 – Alkali-Silica Reactivity (future section)
Part III.6 – Fire Resistance (future section)

Comment: No fire resistance testing has been performed on UHPC to date in the U.S.

End of DRAFT U.S. Design Recommendations

7.3 Implementation Activities

UHPC has been shown to have extreme durability through high resistance to freeze-thaw cycling and chloride penetration, and advanced mechanical performance through increased compressive and flexural strengths, making it a prime candidate for structural highway systems, especially those exposed to aggressive environments like those found in northern regions of the U.S. and coastal areas. However, because of the enhanced properties of UHPC (such as higher compressive strengths), the direct implementation of UHPC into highway systems without a proper design code could result in an inefficiency of the material use. Wasting material is not only expensive; it is irresponsible, particularly in a decade in which engineers are well aware of the adverse effects that CO_2 emissions (from cement production) can have on global climate change. As such, it is imperative to consider efficient designs through optimization of bridge girders sections and deck systems.

140

UHPC appears to lock in some properties through the use of thermal treatment. Compressive strength, modulus of elasticity, Poisson's ratio, chloride penetration, freeze-thaw resistance and the coefficient of thermal expansion exhibited no change in properties once thermally cured. However, several properties and their impact on design and performance are still not well understood. Suggestions for further study address many of these items.

7.4   Suggested Future Work

As a result of this work, several items should be considered in future research. In this research Air-cured specimens were tested at a maximum of 28 days. It is of interest to see what happens over the period of months or years. Do the specimens continue to increase in strength or change modulus and approach an asymptotic ceiling, and if they do what is the limit of an Air-cured specimen? The point at which a thermal cure does not have an impact needs to be located. Also, finding a relationship between the compressive stress and modulus of elasticity of non-thermally cured specimens is of interest.

UHPC exhibits increasing load carrying capacity beyond first-crack because of the fiber reinforcement. More research is needed to better understand, and account for, the increase in flexural capacity of UHPC as a function of crack growth/development. Furthermore, differences in first-crack flexural strength for specimens tested under several curing regimes need to be identified for proper implementation into design codes. Also, the practical limits of allowable cracking for use in the design of structural elements need to be determined.

Thermally curing the specimens while under load is an unanswered question which needs work. Creep-testing research to date has been performed on small thermally cured specimens. The reality is that all prestressed elements would be creep loaded prior to production curing. The

strands would be released and the element would have the compressive force applied, then the element may be cured immediately or possibly stockpiled for some length of time before curing. There are two issues which need addressing. The first is the creep loading on a non-thermally cured specimen, and the second, what happens to the specimen when it is under load and exposed to the high temperatures of a thermal cure.

The durability properties of UHPC may show great improvements and it is foreseeable that it could be used as a sacrificial or wearing course over normal strength concrete. The bond characteristics of these two surfaces would need to be investigated.

Supplemental work is necessary to develop a broad understanding of all types of concretes classified as ultra-high performance concretes. Currently only research on Ductal® has been performed in the United States, and other UHPC materials should be investigated to develop a comprehensive understanding of UHPC performance.

The effects of self-healing in UHPC should be investigated further to determine whether long term benefits exist. Performing an ESEM or petrographic analysis on freeze-thaw specimens post testing may shed more light on this interesting effect. Additional petrographic analysis on the continued hydration of Air-cured versus thermally treated UHPC specimens will also help in properly describing the self-healing phenomena of UHPC.

A closer look at the dynamic response of UHPC undergoing freeze-thaw testing may provide information about the nature of the "skewed" effect on the frequency curves used to determine relative dynamic modulus. Furthermore, UHPC's resistance to freeze-thaw cycling in a saline environment should also be investigated, along with UHPC's resistance to deterioration if cracked prior to freeze-thaw cycling.

Research into the coefficient of thermal expansion of saturated UHPC specimens should also be investigated. The majority of the research to date has focused on the unsaturated CTE values of UHPC. Additionally, the interaction between UHPC elements and NSC or HPC elements due to thermal gradients should be researched to provide practical recommendations when using UHPC with other concretes. Additional studies on the effects of specimen age on UHPC's CTE value are valuable to prestressed concrete manufacturers to accurately estimating strand stress. Determining UHPC's saturated CTE value, thermal interaction with non-UHPC materials, and age effects are crucial to the implementation of UHPC as a viable structural material.

Besides superplasticizer, no admixtures were used in this research. The effects on long term durability by including accelerators during the mixing process may be important for those looking for rapid strength gain and long term durability. Alternate curing regimes, such as water baths have also not been examined thoroughly in the U.S. These studies can provide further flexibility when designing structures using UHPC.

And lastly, while UHPC shows promise as a material of choice for transportation infrastructure, design code development is an integral part of introducing any new material for application. Because of the increased ductility afforded by UHPC, design codes may need to consider a crack-width based approach to design instead of the current stress-based limit states. A rigorous study of section optimization (such as stout double-tee shapes for girders or waffle-slabs systems for slab bridges or deck panels) is warranted. Incorporating results from tests reported herein, in conjunction with other testing results by others as well as those suggested for further study, will provide a comprehensive document for designing UHPC structures.

(This page intentionally left blank)

References

American Concrete Institute-ACI (2005), *Building Code Requirements for Structural Concrete*, ACI Committee 318, Farmington Hills, Michigan.

American Concrete Institute - ACI (2002). "Guide to Durable Concrete." ACI 201.2R-92, ACI Committee 201, Farmington Hills, Michigan.

American Concrete Institute-ACI (1997), "State-of-the Art Report on High-Strength Concrete," *Manual of Concrete Practice-Part I*, ACI Committee 363, Farmington Hills, Michigan.

Ahlborn, T.M., Steinberg, E.P., Hartmann, J.L., Graybeal, B.A., Potter, J.L., and Volygi, J. (2003). "Ultra-High Performance Concrete-Study Tour 2002." *3rd International Symposium on High Performance Concrete*, PCI, Orlando, Florida.

Aitcin, P. (1998) "High-Performance Concrete," Routledge, New York, pp. 549, 551-552.

American Association of State Highway and Transportation Officials – AASHTO (2005)

AASHTO Designation: TP 60-00, Standard Method of Test for Coefficient of Thermal Expansion of Hydraulic Cement Concrete, 2004.

American Society for Testing and Materials. *Annual Book of ASTM Standards*. (2006)

ASTM C 39, Standard Test Method for Compressive Strength of Cylindrical Concrete Specimens, 2004.

ASTM C 78, Standard Test Method for Flexural Strength of Concrete (Using Simple Beam with Third-Point Loading), 2002.

ASTM C 192, Standard Practice for Making and Curing Concrete Test Specimens in the Laboratory, 2000.

ASTM C 215, Standard Test Method for Fundamental Transverse, Longitudinal, and Torsional Frequencies of Concrete Specimens, 2002.

ASTM C 490, Standard Practice for Use of Apparatus for the Determination of Length Change of Hardened Cement Paste, Mortar, and Concrete, 2004.

ASTM C 469, Standard Test Method for Static Modulus of Elasticity and Poisson's Ratio of Concrete in Compression, 2002.

ASTM C 617, Standard Practice for Capping Cylindrical Concrete Specimens, 1998.

ASTM C 666, Standard Test Method for Resistance of Concrete to Rapid Freezing and Thawing, 2003.

ASTM C 1018, Standard Test Method for Flexural Toughness and First-Crack Strength of Fiber-Reinforced Concrete (Using Beam With Third-Point Loading), 1997, (Withdrawn 2006).

ASTM C 1202, Standard Test Method for Electrical Indication of Concrete's Ability to Resist Chloride Ion Penetration, 2005.

ASTM C 1231, Standard Practice for Use of Unbonded Caps in Determination of Compressive Strength of Hardened Concrete Cylinders, 2000.

ASTM C 1437, Standard Test Method for Flow of Hydraulic Cement Mortar, 2001.

AFGV (2002) Association Française de Génie Civil *Interim Recommendations for Ultra High Performance Fibre-Reinforced Concretes*. SETRA (Service d'études techniques des routes et autoroutes). (Bétons Fibrés à Ultra-Hautes Performacnes – Recommandations Provisoires), France.

Banta, T.E. (2005). "Horizontal Shear Transfer Between Ultra High Performance Concrete and Lightweight Concrete." MS Thesis, Virginia Polytechnic Institute and State University, Blacksburg, VA.

Behloul, M., and Cheyrezy, M. (2002a). "Ductal Reference Projects." *Presentation at Bouygues Headquarters – Challenger*, St Quentin en Yveslines, France.

Behloul, M., and Cheyrezy, M. (2002b). "Seonyu Foot Bridge." *Presentation at Bouygues Headquarters – Challenger*, St Quentin en Yveslines, France.

Blais, P., and Couture, M. (1999). "Precast, Prestressed Pedestrian Bridge-World's First Reactive Powder Concrete Structure." *PCI Journal*, Vol. 44, No. 5, September-October 1999, pp. 60-71.

Bonneau, O., Lachemi, M., Dallaire, E., Dugat, J., and Aitcin, P. (1997). "Mechanical Properties and Durability of Two Industrial Reactive Powder Concretes." *ACI Materials Journal*, Vol. 94, No. 4, July/August 1997, pp. 286-290.

Bonneau, O., Vernet, C., Moranville, M., and Aitcin, P. (2000). "Characterization of the Granular Packing and Percolation Threshold of Reactive Powder Concrete." *Cement and Concrete Research*, 30(12), pp. 1861-1867.

Chen, L., Mindess, S., Morgan, D.R., Shah, S.P., Johnston, C.D., and Pigeon, M. (1995). "Comparative Toughness Testing of Fiber Reinforced Concrete." *Testing of Fiber Reinforced Concrete*, eds. Stevens, D.J., Banthia, N., Gopalaratnam, V.S., and Tatnall P.C. American Concrete Institute, Detroit, Michigan, pp. 41-75, 1995.

Cheyrezy, M., Behloul, M., Dowd, W., and Dauriac, C. (1998) "Reactive Powder Concrete (RPC) Application for Seismic Design." *American Concrete Institute Convention*, October 29, 1998, pp. 1-15.

Collins, A.R. (1944). "The destruction of concrete by frost." *Journal of the Institution of Civil Engineers*, 23(1), pp. 29-41.

DASYLab (2004). "DASYLab 8.0." ver. 8.00.04, DasyTech USA, Inc.

Dugat, J., Roux, N., and Rernier, G. (1996). "Mechanical Properties of Reactive Powder Concretes." *Materials and Structures/Matériaux et Constuctions*, Vol. 29, No. 188, May 1996, pp. 233-240.

Ductal® Reference, Lafarge North American, Calgary, Canada.

> Ductal® Reference T 001, Operating Procedure Compressive Test.
>
> Ductal® Reference T 002, Operating Procedure Cylinder & Prism Preparation.
>
> Ductal® Reference T 006, Operating Procedure Flow Test.
>
> Ductal® Reference T 009, Operating Procedure Cylinder End Preparation.

Edvardsen, C. (1999). "Water permeability and autogenous healing of cracks in concrete." *ACI Materials Journal*, Title No. 96-M56, pp. 448-454.

Emanuel, J. and Hulsey, J. (1977). "Prediction of the thermal coefficient of expansion of concrete." *ACI Journal*, 149-155.

Endicott, W.A. (2006) "Iowa Bridge gives Glimpse into the Future." *Ascent*, Summer 2006, pp. 41-46.

Federal Highway Administration (FHWA) (2006). "Achieving the Promise of Ultra-High Performance Concrete." FOCUS. Nov. Turner-Fairbank Highway Research Center Online. Online. 26 Jan. 2007.

Fehling, E., Schmidt, M., Bunje, K., Schreiber, W. (2008) "The "Gartnerplatzbrucke" Design of first hybrid UHPC-steel bridge across the river Fulda in Kassel, Germany." *Ultra-high performance concrete (UHPC)*, Second International Symposium on Ultra High Performance Concrete, Kassel University Press, Kassel, Germany, pp. 581-588.

Gatty, L., Bonnamy, S., Feylessoufi, A., Clinard, C., Richard, P., and VanDamme, H. (1998). "Silica Fume Distribution and Reactivity in Reactive Powder Concretes." *Fly ash, silica fume, slag & natural pozzolans in concrete : proceedings : Sixth CANMET/ACI International Conference : Bangkok, Thailand, SP 178*, American Concrete Institute, Farmington Hills, MI, pp.931-935.

Granger, S., Loukili, A., Pijaudier-Cabot, G., and Chanvillard, G. (2007). "Experimental characterization of the self-healing of cracks in an ultra high performance cementitious material: Mechanical tests and acoustic emission analysis." *Cement and Concrete Research*, 37, 519-527.

Graybeal, B. (2006a). "Material property characterization of ultra-high performance concrete." *Rep. No. FHWA-HRT-06-103*, Federal Highway Administration, Washington, D.C.

Graybeal, B. (2006b). "Nation's First Ultra-High Performance Concrete Bridge Opens in Iowa." *Research & Technology Transporter*, FHWA, June 2006.

Graybeal, B.A. (2005). "Characterization of the Behavior of Ultra-High Performance Concrete." PhD Dissertation, University of Maryland, College Park, Maryland.

Graybeal, B.A., and Hartmann, J.L. (2003) "Strength and Durability of Ultra-High Performance Concrete," *3rd International Symposium on High Performance Concrete*, PCI, Orlando, Florida.

Graybeal, B., Hartmann, J., and Perry, V. (2004). "Ultra-High Performance Concrete for Highway Bridges." AFGC: Concrete Structures: The Challenge of Creativity, *Fib Symposium 2004*, Avignon, France.

Graybeal, B. and Tanesi, J. (2007). "Durability of an Ultrahigh-Performance Concrete." *Journal of Materials in Civil Engineering*, ASCE, 19(10), pp. 848-854.

Hanle, L., Jayaraman, K., and Smith, J. (2004). "CO2 Emissions Profile of the U.S. Cement Industry." *13th Annual Emission Inventory Conference*, U.S. EPA, Clearwater, FL.

Harris, D.K. (2004). "Characterization of Punching Shear Capacity of Thin UHPC Plates." MS Thesis, Virginia Polytechnic Institute and State University, Blacksburg, Virginia.

Harris, D.K. and Roberts-Wollmann, C.L. (2005). "Characterization of the Punching Shear Capacity of Thin Ultra-High Performance Concrete Slabs." *Virginia Transportation Research Council and Virginia Department of Transportation*, Charlottesville, Virginia.

IDOT (2007). Email to C.G. Gilbertson. 9 August. "*Wapello County UHPC Project*."

Hartmann, J. and Graybeal, B. (2001). "U-HPC Testing: Shear," FHWA Structural Testing Laboratory.

Hartmann, J. and Graybeal, B. (2002). "Testing of Ultra-High-Performance Concrete Girders." *PCI Journal,* 47(2), January-February 2002, pp. 148-149.

Jacobsen, S. and Sellevold, E.J. (1996). "Self healing of high strength concrete after deterioration by freeze/thaw." *Cement and Concrete Research*, 26(1), 55-62.

148

JSCE (2006) Japan Society of Civil Engineers. "Recommendations for Design and Construction of Ultra High Strength Fiber Reinforced Concrete Structures (Draft)." Niwa, J., ed.

Jamet, D., Gettu, R., Gopalaratnam, V.S., and Aguado, A. (1995). "Toughness of Fiber-Reinforced High-Strength Concrete from Notched Beam Tests." *Testing of Fiber Reinforced Concrete*, eds. Stevens, D.J., Banthia, N., Gopalaratnam, V.S., and Tatnall P.C. American Concrete Institute, Detroit, Michigan, pp. 23-39, 1995.

Jungwirth, J., and Muttoni, A. (2004). "Structural Behavior of Tension Members in Ultra High Performance Concrete*." International Symposium on UHPC*, Kassel, Germany.

Keierleber, B., Bierwagen, D., Fanous, F., Phares, B., and Couture, I. (2007) "Design of Buchanan County, Iowa, Bridge Using Ultra High Performance Concrete and PI Girders." *Proceedings of the 2007 Mid-Continent Transportation Research Symposium*, Ames, Iowa, August 2007.

Kollmorgen, G.A. (2004). "Impact of Age and Size on the Mechanical Behavior of and Ultra-High Performance Concrete." MS Thesis in Civil Engineering, Michigan Technological University, Houghton, Michigan.

Kowald, T. (2004). "Influence of surface modified Carbon Nanotubes on Ultra-High Performance Concrete." *Proceedings of the International Symposium on Ultra High Performance Concrete*, Kassel University Press, Kassel, Germany, pp 195-202.

Lafarge North America (2006a). "Detroit-Columns." <http://www.imagineductal.com/imagineductal/public/eng/pdf/Detroit-Columns.pdf> (March 16, 2008).

Lafarge North America (2006b). "Wapello Bridge." <http://www.imagineductal.com/imagineductal/public/eng/pdf/WapelloBridge.pdf> (March 16, 2008).

Lee, M.-G., Chiu, C.-T., and Wang, Y.-C. (2005). "The study of bond strength and bond durability of reactive powder concrete." *Journal of ASTM International*, 2(7).

Litvan, G.G. (1972). "Phase transitions of adsorbates IV – Mechanism of frost action in hardened cement paste." *Journal of the American Ceramic Society*, 55(1), 38-42.

Lopez-Anido, R. (1998). "The Life-Cycle Cost Evaluation Report of Fiber Reinforced Polymer (FRP) Composite Bridge Decks." University of Maine. 2 June.

Loukili, A., Richard, P., and Lamirault, J. (1998). "A Study on Delayed Deformations of an Ultra High Strength Cementitious Material." *Recent Advances in Concrete Technology : proceedings : Fourth CANMET/ACI/JCI International Conference :* 136 *Tokushima, Japan, SP-179*, American Concrete Institute, Farmington Hills, MI, pp. 929-949.

Mamlouk, M., and Zaniewski, J. (1999) "Materials for Civil and Construction Engineers."
  Addison Wesley Longman, Inc., Menlo Park, CA, pp. 31-192.

Mehta, P.K., and Monteiro, P.J.M. (2006). "Concrete Microstructure, Properties, and Materials."
  The McGraw-Hill Companies, Inc., New York, NY.

MDOT (2007a). "Capital Scheduled Maintenance Bridge Manual." Michigan.gov. Online. 23
  July.

MDOT (2007b). Email to Dr. Theresa Ahlborn. 25 April. "UHPC progress report - real discount
  rate and deck timeline."

MERL (2006). "Michigan Engineers' Resource Library." (Database of Michigan bid items that
  allows project managers and engineers make road and bridge project estimates).

Mindess, S., Young, J.F., and Darwin, D. (2003). "Concrete 2nd Edition." Pearson Education,
  Inc., Upper Saddle River, New Jersey.

Misson, Donald Li (2008) "Influence of Curing Regimes on the Durability of an Ultra-High
  Performance Concrete." MS Thesis in Civil Engineering, Michigan Technological
  University, Houghton, Michigan.

Mitchell, L.J. (1953). "Thermal expansion tests on aggregates, neat cement, and concretes."
  Proceedings, ASTM, 53, 963-977.

Moore, B., and Bierwagen, D. (2006), "Ultra High Performance Concrete Highway Bridge."
  CTRE Online. Online. Iowa State University. 26 Feb. 2007.

Office of Management and Budget (2007). "Circular No. A-94 Revised." Whitehouse.gov.
  Online. OMB. 15 July.

Ohio LTAP Center (2007). "Preventative Maintenance/Repair Guidelines for Bridges and
  Culverts." ODOT On-line Bridge Maintenance Manual. Online. 15 July.

Nemegeer, D.E., and Tatnall, P.C. (1995). "Measuring Toughness Characteristics of SFRC-A
  Critical Reviwe of ASTM C 1018." *Testing of Fiber Reinforced Concrete*, eds. Stevens,
  D.J., Banthia, N., Gopalaratnam, V.S., and Tatnall P.C. American Concrete Institute,
  Detroit, Michigan, pp. 41-75, 1995.

O'Neil, E.F., Dauriac, C.E, and Gililand, S.K. (1997). "Development of Reactive Powder
  Concrete (RPC) Products in the United States Construction Market." *High- Strength
  Concrete : An International Perspective : papers presented at three halfday sessions at
  the ACI Convention in Montreal, SP-167*, American Concrete Institute, Farmington Hills,
  MI, pp. 249-261.

Perenchio, W. F. (1994). "Corrosion of Reinforcing Steel." *Significance of Tests and Properties of Concrete and Concrete-Making Materials*. STP 169C. Publication Code Number 04-169030-07. American Society for Testing and Materials, Philadelphia, PA. pp. 164-172.

Perry, V.H. (2003) "The World's First Long-Span Roof Constructed in Ductal[®]." Nova Award, 2003, http://www.cif.org/Nom2003/Nom22_03.pdf Viewed 04/17/2007.

Perry, V.H., and Zakariasen, D. (2004). "First Use of Ultra-High Performance Concrete for an Innovative Train Station Canopy." *Concrete Technology Today*, PCA, 25(2).

Perry, V.H., and Zakariasen, D. (2003) "Overview of UHPC Technology, Materials, Properties, Markets & Manufacturing." *3rd International Symposium on High Performance Concrete*, PCI, Orlando, Florida.

Peuse, Erron J., (2008) "Ultra-High Performance Concrete for Michigan Bridges – Material Behavior." MS Thesis in Civil Engineering, Michigan Technological University, Houghton, Michigan.

Pigeon, M. and Pleau, R. (1995). "Durability of Concrete in Cold Climates." *E & FN Spon*, London, UK, pp. 11-23.

Pine Instrument Company (2006). "AFCT1A / AFCT1C Coefficient of Thermal Expansion of Portland Cement Concrete Measurement System Operation Manual." Version 071206, Grove City, PA.

Powers, T.C. (1945). "A working hypothesis for further studies of frost resistance." *Journal of the American Concrete Institute*, 16(4), 245-272.

Powers, T.C. and Helmuth, R.A. (1953). "Theory of volume changes in hardened portland cement pastes during freezing." Proceedings of the Highway Research Board, 29, pp. 184-211.

Rebentrost, M. and Cavill, B. (2006). "Reactive Powder Concrete Bridges." AustRoads Conference, Perth, Australia.

Resplendino, J., and Petitjean, J. (2003). "Ultra-High Performance Concrete: First Recommendations and Examples of Application." *3rd International Symposium on High Performance Concrete*, PCI, Orlando, Florida.

Richard, P., and Cheyrezy, M. (1995). "Composition of reactive Powder Concretes." *Cement and Concrete Research*, Vol. 25, No. 7 October 1995, pp. 1501-1511.

Richard, P. and Cheyrezy, M. (1996). "Reactive Powder Concretes with High Ductility and 200-800 MPa Compressive Strength," *Concrete Technology: Past, Present, and Future*, *SP-144*, American Concrete Institute, Farmington Hills, MI, pp. 507-518.

151

RS Means (2005). Heavy Construction Cost Data 19th edition. Kingston: Reed, 2004.

Russell, H. (1999). "ACI Defines High-Performance Concrete," *Concrete International*, 21(2), February, pp. 56-57.

Schmidt, M., Fehling, E., Teichmann, T., Kai, B., and Roland, B. (2003). "Ultra-High Performance Concrete: Perspective for the precast concrete industry." *Concrete Precasting Plant and Technology*, 69(3), pp. 16-29.

Schmidt, M. and Fehling, E. (2005). "Ultra-High-Performance Concrete: Research, Development and Application in Europe." *Seventh International Symposium on the Utilization of High-Strength/High-Performance Concrete,* ACI Special Publication, Washington, D.C., USA, 228, pp 51-78

Searls, D. (2007). "Ductal Concrete by Lafarge." *Concrete Decor*, <http://www.concretedecor.net/All_Access/703/CD703-Technology.cfm> (March 16, 2008).

Semioli, W.J. (2001). "The New Concrete Technology." *Concrete International*, 2(11), November, pp. 75-79.

Sritharan, S., Bristow, B.J., and Perry, V.H. (2003) "Characterizing an Ultra High Performance Material for Bridge Applications Under Extreme Loads." *3rd International Symposium on High Performance Concrete*, PCI, Orlando, Florida.

Stanish, K.D., Hooton, R.D., and Thomas, M.D.A. (2000). "Testing the Chloride Penetration Resistance of Concrete: A Literature Review." *FHWA Contract DTFH61-97-R-00022*, University of Toronto, Toronto, Ontario, Canada.

Torres, S., and Eggers, J. (2005). "Capping Systems for High-Strength Concrete." *Transportation Research Board Annual Meeting CD-ROM*, 2006

Toutanji, H., McNeil, S., and Bayasi, Z. (1998). "Chloride Permeability and Impact Resistance of Polypropylene-Fiber-Reinforced Silica Fume Concrete." Cement and Concrete Research, 28(7), pp. 961-968

U.S. Department of Labor 2007. "Bureau of Labor Statistics." 30 Nov. 2006. U.S. Department of Labor Online. Online. 24 July. 2007.

Walker, S., Bloem, D.L., and Mullen, W.G. (1952). "Effects of temperature changes on concrete as influenced by aggregates." *ACI Journal Proceedings*, 48(8), 661-680.

Walls, J. III, and Smith, M.R. (1998), "Life-Cycle Cost Analysis in Pavement Design." FHWA-SA-98-079. FHWA, Pavement Division: Washington, DC. Sep.

APPENDIX A: EXPERIMENTAL TEST DATA

Specimen naming scheme

This appendix includes data from all specimens tested herein. A naming system was used to identify each specimen.

Compression Strength, Modulus of Elasticity, Poisson's Ratio, and Flexural Tests

The naming system followed the format of ***Batch number-Specimen geometry-Curing regime-Testing age-(optional character)***. The batch number followed the form of B(number) where the number was 1 through 7 was used with 7 being the batch without fibers. Specimen geometry was designated by C3 for 3 in. diameter cylinders and B2 for 2 in. x 2 in. x 11.25 in. beams. The curing regime followed the same designation as is laid out in Table 1.3.1 where A was Air-cured, TT was thermal treatment, DTT was delayed thermal treatment, and DDTT was double delayed thermal treatment. The testing age designation was the age in days at which the specimen was to be tested. The optional character was used only for the 2 in. x 2 in. x 11.25 in. beams because they were the only specimens in which more than one particular "geometry-curing regime-testing age" came from one batch. In this case, a letter A or B was included to facilitate record keeping.

An example of the specimen nomenclature would be ***B3-B2-A-28-B***. This specimen would have been cast out of batch 3, was a 2 in. x 2 in. x 11.25 in. beam, air treated, tested at an age of 28 days and been the second of the 2 in. x 2 in. x 11.25 in. beams made from the batch. Another example would be ***B2-C3-TT-14***. This specimen was cast from the second batch, a

3 in. x 6 in. cylinder, thermally treated, and tested at 14 days. Because no other 3 in. x 6 in. cylinders thermally treated and being tested at 14 days came from batch 2, the optional A or B tag was left off the specimen identifier.

Rapid Chloride Penetration, Freeze-Thaw Resistance, Coefficient of Thermal Expansion

A total of nine batches were cast for testing (with several more cast for specimen shakedown) and 79 samples were tested to observe the durability characteristics of UHPC (**Error! Reference source not found.**). A specimen nomenclature was used to identify batch number, test procedure, curing regime and testing age. All specimens were marked with the following nomenclature after demolding: ***Batch number-Test procedure-(optional side study label)Curing regime-Testing age(optional letter within batch)***. Batch numbers began at ***A*** and ended at ***D*** for the batches incorporating coefficient of thermal expansion and rapid chloride penetration test specimens, and began again at ***M*** and ended at ***S*** (skipping the letter ***O*** label to avoid confusion) for batches comprising of primarily freeze-thaw test specimens. Supplementary CTE and RCPT specimens were also cast in batches ***M*** through ***S*** with excess material. The test procedures were designated on each specimen as ***CTE*** for the coefficient of thermal expansion test, ***RCP*** for the rapid chloride penetration test, ***FT*** for the freeze-thaw test, and ***C*** for the compression test. Curing regime designations followed the format of ***TT*** for thermal treatment curing and ***A*** for ambient air curing (Note: In this report, when referring to the type of curing regime, the abbreviation "Air" is used. When referring to a specific specimen's nomenclature, the entire nomenclature will be used). Additionally, when a specimen was used for a side study test rather than actual testing, ***SS*** was added before the curing regime notation. So a side study air cured specimen would have the label of ***SSA***

rather than *A*. The final number in the nomenclature specifies the number of days after casting that a specimen was tested. For example, *Specimen X* marked **N-FT-A-28** would imply that *Specimen X* was cast from batch N for the purpose of freeze-thaw testing and was ambient air cured for 28-days prior to testing. Similarly, *Specimen Y* marked **N-FT-SSA-28** means that *Specimen Y* was cast from batch N for the purpose of freeze-thaw side study testing and was ambient cured for 28-days prior to testing. However, when two or more specimens from a particular batch were cured the same, for the same amount of time, and tested under the same test (e.g. – companion compression test cylinders), an additional letter (*A* – *D*) was added at the end of the specimen nomenclature. For example, Batch S included three specimens designated as *S-C-TT-28A*, *S-C-TT-28B*, and *S-C-TT-28C* to distinguish between the individual specimens. In this study, only companion compression test cylinders employed this additional nomenclature scheme.

Table A.1: Data for Air-Cured Cylindrical Specimens

Specimen	Compressive Stress (ksi)	Modulus of Elasticity (ksi)	Poisson's Ratio	Degrees out of Perpendicularity
B1-C3-A-3	13.517	NR	NR	0.327
B2-C3-A-3	14.656	NR	NR	0.418
B3-C3-A-3	14.162	6859.481	0.2003	0.155
B4-C3-A-3	14.578	6912.080	0.1900	0.189
B5-C3-A-3	15.098	6954.998	0.2020	0.132
B6-C3-A-3	14.667	6911.809	0.1995	0.195
B1-C3-A-7	20.378	7688.747	0.2068	0.332
B2-C3-A-7	20.141	7493.304	0.2044	0.327
B3-C3-A-7	19.948	7666.874	0.2031	0.218
B4-C3-A-7	19.939	7537.427	0.2064	0.074
B5-C3-A-7	19.281	7356.481	0.2109	0.103
B6-C3-A-7	19.828	7376.915	0.1989	0.120
B1-C3-A-14	22.049	7777.159	0.2085	0.172
B2-C3-A-14	22.727	7899.073	0.2095	0.149
B3-C3-A-14	21.710	7906.809	0.2050	0.149
B4-C3-A-14	21.972	7813.602	0.2020	0.126
B5-C3-A-14	21.796	7850.511	0.2065	0.218
B6-C3-A-14	23.542	7943.388	0.2062	0.160
B1-C3-A-28	24.606	7905.299	0.2114	0.115
B2-C3-A-28	23.378	7727.810	0.1961	0.149
B3-C3-A-28	23.316	8056.596	0.2190	0.223
B4-C3-A-28	24.037	7993.116	0.1999	0.235
B5-C3-A-28	23.934	7736.127	0.2035	0.149
B6-C3-A-28	24.354	7756.123	0.1995	0.212
B7-C3-A-28A	25.585	7795.399	0.1952	0.109
B7-C3-A-28B	24.501	7792.813	0.2022	0.080
B7-C3-A-28C	25.716	7540.652	0.2012	0.109
B7-C3-A-28D	24.742	7668.635	0.2048	0.132
B7-C3-A-28E	25.160	7675.370	0.1980	0.109
B7-C3-A-28F	23.713	7701.819	0.1995	0.092

Table A.2: Data for TT Cylindrical Specimens

Specimen	Compressive Stress (ksi)	Modulus of Elasticity (ksi)	Poisson's Ratio	Degrees out of Perpendicularity
B1-C3-TT-7	30.503	8047.005	0.2012	0.338
B2-C3-TT-7	31.180	8079.182	0.2090	0.418
B3-C3-TT-7	30.152	7879.787	0.2060	0.080
B4-C3-TT-7	28.591	7948.310	0.2135	0.126
B5-C3-TT-7	30.572	8151.638	0.2024	0.120
B6-C3-TT-7	30.676	8231.884	0.2047	0.092
B1-C3-TT-14	30.215	8175.464	0.1968	0.138
B2-C3-TT-14	32.014	8359.577	0.2064	0.080
B3-C3-TT-14	30.081	8155.241	0.2063	0.172
B4-C3-TT-14	28.153	8127.066	0.2124	0.103
B5-C3-TT-14	29.046	8127.497	0.2063	0.115
B6-C3-TT-14	31.000	8348.119	0.2064	0.120
B1-C3-TT-28	31.095	8166.650	0.2068	0.138
B2-C3-TT-28	30.845	8080.693	0.2050	0.115
B3-C3-TT-28	30.808	8124.252	0.2119	0.115
B4-C3-TT-28	30.994	8048.575	0.2046	0.143
B5-C3-TT-28	31.884	8198.986	0.2025	0.138
B6-C3-TT-28	30.944	8066.015	0.1991	0.126
B7-C3-TT-28A	33.025	7793.664	0.1968	0.052
B7-C3-TT-28B	29.456	7844.217	0.1992	0.074
B7-C3-TT-28C	30.154	7858.390	0.2096	0.097
B7-C3-TT-28D	32.667	7929.705	0.2054	0.103
B7-C3-TT-28E	34.063	8020.766	0.2029	0.103

Table A.3: Data for DTT and DDTT Cylindrical Specimens

Specimen	Compressive Stress (ksi)	Modulus of Elasticity (ksi)	Poisson's Ratio	Degrees out of Perpendicularity
B1-C3-DTT-14	29.859	9003.986	0.2233	0.097
B2-C3-DTT-14	29.712	8098.644	0.2115	0.166
B3-C3-DTT-14	28.572	8082.995	0.1987	0.097
B4-C3-DTT-14	28.869	8393.630	0.2078	0.092
B5-C3-DTT-14	30.795	8180.276	0.2005	0.103
B6-C3-DTT-14	30.740	8128.955	0.2063	0.166
B1-C3-DTT-28	30.424	8181.310	0.2085	0.080
B2-C3-DTT-28	29.375	8172.989	0.1977	0.057
B3-C3-DTT-28	29.210	8096.720	0.2226	0.086
B4-C3-DTT-28	29.420	8144.191	0.2091	0.086
B5-C3-DTT-28	30.378	8129.613	0.1980	0.120
B6-C3-DTT-28	30.761	8239.005	0.2085	0.115
B7-DTT-28A	24.785	7786.891	0.1995	0.109
B7-DTT-28B	32.340	7807.098	0.2025	0.126
B7-DTT-28C	32.278	7872.662	0.1988	0.103
B7-DTT-28D	30.282	7544.063	0.1984	0.155
B7-DTT-28E	30.015	7979.124	0.1994	0.086
B1-C3-DDTT-28	28.098	8178.926	0.2025	0.298
B2-C3-DDTT-28	30.706	8121.966	0.2031	0.109
B3-C3-DDTT-28	29.154	8164.106	0.2012	0.103
B4-C3-DDTT-28	29.726	8001.333	0.2025	0.097
B5-C3-DDTT-28	29.431	8026.161	0.2065	0.149

Table A.4: Data for Air-Cured Flexural Specimens

Specimen	Corrected First Crack Strength (ksi)	First Crack Strength (ksi)	Deflection at First Crack (in.)	Equivalent Flexural Strength (ksi)	Ultimate Load (kip)	I_5	I_{10}	I_{20}	I_{30}	I_{40}	$R_{5,10}$	$R_{10,20}$	$R_{20,30}$	$R_{30,40}$
B1-B2-A-28A	0.778	1.402	0.00190	4.862	4.322	6.8	17.4	44.2	74.2	107.4	212	268	300	332
B1-B2-A-28B	0.757	1.365	0.00183	4.637	4.225	6.9	18.5	46.8	77.1	109.5	232	284	302	325
B2-B2-A-28A	0.772	1.391	0.00176	5.482	4.994	6.9	18.0	46.7	78.5	113.4	221	288	318	348
B2-B2-A-28B	0.772	1.392	0.00182	4.603	3.990	6.7	17.7	45.2	76.2	108.8	221	275	310	326
B3-B2-A-28A	0.716	1.291	0.00168	4.643	4.127	6.9	18.0	46.4	78.8	112.1	222	285	323	333
B3-B2-A-28B	0.566	1.021	0.00146	3.575	3.724	6.9	17.6	44.9	76.6	109.9	214	273	317	334
B4-B2-A-28A	0.700	1.262	0.00163	4.878	4.445	6.8	18.1	46.9	79.5	114.2	225	288	327	347
B4-B2-A-28B	0.642	1.157	0.00168	4.862	4.770	7.3	19.3	49.4	84.2	121.1	238	302	348	369
B5-B2-A-28A	0.747	1.348	0.00198	4.213	4.069	6.9	17.4	42.7	70.3	100.4	211	253	277	300
B5-B2-A-28B	0.823	1.484	0.00185	4.308	3.829	6.1	16.3	40.8	67.5	95.3	204	245	267	278
B6-B2-A-28A	0.792	1.429	0.00186	4.308	3.829	6.6	16.7	41.3	67.4	93.6	202	246	261	262
B6-B2-A-28B	0.873	1.574	0.00203	4.626	4.215	6.6	16.5	41.2	68.7	97.7	198	247	275	290
B7-B2-A-28A	0.888	1.601	0.00215	Not Applicable										
B7-B2-A-28B	0.741	1.336	0.00198	Not Applicable										
B7-B2-A-28C	0.864	1.559	0.00203	Not Applicable										

Table A.5: Data for TT Flexural Specimens

Specimen	Corrected First Crack Strength (ksi)	First Crack Strength (ksi)	Deflection at First Crack (in.)	Equivalent Flexural Strength (ksi)	Ultimate Load (kip)	I_5	I_{10}	I_{20}	I_{30}	I_{40}	$R_{5,10}$	$R_{10,20}$	$R_{20,30}$	$R_{30,40}$
B1-B2-TT-28A	1.078	1.943	0.00248	5.764	5.124	6.6	16.0	39.3	65.2	92.9	188	233	258	277
B1-B2-TT-28B	1.101	1.986	0.00263	5.367	4.770	6.8	16.5	40.1	66.0	91.9	194	236	259	259
B2-B2-TT-28A	1.038	1.873	0.00240	5.644	5.017	6.5	16.4	40.6	67.4	NR	199	242	269	NR
B2-B2-TT-28B	0.967	1.744	0.00247	5.197	4.619	7.0	17.5	42.6	70.4	99.4	211	250	278	291
B3-B2-TT-28A	0.967	1.743	0.00230	5.230	4.649	6.5	16.5	40.4	67.1	95.7	200	238	268	286
B3-B2-TT-28B	1.042	1.878	0.00233	4.987	4.433	6.0	14.8	35.9	59.7	85.3	177	211	238	257
B4-B2-TT-28A	0.965	1.739	0.00203	5.622	4.997	6.7	16.8	42.1	69.6	98.9	202	253	275	293
B4-B2-TT-28B	0.989	1.783	0.00229	5.444	4.960	6.7	16.9	42.6	70.5	99.3	204	257	279	288
B5-B2-TT-28A	1.187	2.140	0.00264	4.978	4.314	6.5	15.7	37.2	59.2	NR	185	215	220	NR
B5-B2-TT-28B	1.209	2.180	0.00258	6.124	5.307	6.2	15.4	38.1	62.6	88.8	184	227	246	262
B6-B2-TT-28A	1.134	2.045	0.00238	5.348	4.873	6.1	15.0	36.0	59.4	84.3	178	210	234	248
B6-B2-TT-28B	1.047	1.889	0.00226	5.539	4.924	6.2	15.9	38.8	63.8	91.1	194	229	250	272
B7-B2-TT-28A	1.051	1.896	0.00253	Not Applicable										
B7-B2-TT-28B	1.123	2.026	0.00284	Not Applicable										
B7-B2-TT-28C	1.201	2.166	0.00288	Not Applicable										

A-9

Table A.6: Data for DTT Flexural Specimens

Specimen	Corrected First Crack Strength (ksi)	First Crack Strength (ksi)	Deflection at First Crack (in.)	Equivalent Flexural Strength (ksi)	Ultimate Load (kip)	I_5	I_{10}	I_{20}	I_{30}	I_{40}	$R_{5,10}$	$R_{10,20}$	$R_{20,30}$	$R_{30,40}$
B1-B2-DTT-28A	1.219	2.197	0.00277	NR	NR	6.5	16.1	39.2	NR	NR	192	231	NR	NR
B1-B2-DTT-28B	1.184	2.136	0.00276	5.773	5.132	6.6	16.1	39.0	64.0	90.7	192	229	249	267
B2-B2-DTT-28A	1.161	2.094	0.00256	5.185	4.609	6.5	15.5	37.5	61.4	NR	181	220	239	NR
B2-B2-DTT-28B	1.133	2.043	0.00249	4.575	4.067	6.0	14.7	35.3	56.9	NR	175	205	217	NR
B3-B2-DTT-28A	1.013	1.827	0.00247	4.534	4.365	6.3	15.2	37.1	60.7	84.7	178	219	236	239
B3-B2-DTT-28B	0.961	1.733	0.00267	4.832	4.768	6.7	16.7	40.2	66.2	93.5	200	235	259	273
B4-B2-DTT-28A	1.136	2.049	0.00271	4.481	4.083	6.1	14.8	35.2	56.2	76.7	174	204	209	205
B4-B2-DTT-28B	1.168	2.106	0.00267	4.732	4.311	6.2	15.3	35.7	57.3	79.3	183	204	215	220
B5-B2-DTT-28A	1.284	2.315	0.00285	4.475	4.077	6.2	14.7	33.4	51.4	NR	171	187	180	NR
B5-B2-DTT-28B	1.250	2.255	0.00287	5.227	4.646	6.1	14.8	34.7	55.9	NR	175	199	212	NR
B6-B2-DTT-28A	1.305	2.354	0.00295	5.405	4.925	6.1	14.8	34.5	55.7	NR	175	197	212	NR
B6-B2-DTT-28B	1.288	2.322	0.00299	5.642	5.015	6.4	15.6	36.8	59.9	NR	183	213	231	NR
B7-B2-DTT-28A	1.142	2.059	0.00282	Not Applicable										
B7-B2-DTT-28B	1.187	2.141	0.00314	Not Applicable										
B7-B2-DTT-28C	1.293	2.331	0.00324	Not Applicable										

Table A.7: RCPT Specimen Data Sorted by Batch

Specimen ID	Age	Charge Passed (coulombs)	Chloride Ion Penetrability
1A-RCP-TT-7	7	12	Negligible
1A-RCP-A-28	28	93	Negligible
1A-RCP-TT-28	28	16	Negligible
1B-RCP-TT-7	7	9	Negligible
1B-RCP-A-28	28	78	Negligible
1B-RCP-TT-28	28	13	Negligible
1C-RCP-A-28	28	57	Negligible
1C-RCP-TT-28	28	11	Negligible
D-RCP-A-28	28	73	Negligible
D-RCP-TT-28	28	19	Negligible
S-RCP-TT-7	8	10	Negligible

Table A.8: RCPT Specimen Data Sorted by Curing Regime

Specimen ID	Specimen age at time of testing (days)	Charge Passed (coulombs)	Chloride Ion Penetrability
1A-RCP-TT-7	7	12	Negligible
1B-RCP-TT-7	7	9	Negligible
S-RCP-TT-7	8	10	Negligible
	Average	**10**	
	St. Dev.	**1.5**	
	COV (%)	**15**	
1A-RCP-TT-28	28	16	Negligible
1B-RCP-TT-28	28	13	Negligible
1C-RCP-TT-28	28	11	Negligible
D-RCP-TT-28	28	19	Negligible
	Average	**15**	
	St. Dev.	**3.5**	
	COV (%)	**24**	
1A-RCP-A-28	28	93	Negligible
1B-RCP-A-28	28	78	Negligible
1C-RCP-A-28	28	57	Negligible
D-RCP-TT-28	28	73	Negligible
	Average	**75**	
	St. Dev.	**15**	
	COV (%)	**20**	

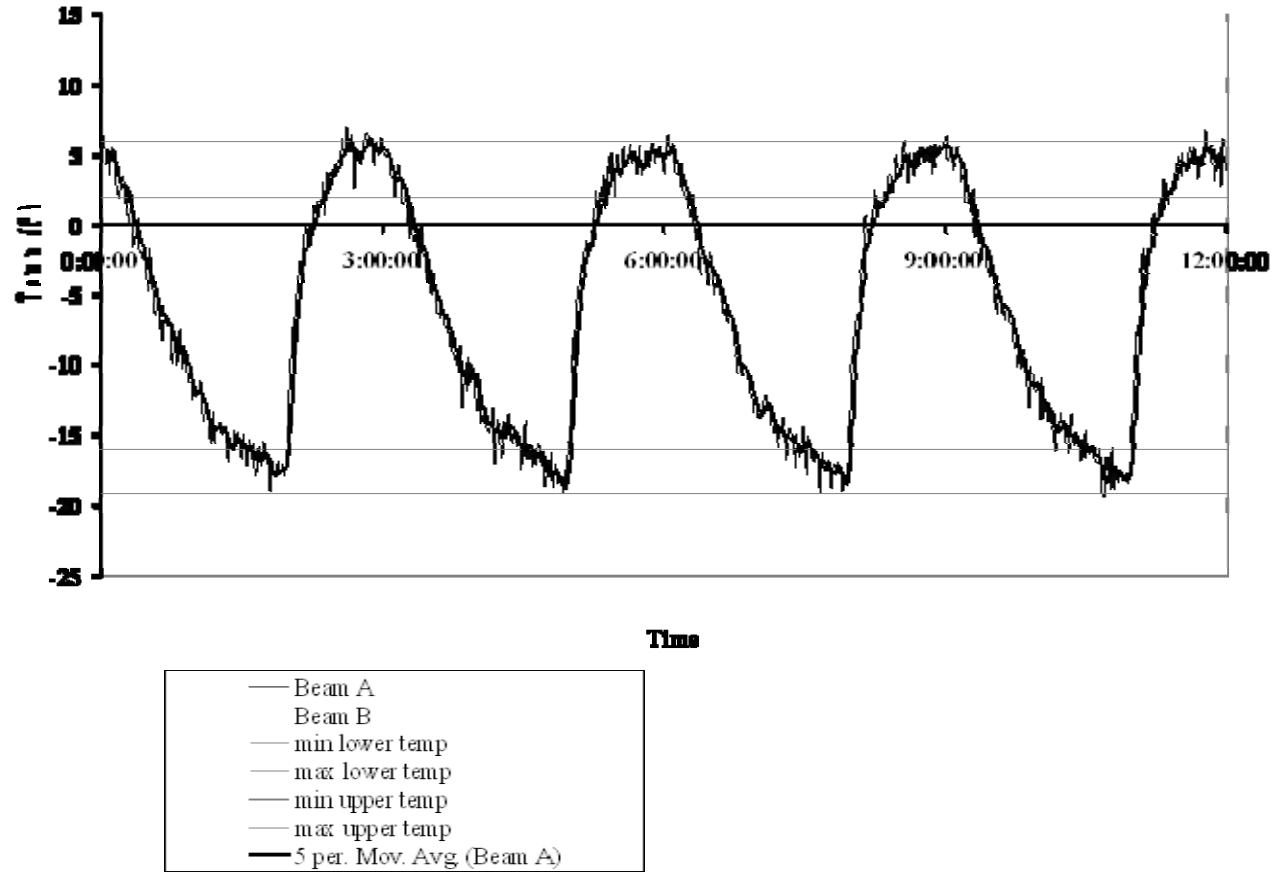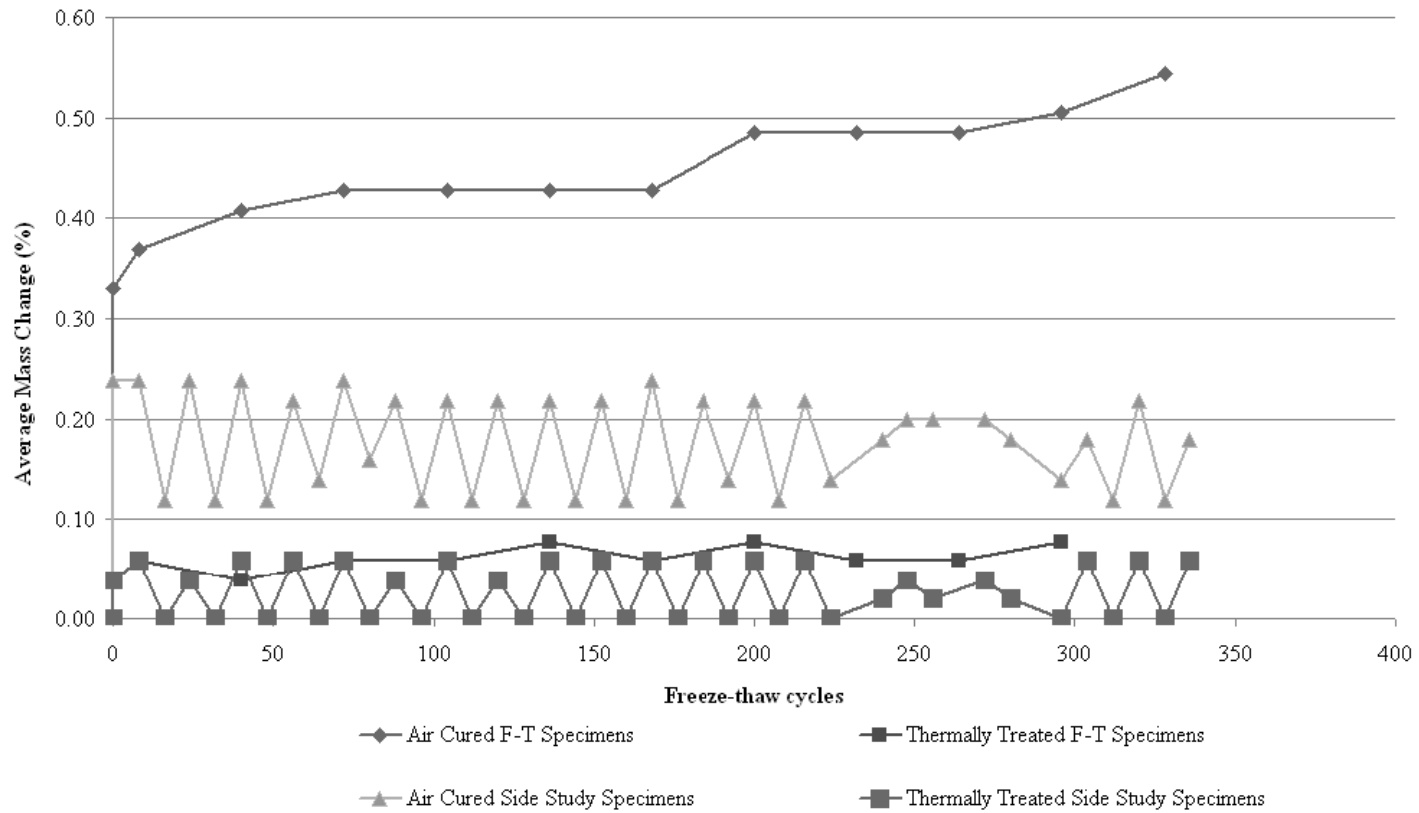**Figure A.9: Sample Freeze-Thaw Cycle Temperature – Position A17**

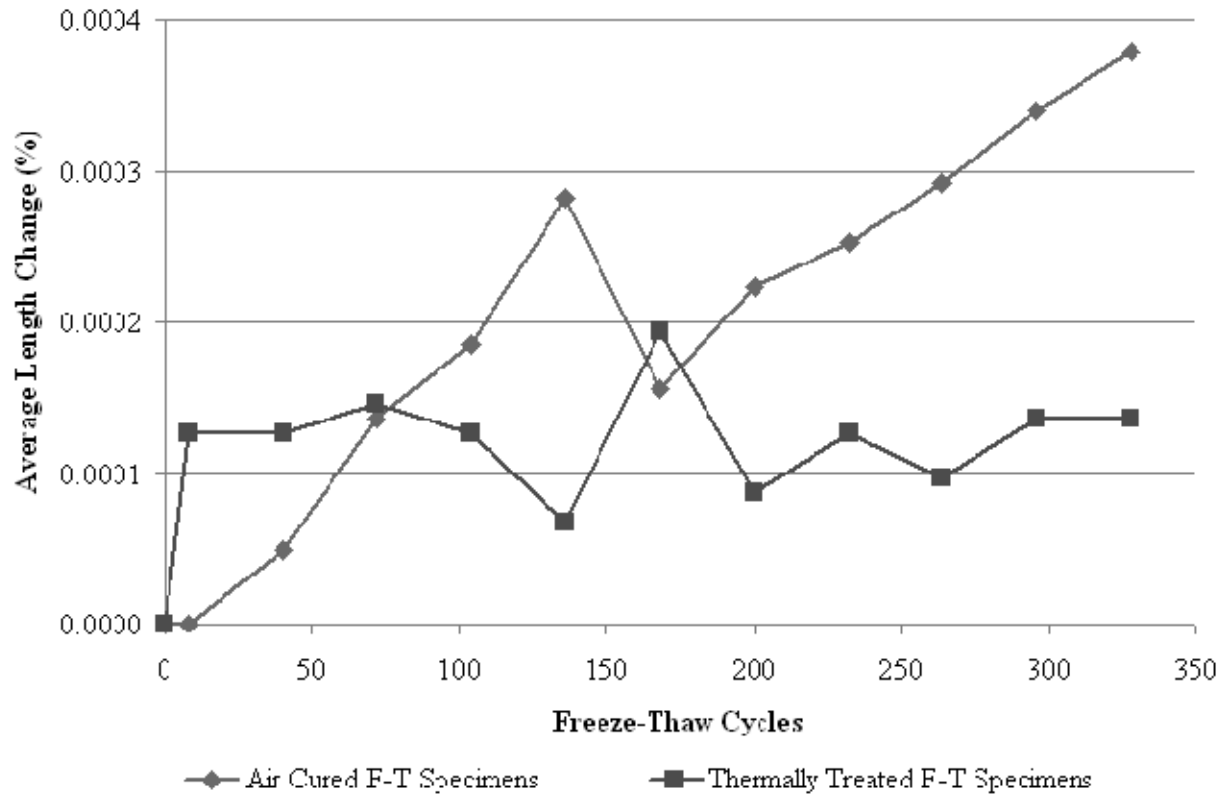**Figure A.10: Average Mass Change of UHPC Freeze-Thaw and Side Study Specimens**

Figure A.11: Average Length Change of UHPC Specimens Undergoing Freeze-Thaw Cycling

Table A.12: Michigan Tech CTE Summary Report on UHPC

Date	Core	Frame S/N	L_o	ΔL_{m1}	ΔL_{m2}	CTE_1	CTE_2	CTE_{avg} (°C)	CTE_{avg} (°F)	Not tested on correct day
5/22/2007	1A-CTE-A-3	1135	175.49	-0.1050	0.1067	13.3E-06	13.5E-06	13.4E-06	7.44E-06	
5/27/2007	1A-CTE-A-7	1135	177.70	0.1067	-0.1056	14.0E-06	13.8E-06	13.9E-06	7.73E-06	x
6/3/2007	1A-CTE-A-14	1135	177.20	0.1077	-0.1077	14.0E-06	14.0E-06	14.0E-06	7.79E-06	
6/15/2007	1A-CTE-A-28	1135	177.99	0.1040	-0.1040	13.7E-06	13.7E-06	13.7E-06	7.59E-06	
6/16/2007	1A-CTE-TT-28	1135	177.80	0.1088	-0.1093	14.3E-06	14.4E-06	14.3E-06	7.97E-06	
5/26/2007	1B-CTE-A-3	1135	178.12	-0.1029	0.1040	13.5E-06	13.7E-06	13.6E-06	7.56E-06	
5/30/2007	1B-CTE-A-7	1135	177.75	0.1023	-0.1023	13.4E-06	13.4E-06	13.4E-06	7.44E-06	x
6/5/2007	1B-CTE-A-14	1135	178.76	0.1018	-0.1023	13.5E-06	13.6E-06	13.6E-06	7.53E-06	
6/19/2007	1B-CTE-A-28	1135	177.82	-0.1072	0.1083	14.1E-06	14.2E-06	14.2E-06	7.89E-06	
5/29/2007	1C-CTE-A-3	1135	176.73	0.1066	-0.1050	13.8E-06	13.5E-06	13.7E-06	7.59E-06	
6/1/2007	1C-CTE-A-7	1135	177.25	-0.1061	0.1067	13.8E-06	13.9E-06	13.8E-06	7.69E-06	
6/8/2007	1C-CTE-A-14	1135	177.03	0.1067	-0.1077	13.8E-06	14.0E-06	13.9E-06	7.73E-06	
6/22/2007	1C-CTE-A-28	1135	178.07	0.1061	-0.1050	14.0E-06	13.8E-06	13.9E-06	7.73E-06	
6/24/2007	1C-CTE-TT-28	1135	177.64	0.1120	-0.1137	14.7E-06	15.0E-06	14.8E-06	8.25E-06	x
6/6/2007	1D-CTE-A-7	1135	177.05	0.1061	-0.1050	13.8E-06	13.6E-06	13.7E-06	7.61E-06	
7/3/2007	M-CTE-A-7	1135	176.09	0.1066	-0.1056	13.6E-06	13.5E-06	13.6E-06	7.53E-06	
7/23/2007	M-CTE-TT-28	1135	177.80	0.1142	-0.1126	15.1E-06	14.8E-06	15.0E-06	8.31E-06	

Table A.12 (continued): Michigan Tech CTE Summary Report on UHPC

Date	Core	Frame S/N	L_o	ΔL_{m1}	ΔL_{m2}	CTE_1	CTE_2	CTE_{avg} (^oC)	CTE_{avg} (^oF)	Not tested on correct day
7/6/2007	N-CTE-A-7	1135	176.36	-0.1083	0.1072	13.9E-06	13.8E-06	13.9E-06	7.69E-06	
7/26/2007	N-CTE-TT-28	1135	177.09	0.1137	-0.1126	14.8E-06	14.7E-06	14.8E-06	8.21E-06	
7/11/2007	P-CTE-TT-7	1135	178.41	0.1110	-0.1110	14.7E-06	14.7E-06	14.7E-06	8.19E-06	
7/14/2007	R-CTE-TT-7	1135	177.85	0.1110	-0.1115	14.6E-06	14.7E-06	14.7E-06	8.14E-06	
7/17/2007	S-CTE-TT-7	1135	177.58	0.1131	-0.1131	14.9E-06	14.9E-06	14.9E-06	8.26E-06	

Table A.13: Mass change study on epoxy coated UHPC CTE specimens

Air-cured UHPC Specimens				Thermally-treated UHPC Specimens		
Specimen	Age of specimen at testing (days)	Mass Change (%)		Specimen	Age of specimen at testing (days)	Mass Change (%)
1A-CTE-A-3	3	0.00		1A-CTE-TT-28	28	0.03
1A-CTE-A-7	7	0.00		1C-CTE-TT-28	28	0.03
1A-CTE-A-14	14	0.05		M-CTE-TT-28	28	N/A
1A-CTE-A-28	28	0.03		N-CTE-TT-28	28	N/A
1B-CTE-A-3	3	N/A		P-CTE-TT-7	7	0.05
1B-CTE-A-7	7	0.05		R-CTE-TT-7	7	0.00
1B-CTE-A-14	14	0.00		S-CTE-TT-7	7	0.01
1B-CTE-A-28	28	0.03		Mean		0.02
1C-CTE-A-3	3	N/A		Standard Dev.		0.02
1C-CTE-A-7	7	0.03		COV (%)		84.94
1C-CTE-A-14	14	0.03				
1C-CTE-A-28	28	0.03				
D-CTE-A-7	7	0.03				
D-CTE-A-28	28	0.03				
M-CTE-A-7	7	0.03				
N-CTE-A-7	7	0.03				
Mean		0.03				
Standard Dev.		0.02				
COV (%)		66.44				

APPENDIX B – CTE Test Procedure Modifications

SECTION C - DESCRIPTION/SPECIFICATIONS/WORK STATEMENT

NOTE: Please see Section J for Attachments and References.

BACKGROUND

The Federal Highway Administration requests proposals for the development and manufacture of automated testing equipment for the measurement of the Coefficient of Thermal Expansion (CTE) of Portland Cement Concrete (PCC). The equipment is to be accurate, practical, and capable of being made commercially available for the testing of concrete cores and cylinders used to characterize the thermal properties of saturated hydraulic cement concrete for pavements structures.

The CTE equipment developed must generally meet the objectives and requirements of the American Association of State Highway and Transportation Officials (AASHTO), "Standard Test Method for the Coefficient of Thermal Expansion of Hydraulic Cement Concrete" (AASHTO Designation TP60-00). Consideration will also be given to equipment and procedures that improves on the technology and practicality of the AASHTO procedure. *A copy of TP60-00 is available for inspection upon request. See Reference 1.*

The precision of the equipment developed must be as good as or better than that exhibited by several sets of prototype equipment designed and fabricated at the FHWA Turner-Fairbank Highway Research Center (TFHRC). This prototype equipment is currently being used to test the CTE of cores taken from PCC pavements across the United States as part of the Long Term Pavement Performance (LTPP) program. In limited duplicate tests made on about 130 specimens from the LTPP program data set, the median difference between the two test results for CTE was 0.4×10^{-6} per °C, and 75 percent of the differences between the two results were less than 0.9×10^{-6} per °C. It also expected that results obtained from new equipment will be comparable to results from the same samples tested in the existing TFHRC prototype equipment, taking into account the within laboratory precision exhibited for the LTPP work.

AASHTO TP60-00 contains schematic figures depicting a CTE test frame like the one used at TFHRC. Photographs and a description of the TFHRC equipment are provided in Attachment 5, and in the section of "Thermal Concrete of Portland Cement Concrete" from the FHWA website, a copy of which is provided as Attachment 6.

OBJECTIVE

The initial purpose for developing automated and practical equipment for the determination of the CTE of concrete is to enable performance of detailed ruggedness studies, to be run in at least three laboratories in accordance with ASTM Practice C 1067, "Conducting a Ruggedness or Screening Program for Test Methods for Construction Materials". The ruggedness evaluation will use the newly developed equipment and the appropriate procedures in general accord with AASHTO TP60. If the ruggedness testing is satisfactory it is anticipated that revisions to

AASHTO TP60 will be proposed as needed, and a more comprehensive interlaboratory study will be initiated to develop a precision statement for the method. At that time, additional laboratories will need to acquire the new equipment to participate in the precision study.

It is difficult to estimate the overall commercial market for automated equipment to measure CTE. CTE has been identified as a key parameter in concrete pavement design and will be included in the new AASHTO Pavement Design Guide now in the evaluation process prior to publication by AASHTO. Because of this the State Departments of Transportation (DOTs) may want to acquire the CTE equipment to evaluate PCC for pavements and structures. In addition, Federal Government laboratories, private consultants, and universities performing research, design, and forensic analyses of PCC pavements, airfields, and structures may require the equipment to measure CTE accurately and efficiently. Reference 2 provides links to two websites that discuss the development of the new AASHTO Pavement Design Guide. Reference 3 provides general discussion on the importance of the thermal characteristics of concrete and concrete aggregates.

SPECIFICATIONS

The CTE equipment must meet, at a minimum, the following criteria:

- Ability to test concrete cores or cylinders with diameters ranging from 90 to 160 mm and lengths ranging from 170 to 210 mm.

- Ability to run at least two tests (i.e. tests on two different specimens) at one time.

- Ability to maintain specimens in a saturated state during the test, to accurately cycle the temperature of the concrete through the test range, and to facilitate the stabilization of the length change of the specimens at thermal equilibrium for each of the target test temperatures ($5°$ C to $60°$ C).

- Ability to select the point temperatures to the nearest $1°$ C and to maintain the temperature of the specimens and the surrounding water at a stable temperature (within $\pm 0.1°$ C of set point.

    1. Clarification of temperature requirements from FHWA 10/19/04:
       The unit shall be... Settable to 1°C,
       Readable to 0.1°C,
       Accurate to 0.2°C,
       Stable to 0.1°C, and
       Reported to 0.1°C.

- Ability to detect and record the actual temperature of each of the specimens (if specimens have embedded thermocouples or other means of temperature detection) and the surrounding water to the nearest $0.1°$ C. At least four temperature-measuring devices shall be used to assure consistency and accuracy of the temperature during the test.

- Ability to detect and record the actual length change of each of the specimens to the

B-2

- Ability to run the test and acquire data automatically after the specimens have been mounted in the device, using a programmable controller and data acquisition device(s) or other suitable means. This shall include:

    o The ability to automatically cycle the water bath (or other testing chamber) according to the requirements of AASHTO TP60-00
    o The ability to detect when temperature and length have stabilized (e.g., to ensure consistency of length change readings to within 0.00125 mm [0.00005 in.] and temperature to within 0.1˚ C over a 30-minute time period before moving to the next cycle change)
    o The ability to collect data for temperature and length change at user-defined time intervals
    o The ability to easily transfer data electronically to other data storage or computers for calculation and evaluation

- Ability to use either SI or English units and values for running the test.

- The equipment shall be designed for durability and long life. Non-corroding materials and parts shall be used to minimize the need for coatings and frequent maintenance.

- Other material and manufacturing considerations with regard to durability and longevity shall be identified and incorporated to the extent practicable.

- All accessories required for operation and calibration (other than standard, readily available tools and supplies) shall be provided. Any standard tools or supplies that are required accessories for operation or calibration shall be specified in sufficient detail to allow the user to obtain correct items. (For example, caliper, comparator, or another suitable device to measure the length of each specimen to the nearest 0.1 mm. Micrometer, or another suitable devices for calibrating the linear variable differential transformer (LVDT) or other length change measuring device over the range to be used in the test with a minimum resolution of 0.00125 or 0.00005 in.). (Note – This differs from AASHTO TP 60, section 5.8; however, a change will be recommended to AASHTO).

- A complete set of operating instructions, including instructions for normal operation, calibration, and troubleshooting, shall be provided.

(This page intentionally left blank)